

AN INVESTIGATION OF ELECTRON  
DONOR-ACCEPTOR COMPLEX FORMATION BY  
CARBON-13 MAGNETIC RESONANCE

A Thesis  
Presented to the  
Faculty of Graduate Studies  
The University of Manitoba

In Partial Fulfillment of the  
Requirements for the Degree of  
Master of Science

Kenneth J. Friesen  
1978

AN INVESTIGATION OF ELECTRON  
DONOR-ACCEPTOR COMPLEX FORMATION BY  
CARBON-13 MAGNETIC RESONANCE

BY

KENNETH J. FRIESEN

A dissertation submitted to the Faculty of Graduate Studies of  
the University of Manitoba in partial fulfillment of the requirements  
of the degree of

MASTER OF SCIENCE

© 1978

Permission has been granted to the LIBRARY OF THE UNIVERSITY OF MANITOBA to lend or sell copies of this dissertation, to the NATIONAL LIBRARY OF CANADA to microfilm this dissertation and to lend or sell copies of the film, and UNIVERSITY MICROFILMS to publish an abstract of this dissertation.

The author reserves other publication rights, and neither the dissertation nor extensive extracts from it may be printed or otherwise reproduced without the author's written permission.

To Elaine

### ACKNOWLEDGEMENTS

It has been a privilege to work in Dr. Barry Blackburn's laboratory and I thank him for his guidance, friendship and support throughout this research project.

I express special thanks to Dr. Rod Wasylshen for sharing so much of his expertise in nmr with me. I appreciate the interest that Dr. Ted Schaefer showed in this project. I also thank Miss Moira Graham for assistance in the synthesis and Mr. Walter Hiebert for his suggestions regarding computer programming. I am indebted to Professor J.-M. Lehn for providing the program used in the determination of molecular dynamics.

I owe an expression of thanks to the University of Winnipeg and the Chemistry Department, in particular, for encouraging this study.

Finally, above all, I appreciate the patience and support of my wife, Elaine. In addition, her typing skills were invaluable in the preparation of this thesis. I also appreciate the patience and understanding of my children, Travis and Jeri, throughout my studies.

## ABSTRACT

Carbon-13 pulse Fourier transform nuclear magnetic resonance has been used to study electron donor-acceptor complex formation.

Carbon-13 chemical shifts were used to determine the equilibrium constants of two hydrocarbon complexes of *p*-benzoquinone. The shifts of the protonated carbons of *p*-benzoquinone were measured as a function of the hydrocarbon concentration in carbon tetrachloride at 34.5°C. The data was treated by a method of successive approximations to give equilibrium constants of 0.62 and 0.49 (kg solvent)mol<sup>-1</sup> for complex formation of *p*-benzoquinone with hexamethylbenzene and pentamethylbenzene respectively.

The major portion of this study was based on complex formation between 2-methylindole and 1,3,5-trinitrobenzene. Two carbon-13 enriched compounds, 2-methylindole-(methyl,3)-<sup>13</sup>C<sub>2</sub> and 2-methylindole-2-<sup>13</sup>C, were prepared by the *Fischer indole synthesis* in order to improve the signal-to-noise and permit experiments at lower concentrations.

The equilibrium constant for complex formation between 2-methylindole and trinitrobenzene (TNB) in 1,2-dichloroethane at 35.0°C was determined by monitoring the methyl shift of 2-methylindole-(methyl,3)-<sup>13</sup>C<sub>2</sub> and the C-2 shift of 2-methylindole-2-<sup>13</sup>C as a function of the TNB concentration. Equilibrium constants of 0.95 and 1.61 (kg solvent)mol<sup>-1</sup> were obtained from the methyl and C-2 shifts respectively.

Carbon-13 spin-lattice relaxation times ( $T_1$ 's) are reported for C-3 of 2-methylindole-(methyl,3)- $^{13}\text{C}_2$  as a function of the concentration of TNB in 1,2-dichloroethane at 35.0°C. The observed decreases in  $T_1$  with increasing concentrations of TNB are interpreted in terms of the formation of increasing amounts of complex and increases in viscosity. An equation is derived which makes it possible to obtain estimates of the equilibrium constants for complex formation and the spin-lattice relaxation time of the complex from the observed  $T_1$ 's and viscosity measurements. From the data obtained, values of 6.7 and 14.7 psec were calculated for the effective correlation times of free 2-methylindole and its TNB complex respectively, at 35°C and 0.686 centipoise. The  $T_1$  in the pure complex obtained by this method was 3.0 sec.

The molecular dynamics of complex formation between 2-methylindole and TNB have been determined by fitting the theoretical dependence of  $T_1$  on the fraction complexed, to the experimental data corrected for the effects of viscosity. The results indicate that the rate of chemical exchange relative to the rate of reorientation of the complex,  $k_4/k_2$ , for this system is *ca.*  $10^{-1}$ . The  $T_1$  for C-3 of 2-methylindole in the complex was found to be 2.4 sec, corresponding to an effective correlation time of 18.4 psec, by this method.

Hydrodynamical models of molecular reorientation are considered for the rotation of 2-methylindole and its TNB complex in solution.

## TABLE OF CONTENTS

ACKNOWLEDGEMENTS	ii
ABSTRACT	iii
TABLE OF CONTENTS	v
LIST OF FIGURES	x
LIST OF TABLES	xii
I. INTRODUCTION	1
II. THEORETICAL DISCUSSION	3
A. THE FISCHER INDOLE SYNTHESIS	3
1. Introduction	3
2. Synthesis of 2-methylindole	4
3. The accepted mechanism	5
B. ELECTRON DONOR-ACCEPTOR COMPLEXES	7
1. General	7
2. Electron donors and acceptors	7
3. Characteristics of EDA systems	8
4. Description of the EDA interaction	11
(a) Historical development	11
(b) Mulliken's valence-bond treatment	12
(c) Simple molecular orbital treatment	16
C. USE OF CHEMICAL SHIFTS IN STUDYING COMPLEX FORMATION	17
1. General	17
2. Origin of chemical shifts	19
3. NMR in the liquid phase	20
(a) Medium effects	20
(b) NMR and chemical exchange rates	21

4.	Determination of association constants in dilute solution	22
	(a) Hanna-Ashbaugh-Foster-Fyfe method	22
	(b) Methods not requiring a large excess of one component	28
	(c) Application to EDA equilibria	28
	(d) Criticism of the method	31
D.	CARBON-13 SPIN-LATTICE RELAXATION	32
1.	Introduction	32
	(a) General	32
	(b) Free induction decay and Fourier transformation	34
2.	Spin-lattice relaxation	37
	(a) The origin of magnetic relaxation	37
	(b) The dipole-dipole relaxation mechanism	38
	(c) Other relaxation mechanisms	43
	(d) Determination of $T_1$ by inversion recovery	44
3.	Relaxation and nuclear Overhauser enhancement	48
	(a) The nuclear Overhauser effect	48
	(b) Differentiation of relaxation mechanisms	49
4.	Molecular reorientation in liquids	50
	(a) Introduction	50
	(b) Isotropic reorientation	51
	(c) Anisotropic reorientation	52
	(d) Boundary conditions	54



5.	Molecular dynamics of complex formation	55
	(a) Effect of chemical exchange on relaxation	55
	(b) Evaluation of the rate constants	59
	(i) Determination of relative exchange rates	59
	(ii) Curve fitting	60
III.	EXPERIMENTAL	62
	A. MATERIALS	62
	B. NMR SAMPLE PREPARATION	65
	C. HIGH RESOLUTION CARBON-13 NMR SPECTRA	68
	D. SPIN-LATTICE RELAXATION TIMES	69
	E. NUCLEAR OVERHAUSER ENHANCEMENTS	71
	F. VISCOSITY DETERMINATIONS	72
IV.	RESULTS AND DISCUSSION	73
	A. SYNTHESIS OF CARBON-13 ENRICHED 2-METHYLINDOLES	73
	1. Difficulties in the synthesis	73
	2. Position of enrichment	76
	(a) Consideration of the mechanism	76
	(b) Carbon-13 nmr spectra	77
	B. CARBON-13 CHEMICAL SHIFT STUDIES OF SEVERAL EDA INTERACTIONS	80
	1. Method of analysis	80
	2. Hydrocarbon complexes of <i>p</i> -benzoquinone	82
	3. The 2-methylindole:1,3,5-trinitrobenzene complex	88

C.	A CARBON-13 SPIN-LATTICE RELAXATION TIME STUDY OF THE EDA INTERACTION OF 2-METHYLINDOLE AND 1,3,5-TRINITROBENZENE	94
1.	Introduction	94
2.	Method of analysis of K	98
3.	The assumptions involved in the determination of K from $T_1$ data	102
4.	$T_1$ in the pure complex	103
5.	Effective correlation times	103
6.	Discussion of $T_1$ values	104
7.	Criticism of the method	109
D.	MOLECULAR DYNAMICS OF 2-METHYLINDOLE: 1,3,5-TRINITROBENZENE COMPLEX FORMATION	110
1.	Experimental dependence of $T_1$ on fraction complexed	110
2.	Theoretical dependence of dipolar relaxation times on fraction complexed	112
3.	The rate constants for the 2-MeI:TNB system	113
4.	$T_1$ in the pure complex	116
E.	SPIN-LATTICE RELAXATION AND HYDRODYNAMICAL ROTATION OF 2-METHYLINDOLE	118
1.	Isotropic reorientation	118
2.	Anisotropic reorientation	119
(a)	Determination of the geometry	119
(b)	Application of boundary conditions	119
(c)	Determination of the experimental viscosity dependence of $\tau_c$	122
(i)	Variation of temperature	122
(ii)	Variation of the solvent system	124

	(d) Comparison of experimental data with theory	124
	(e) Application to the TNB complex of 2-methylindole	127
V.	BIBLIOGRAPHY	131
VI.	APPENDICES	137
	A. 'SHIFT'	137
	B. 'EDA'	138
	C. 'QUADEX'	141

## LIST OF FIGURES

Figure		Page
1.	Energy diagram for a weak electron donor-acceptor interaction.	15
2.	Effect of chemical exchange rates on nmr line-shapes.	23
3.	Nmr spectra showing the effects of complex formation on chemical shifts.	26
4.	Effect of rf excitation on the net magnetization of a sample in an external magnetic field.	33
5.	Examples of free induction decay patterns.	36
6.	Dependence of $T_1$ and $T_2$ on the effective correlation times.	40
7.	Transition probabilities for the $^{13}\text{C}-^1\text{H}$ two-spin system.	42
8.	Illustration of the $180^\circ-t_i-90^\circ$ pulse sequence used to determine $T_1$ .	45
9.	The recovery of the longitudinal magnetization in the inversion recovery method for the determination of $T_1$ .	47
10.	Effect of chemical exchange rates on relaxation behaviour.	58
11.	Apparatus used for vacuum degassing and sealing nmr samples.	67
12.	Obtaining high resolution $^{13}\text{C}$ nmr spectra from the free induction decay.	70
13.	Carbon-13 nmr spectra of 2-methylindole, 2-methylindole-(methyl,3)- $^{13}\text{C}_2$ and 2-methylindole-2- $^{13}\text{C}$ in 1,2-dichloroethane.	79
14.	Plot used in the determination of the equilibrium constant for the <i>p</i> -benzoquinone: hexamethylbenzene system from chemical shift data.	85

Figure		Page
15.	Plot used in the determination of the equilibrium constant for the <i>p</i> -benzoquinone: pentamethylbenzene system from chemical shift data.	86
16.	Plot used in the determination of the equilibrium constant for the 2-methylindole: trinitrobenzene system from C-2 shifts of 2-methylindole.	90
17.	Plot used in the determination of the equilibrium constant for the 2-methylindole: trinitrobenzene system from the methyl shifts of 2-methylindole.	92
18.	Spectra obtained by the inversion recovery method for the determination of $T_1$ for C-3 of 2-methylindole.	96
19.	Magnetization recovery plots for C-3 of 2-methylindole with and without TNB added.	97
20.	Spectra obtained in the nOe measurement of C-3 of 2-methylindole.	99
21.	Plot used in the determination of the equilibrium constant for the 2-methylindole: trinitrobenzene system from $T_1$ data.	101
22.	Dependence of $T_1$ and $T_2$ on the correlation time for the CFT-20 nmr spectrometer.	105
23.	Dependence of the nOe on the correlation time for the CFT-20 nmr spectrometer.	106
24.	Pulse width calibration for the CFT-20.	108
25.	Dependence of $T_1$ of C-3 of 2-methylindole on the fraction complexed.	114
26.	Approximation of 2-methylindole as an oblate spheroid.	121
27.	Viscosity dependence of $1/T_1$ of C-3 of 2-methylindole.	126
28.	Comparison of theoretical and experimental viscosity dependence of the correlation time for 2-methylindole.	128

## LIST OF TABLES

Table		Page
1.	Common electron donors and acceptors.	9
2.	Magnetic properties of several nuclei frequently used in nmr.	18
3.	Carbon chemical shifts of 2-methylindole relative to TMS.	78
4.	Chemical shifts of the protonated carbon of <i>p</i> -benzoquinone as a function of the hexamethylbenzene concentration.	84
5.	Chemical shifts of the protonated carbon of <i>p</i> -benzoquinone as a function of the pentamethylbenzene concentration.	84
6.	Comparison of $^{13}\text{C}$ results with $^1\text{H}$ results for complex formation of <i>p</i> -benzoquinone with hexa- and pentamethylbenzene.	87
7.	Chemical shifts for C-2 of 2-methylindole as a function of the TNB concentration.	89
8.	Chemical shifts for the methyl carbon of 2-methylindole as a function of the TNB concentration.	89
9.	Spin-lattice relaxation times for C-3 of 2-methylindole as a function of the TNB concentration.	95
10.	Spin-lattice relaxation times for C-3 of 2-methylindole as a function of the fraction complexed.	111
11.	Rate constants and $T_1$ 's for complex formation of 2-methylindole with TNB.	115
12.	Viscosity dependence of $T_1$ determined by variation of the temperature.	123
13.	Viscosity dependence of $T_1$ determined by variation of the solvent system.	125
14.	Viscosity dependence of the correlation time of 2-methylindole.	127
15.	Hydrodynamical rotation of the TNB complex of 2-methylindole.	129

## I. INTRODUCTION

There has been an increase in research activity in the area of molecular complexes of the electron donor-acceptor, sometimes called charge-transfer, type (1) in the last two decades. This can be attributed partly to the fact that such molecular associations are likely of importance in biological systems (2, 3), but also to the advancement of physical techniques such as differential refractometry, gas-liquid chromatography, osmometry, calorimetry, fluorescence and nuclear magnetic resonance (nmr) spectroscopy (4).

Although the geometries of many complexes have been determined in the solid state by X-ray crystallography, the earliest methods of analysis of complexes in solution were by ultraviolet-visible spectroscopy. More recently nmr, proton ( $^1\text{H}$ ) and to some extent fluorine ( $^{19}\text{F}$ ), has become a well documented technique for the analysis of electron donor-acceptor (EDA) systems (5). In these experiments changes in chemical shifts of nuclei in the minor component are monitored as a function of the concentration of the major component. The results allow calculation of the equilibrium constants and provide potential information on the composition and thermodynamics of the system (1).

When this study was initiated there were, to the best of this author's knowledge, no publications on the use of carbon-13 nmr in the study of EDA systems, due to the low natural abundance and small magnetic moment of the  $^{13}\text{C}$  nucleus (6). This difficulty was overcome to a large extent with the de-

velopment of  $^{13}\text{C}$  Fourier transform (FT) nmr. It was felt that the advantages offered by  $^{13}\text{C}$  nmr over  $^1\text{H}$  nmr, namely the greater dispersion of peaks and more readily interpretable spin-lattice relaxation time ( $T_1$ ) data, may be utilized in this type of study. These advantages, together with the fairly recent increase in the availability of  $^{13}\text{C}$  enriched compounds made the idea of studying EDA systems by  $^{13}\text{C}$  nmr quite attractive.

The usefulness of both chemical shifts and spin-lattice relaxation times in the determination of equilibrium constants, with particular emphasis on the EDA interaction of 2-methylindole with 1,3,5-trinitrobenzene, was investigated in this thesis. Furthermore, the investigation was to determine whether the  $T_1$  data could provide information about the lifetimes and reorientation rates of both the free and complexed forms of the minor component. A study of the viscosity dependence of  $T_1$  was to aid in determining the reorientational behaviour of 2-methylindole, the minor component in a large part of this work, in solution.

In studies of this type changes must be monitored in the minor component. This presented little difficulty for most of the chemical shift work. However, to gain sufficient signal-to-noise, particularly for the  $T_1$  study and for the chemical shift work with carbon-2 of 2-methylindole, it was necessary to synthesize several carbon-13 enriched compounds.

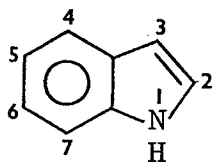


## II. THEORETICAL DISCUSSION

### A. THE FISCHER INDOLE SYNTHESIS

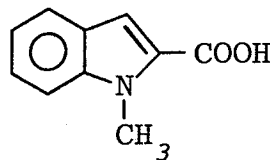
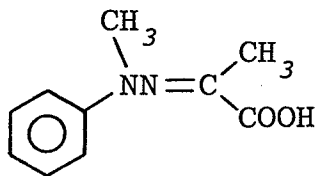
#### 1. INTRODUCTION

Treatment of arylhydrazones of certain aldehydes and ketones with an appropriate catalyst, usually zinc chloride, results in the elimination of ammonia and formation of the indole nucleus



in a reaction known as the *Fischer indole synthesis* (7). The arylhydrazones, readily prepared by treating the aldehyde or ketone with an arylhydrazine, can usually be subjected to indolization without prior isolation and purification.

This reaction was discovered in 1883 when Fischer and Jourdan treated pyruvic acid 1-methylphenylhydrazone with alcoholic hydrogen chloride (8). A year later the product of this reaction was identified as 1-methylindole-2-carboxylic acid by Fischer and Hess (9).



The Fischer synthesis does, however, have certain limitations. For example, *m*-substituted phenylhydrazones will give a mixture of indoles since ring closure can take place in two ways. Nevertheless, the discovery of this reaction has provided a most versatile method for the preparation of indoles, one which has been utilized in the synthesis of many of the mono- and dimethylindoles.

## 2. SYNTHESIS OF 2-METHYLINDOLE

There have been a number of publications reporting the synthesis of 2-methylindole from acetone phenylhydrazone using slight variations in procedure.

Marion and Oldfield (10) report a yield of 2-methylindole of 53% by heating a mixture of equal weights of freshly fused zinc chloride and the phenylhydrazone of acetone.

Chapman, Clarke and Hughes (11) obtained yields of 85% on boiling equal weights of anhydrous zinc chloride and acetone phenylhydrazone in dry cumene for 1 hour under nitrogen.

Kissman, Farnsworth and Witkop (12) heat a mixture of phenylhydrazine, acetone and polyphosphoric acid to 203°C. Purification of the product resulted in an overall yield of 60%.

The group of Shukri, Alazawe and Al-Tai (13) report the use of glacial acetic acid and boron trifluoride as cyclizing agents in the synthesis of several 2-substituted indole derivatives with yields ranging from 40-82%.

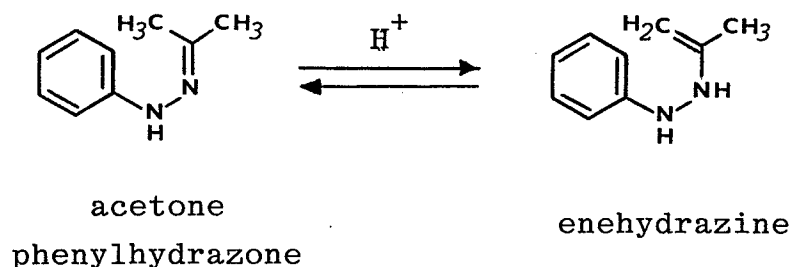
### 3. THE ACCEPTED MECHANISM

The currently accepted mechanism for the *Fischer indole synthesis*, first proposed by Robinson and Robinson (14), consists of three basic steps.

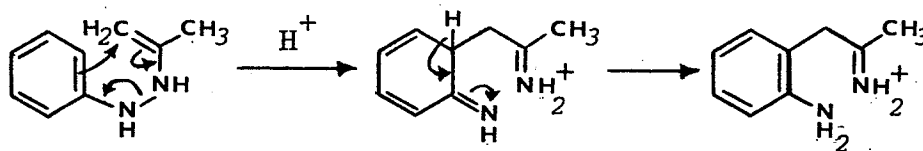
First, the catalyst is believed to catalyze the conversion of the arylhydrazone to its enehydrazine tautomer. A sigmatropic rearrangement (15) then takes place in which the enehydrazine undergoes an intramolecular electrophilic substitution resulting in the formation of a new carbon-carbon bond. Finally, ring closure is effected as nitrogen is eliminated as ammonia.

The steps in the mechanism are illustrated (below) for the synthesis of 2-methylindole from acetone phenylhydrazone.

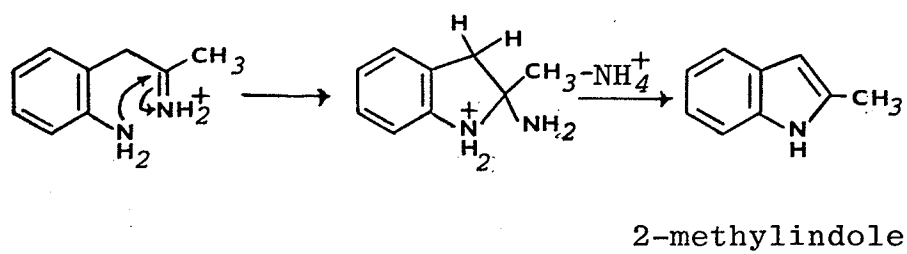
(a) Hydrazone-enehydrazine equilibrium



(b) Sigmatropic rearrangement



(c) Loss of nitrogen and ring closure



## B. ELECTRON DONOR-ACCEPTOR COMPLEXES (20)

### 1. GENERAL

Molecules experience a range of interactions from weak physical forces, such as the van der Waals attractions which are experienced by all molecules, to the strong "chemical" forces which result in the formation of new covalent or ionic bonds and the production of a new compound.

Electron donor-acceptor (EDA) complexes, also known as charge-transfer complexes, result from an intermediate degree of interaction between an electron donor and an electron acceptor molecule or ion. However, due to the continuum of interactions between molecules there are no sharp boundaries which define a particular interaction to be of the EDA type.

### 2. ELECTRON DONORS AND ACCEPTORS

An organic electron donor (D) may donate electron density either through unshared pairs of electrons in non-bonding orbitals, in which case it is known as a n-donor, or through the delocalized  $\pi$ -cloud of an olefin or an aromatic ring. Aliphatic amines, alcohols and ethers act as n-donors; whereas the stronger  $\pi$ -donors, as the latter group is known, include aromatic amines, aromatic hydrocarbons and certain heterocyclic systems. Since electron density is donated from these molecules during the formation of an EDA complex, molecules with a low ionization potential (IP) -i.e. the ease with which an electron can be removed from D- are more effective donors. Adding electron releasing groups

to the donor lowers its IP and results in the formation of more stable complexes.

The most common organic acceptors, the  $\pi$ -acceptors, are usually aromatic compounds or olefins containing strong electron-withdrawing substituents such as  $\text{NO}_2$ , CN, or the halogens, as well as quinones and acid anhydrides. The electron withdrawal by the substituents makes the molecule a better electron acceptor. This increased electrophilic nature will lead to the formation of more stable complexes on interaction of these molecules with electron donors.

Several common organic electron donors and electron acceptors are given in Table 1. Although the compounds shown are listed as donors or acceptors *per se*, it should be noted that this is a generalization, since some molecules are known to behave as both donor and acceptor in different situations (5).

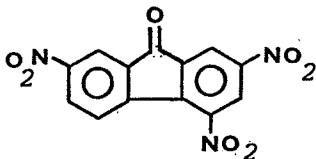
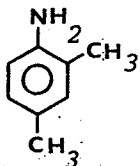
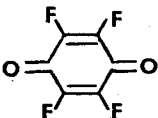
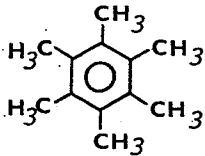
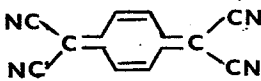
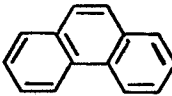
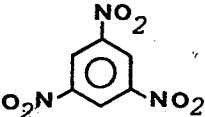
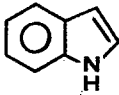
### 3. CHARACTERISTICS OF EDA SYSTEMS

Despite the lack of sharp boundaries defining interactions as being of the EDA type, a number of observations have been made which are fairly characteristic of EDA complexes (1, 5, 16).

Though many complexes exist only in solution in equilibrium with their components, a number have been isolated as stable crystalline adducts (19).

The enthalpies of formation of these complexes are usually of the order of 4 kcal/mole or less, indicative of the

TABLE 1. Common organic electron donors and electron acceptors.

ACCEPTORS	DONORS
	
2,4,7-Trinitrofluorenone	2,4-Dimethylaniline
	
Fluoranil	Hexamethylbenzene
	
7,7,8,8-Tetracyanoquinodimethane (TCNQ)	Phenanthrene
	
1,3,5-Trinitrobenzene (TNB)	Indole

weak interactions involved.

X-ray diffraction studies on solid EDA complexes of the  $\pi$ - $\pi$  type have shown that the donor and acceptor are arranged in parallel planes with a separation of 3-3.5Å. This relatively large separation ruled out the possibility that these complexes were held together by normal covalent bonds.

It is also known that large substituents on aromatic rings greatly reduce the stability of the EDA complex (32), presumably for steric reasons. For example, hexaethylbenzene forms a much weaker complex with 1,3,5-trinitrobenzene than does hexamethylbenzene (1).

Complexes are usually formed with simple, frequently 1:1, ratios of donor and acceptor.

EDA complexes have dipole moments even if the component molecules do not. Polarized UV spectroscopy has shown that the plane of greatest polarizability in the complexes is perpendicular to the planes of the molecules.

Finally, EDA complexes frequently show an absorption band in their electronic spectrum which is not present in the spectrum of either component. Since this absorption is in the visible or near-UV region many complexes are intensely colored. The description of these interactions as "charge-transfer complexes" originated out of the fact that this "extra" absorption band could be accounted for by assuming transfer of charge from the donor to the acceptor. This description has certain difficulties since it is now known that charge-transfer forces normally do not contribute to a large



degree to the stabilization of the ground state of the complex as implied by this term. Therefore, "electron donor-acceptor complex" is a more accurate description of this type of interaction.

#### 4. DESCRIPTION OF THE EDA INTERACTION

##### (a) Historical Development (1)

The properties of the adducts produced by the apparently instantaneous reaction of two compounds were documented as early as 1927 by P. Pfeiffer.

Early attempts to describe the bonding in these complexes included theories of covalent bonding between the two molecules (J. J. Sudborough-1901), electrostatic attractions between dipoles and induced dipoles within the components (G. Briegleb-1932), and the formation of an ionic complex (J. J. Weiss-1941). Each of these theories had trouble accounting for available experimental data. The idea of covalent bonding was dispelled after crystallographic studies showed a separation of components much larger than reasonable for covalent bonding. The "ionic" complex model was not consistent with the small enthalpies of formation which had been measured and Briegleb's theory could not account for the intense coloration of these complexes.

The idea of "complex resonance", using one nonbonded and one covalently bonded contributing structure, was used by Brackmann (1949) to describe the complex. However, he failed to suggest that the bonded structure was the result

of an electron transfer between the component molecules. At this time Benesi and Hildebrand observed an absorption band for the complex between an aromatic hydrocarbon and iodine which was not present in the spectra of either of the individual components. In 1950 Mulliken suggested that this absorption could be explained by an intermolecular charge-transfer between the components, which led to his "valence-bond" description of such complexes (17).

(b) Mulliken's Valence-Bond Treatment (1, 5, 17)

For a relatively weak interaction between an electron donor (D) and an electron acceptor (A), Mulliken (17) has approximated the ground state of the complex with a quantum mechanical wave function of the form

$$[1] \quad \psi_N(AD) = a\psi_0(A,D) + b\psi_1(A^-D^+)$$

This wave function describes the complex as a resonance hybrid of two contributing structures (18).



The function  $\psi_0(A,D)$ , known as the "no-bond" structure, corresponds to a structure in which only Coulombic forces such as dipole-dipole, dipole-induced-dipole, hydrogen-bonding and van der Waals attractions bind the donor to the acceptor. The other contributing structure, represented by the wave function  $\psi_1(A^-D^+)$ , symbolizes the "charge-transfer" structure in which one electron has been completely transferred from the donor to the acceptor without a change in the spin

multiplicity of the system. Since crystallographic data (19) on weak  $\pi$ - $\pi$  complexes indicates that the components are separated by 3-3.5Å, this second, covalently bonded structure makes only a minor contribution to the binding energy of the ground state of the complex, i.e.  $a \gg b$  in the ground-state wave function  $\psi_N$ . Since this "charge-transfer" structure makes only a small contribution to the ground state, it must mean that only a small amount of charge (a fraction of an electron) is transferred (18).

For weak EDA interactions, the energy of the complex in its ground state,  $W_N$ , can qualitatively be represented as

$$[2] \quad W_N = W_0 - X_0$$

where  $W_0$  represents the energy of the state  $\psi_0$ , i.e. the energy of all the Coulombic interactions together with the energy of the infinitely separated components, A and D; and  $X_0$  represents a resonance stabilization due to the small contribution of the "charge-transfer" structure to the ground state of the complex.

Continuing with Mulliken's treatment, a wave function describing an excited state of the complex can be approximated as

$$[3] \quad \psi_E(AD) = a*\psi_1(A^-D^+) - b*\psi_0(A,D)$$

where  $a \approx a$  and  $b \approx b$ .

The energy of the excited state can be represented by

$$[4] \quad W_E = W_I + X_I$$

where  $W_I$  takes into account the energy of the separated components A and D, the energy required to remove an electron from D (the ionization potential of D,  $(IP)_D$ ), the energy released as A accepts the electron (the electron affinity of A,  $(EA)_A$ ), and the Coulombic forces of attraction as the ions are brought to their equilibrium distance of separation; and  $X_I$  represents the resonance energy due to a small contribution from the "no-bond" structure in the excited state.

Since the excited state  $\psi_E$  is not quite purely "charge-transferred" the energy of this state is somewhat greater than  $W_I$ .

For the weak interactions considered here perturbation theory can be used to get a reasonable approximation of the energy terms  $W_N$  and  $W_E$ , since one resonance structure predominates and the other(s) can be treated as a small perturbation to the system. The qualitative energy diagram (Figure 1) shows how  $W_E$  and  $W_N$  vary with the distance between the molecules (or ions). The effect of resonance on the states  $\psi_0$  and  $\psi_1$  has been illustrated as well. Note in particular that resonance (or overlap) becomes more important as the intermolecular distance decreases.

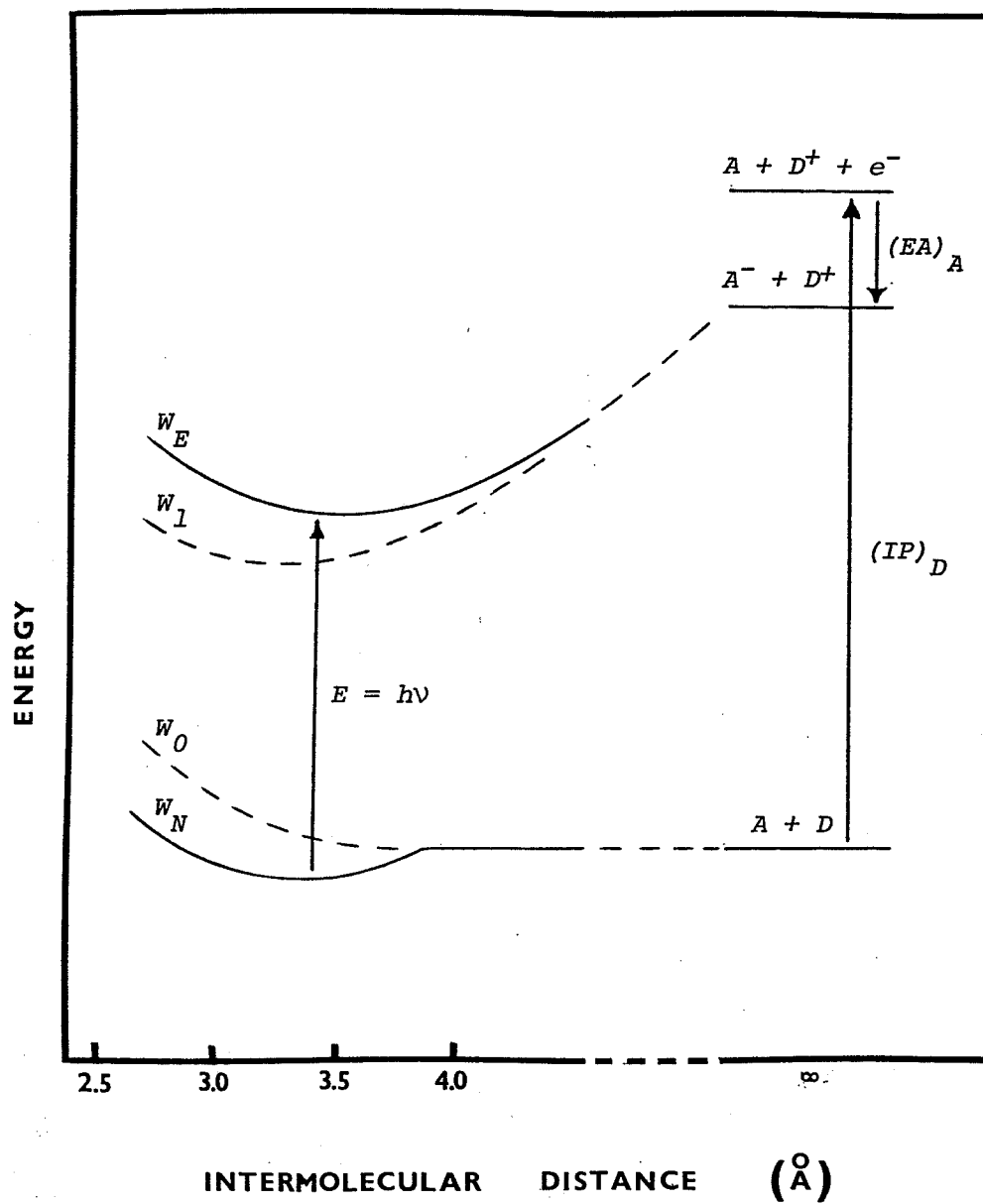


FIGURE 1. Energy diagram for a weak electron donor-acceptor interaction showing the dependence of the energies of the ground and excited states,  $W_N$  and  $W_E$ , with the intermolecular distance A-D, and a possible electronic transition. (After R. S. Mulliken (17).)

The electronic absorption characteristic of the complex involves the transition of an electron from the ground to the excited state of the complex,  $\psi_N \rightarrow \psi_E$ . For weak interactions this involves the transfer of an outer electron from a molecular orbital (MO) of the donor into an unoccupied MO in the acceptor (ie. essentially a transition  $\psi_0 \rightarrow \psi_1$ ). Since many complexes utilize  $\pi$ -MO's this intermolecular bond is not necessarily localized between two atoms. The MO's (or AO's) involved in this transfer must be of the same group-theory species (ie. there must be proper symmetry) for there to be any resonance or overlap. However, the overlap is not strong since  $a \gg b$  for these complexes. Although this extra absorption(s) is observed in a number of EDA complexes, it may be difficult to identify since it may be hidden by the peaks of the component molecules.

It should be emphasized that the above discussion is applicable only to fairly weak EDA interactions between neutral molecules of the type discussed in this thesis.

### (c) Simple Molecular Orbital Treatment

A molecular orbital treatment of weak EDA interactions (21) generally involves calculation of the energies of the highest occupied molecular orbital (HOMO) of the donor and the lowest unoccupied molecular orbital (LUMO) of the acceptor by a Hückel treatment. Transfer of charge from the HOMO of D to the LUMO of A accounts for the new bands in the electronic spectrum. The reader is referred to the discussion by Dewar and Lepley for the details of the MO treatment for weak EDA interactions.

## C. USE OF CHEMICAL SHIFTS IN STUDYING COMPLEX FORMATION

### 1. GENERAL

For nuclei with a spin quantum number  $I = \frac{1}{2}$ , (for example  $^1\text{H}$ ,  $^{13}\text{C}$ ,  $^{19}\text{F}$  and  $^{31}\text{P}$ ), the interaction of the magnetic moment of the nucleus with the external magnetic field  $H_0$  splits the system into two energy levels or spin states, the degree of interaction being directly proportional to the strength of the applied field. The resonance condition or the external magnetic field at which a nucleus absorbs energy from a radiofrequency field superimposed on the sample is given by

$$[5] \quad \nu = (\gamma/2\pi) H_0$$

where  $H_0$  = the applied magnetic field strength,

$\nu$  = the frequency of the applied  
electromagnetic radiation,

$\gamma$  = the magnetogyric ratio of the  
nucleus.

Since nuclear isotopes have widely varying magnetogyric ratios, different frequencies and magnet strengths are required to study different nuclei. Table 2 summarizes the absorption characteristics of several important magnetic nuclei.

For a detailed quantum mechanical treatment of nuclear magnetic resonance, the reader is referred to several books (6, 22-24).

TABLE 2. Magnetic properties of several nuclei  
frequently used in nmr (5, 24).

ISOTOPE	NATURAL ABUNDANCE	SPIN (I)	RELATIVE SENSITIVITY	NMR FREQUENCY MHZ at 14.092G
$^1\text{H}$	99.985%	$\frac{1}{2}$	1.000	60.000
$^2\text{H}$	0.015	1	0.0097	9.210
$^{13}\text{C}$	1.108	$\frac{1}{2}$	0.0159	15.087
$^{14}\text{N}$	99.63	1	0.001	4.334
$^{19}\text{F}$	100.0	$\frac{1}{2}$	0.833	56.446
$^{31}\text{P}$	100.0	$\frac{1}{2}$	0.066	24.288



## 2. ORIGIN OF CHEMICAL SHIFTS

Since electrons shield nuclei from  $H_0$ , different nuclei "see" and therefore resonate at different fields,  $H_i$  where

$$[6] \quad H_i = H_0(1 - \sigma_i)$$

and  $\sigma$  is the screening constant, a tensor quantity representing the shielding of the nucleus.

The small magnetic fields ( $\sigma H_0$ ) produced by the field-induced circulation of electrons may originate within the molecule being observed as well as from the molecules of the medium immediately surrounding it. The shielding term may therefore be written (25) as

$$[7] \quad \sigma = \sigma_{intra} + \sigma_{inter}$$

The intermolecular (usually small) effects contributing to shielding will be discussed in the next section. The various factors which have been postulated (6,24) to contribute to  $\sigma_{intra}$  can be summarized as follows:

$$[8] \quad \sigma_{intra} = \sigma_d + \sigma_p + \sigma_a + \sigma_r + \sigma_e$$

The field-induced spherical circulation of electron density about the nucleus creates an induced field which opposes  $H_0$  at the nucleus. This isotropic shielding term, known as the diamagnetic contribution ( $\sigma_d$ ), is particularly important in  $^1\text{H}$  nmr.

However, due to the absence of spherical symmetry in most molecules, an anisotropic paramagnetic term ( $\sigma_p$ ) is added. This deshielding term, which arises due to the mixing of low-lying excited states with the ground state of the molecule by  $H_0$ , reflects the nonspherical circulation of electron density caused by the presence of other nuclei in the molecule. The paramagnetic contribution, so called because it opposes  $\sigma_d$ , is especially important where p orbitals are involved, as in  $^{19}\text{F}$  and  $^{13}\text{C}$  nmr.

Neighbor anisotropic contributions ( $\sigma_a$ ) are effects felt by the nucleus being observed due to the interaction of neighbor atoms with  $H_0$ .

Ring currents of delocalized electrons ( $\sigma_r$ ) also make a contribution to shielding.

Finally an electric field effect ( $\sigma_e$ ) due to a polar group in the molecule affects the electron density at the nucleus being observed.

Although chemical shifts are not well understood, for the moment it appears that the intramolecular effects cited are the major contributors to the shielding of nuclei.

### 3. NMR IN THE LIQUID PHASE (1, 5, 24)

#### (a) Medium Effects

The observed chemical shifts ( $\delta$ ) will depend to some extent on the medium in which the measurements are made. These intermolecular shielding effects ( $\sigma_{inter}$ ) may be due to the interaction of the nucleus in question with surrounding solvent molecules or with other solute molecules in the medium.

Solvent effects which contribute to shielding include (1,24) the bulk magnetic susceptibility of the solvent ( $\sigma_B$ ), the solvent anisotropy ( $\sigma_A$ ), van der Waals interactions between the solute and the solvent ( $\sigma_W$ ) and a polar effect ( $\sigma_E$ ) in which a dipole moment in the solute induces an electric field in the solvent.

Finally, specific complex formation also makes a contribution ( $\sigma_C$ ) to the shielding of the nuclei in the molecule under observation.

The intermolecular interactions which contribute to shielding may therefore be summarized as

$$[9] \quad \sigma_{inter} = \sigma_B + \sigma_A + \sigma_W + \sigma_E + \sigma_C.$$

In this study we are particularly interested in the last term, the effect of complex formation on the observed shift.

#### (b) NMR and Chemical Exchange Rates

For nuclei which are involved in exchange between two chemical environments,



the observed nmr spectrum will depend on the kinetics of the exchange (5).

If the rate of exchange between two species is slow relative to the rate of exchange between the magnetic states of the nucleus under observation, the nonequivalence of that nucleus can be detected, resulting in the appearance of two sharp resonances in the spectrum. As the relative chemical

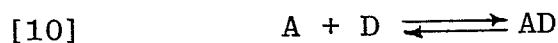
exchange rate increases the lines broaden and then coalesce as shown in Figure 2. When the relative exchange is fast only a time-averaged field is felt by the nucleus resulting in a single sharp resonance. The chemical shift of this resonance will be a population weighted average of the chemical shifts of the nucleus being measured (say A) in its two environments, as given by [14]. Factors such as temperature and concentration which affect the position of equilibrium (hence the relative populations in the two states) will influence the observed chemical shift.

Any interaction between two molecules should affect the chemical shift of a particular nucleus (6). The weak interactions between electron donors and electron acceptors generally fall into the category of fast exchange reactions (1). However, as the strength of binding between the interacting species increases the line shape could conceivably be affected (5).

#### 4. DETERMINATION OF ASSOCIATION CONSTANTS IN DILUTE SOLUTION (1, 5)

##### (a) Hanna-Ashbaugh-Foster-Fyfe Method

For the interaction of an electron donor and an electron acceptor under the conditions of microscopic reversibility (ie. fast exchange) to form a 1:1 complex,



a thermodynamic equilibrium constant can be written as

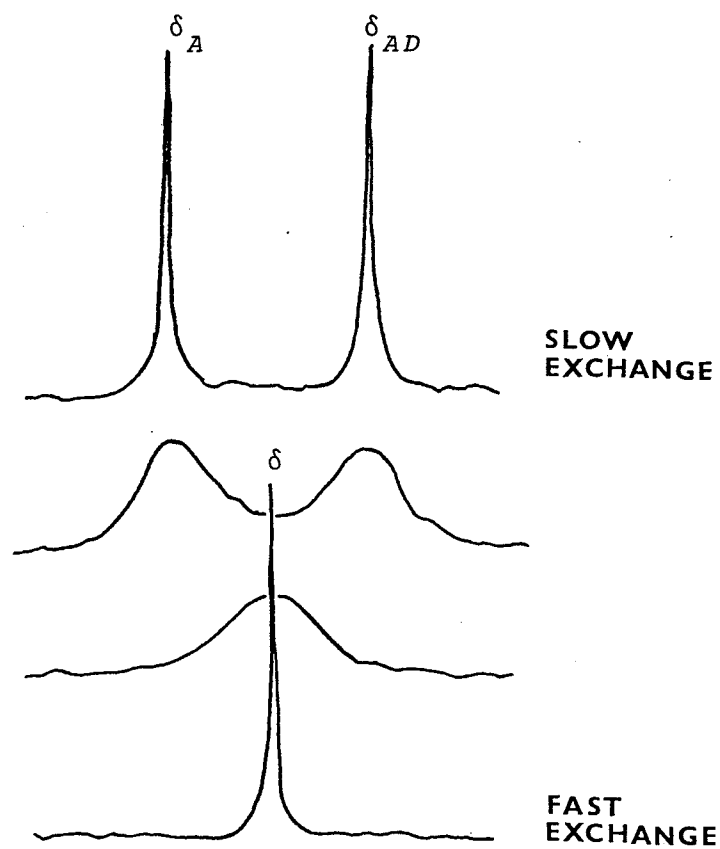


FIGURE 2. The effect of chemical exchange rates on nmr line-shapes, shown here for exchange between environments with equal populations.

$$[11] \quad K = \frac{[AD] \gamma_{AD}}{[D][A] \gamma_D \gamma_A}$$

where [A], [D], and [AD] represent the equilibrium concentrations of the three species involved. A number of concentration scales (molar, molal, mole fraction, etc.) are used in the literature (1, 5) affecting the magnitude and units of reported equilibrium constants.

Since the measurements are normally made on dilute solutions the activity coefficient term  $\gamma_{AD}/\gamma_D\gamma_A$  is assumed to be 1. The thermodynamic equilibrium constant is then approximated by the equilibrium quotient. In terms of the initial concentrations of acceptor and donor,  $[A]_0$  and  $[D]_0$ , the equilibrium constant expression is written as

$$[12] \quad K = \frac{[AD]}{([D]_0 - [AD])([A]_0 - [AD])}$$

For systems where K is small this expression can be simplified by keeping one component in large excess, so that its concentration is virtually unchanged by complex formation.

Experimentally the donor is usually in large excess due to the low solubility of organic acceptors. Therefore, where  $[D]_0 \gg [A]_0$

$$[13] \quad K = \frac{[AD]}{[D]_0([A]_0 - [AD])}$$

An analogous equation and subsequent treatment apply to situations where  $[A]_0 \gg [D]_0$ .

Recall that under the conditions of fast exchange the observed chemical shift of the nucleus A is a population weighted average of the shifts of this nucleus in the two environments, *ie.*

$$[14] \quad \delta = \delta_A P_A + \delta_{AD} P_{AD}$$

where  $\delta_A$  = the chemical shift for pure A,

$\delta_{AD}$  = the chemical shift of the same nucleus in A for the pure complex,

$\delta$  = the observed chemical shift for this nucleus in the equilibrium mixture,

$P_A$  = the mole fraction of A uncomplexed,

$P_{AD}$  = the mole fraction of A complexed.

Since  $(P_A + P_{AD}) = 1$ , [14] becomes

$$[15] \quad \delta = P_{AD}(\delta_{AD} - \delta_A) + \delta_A.$$

If, as illustrated in Figure 3, we let

$\Delta_0 = (\delta_A - \delta_{AD})$  *ie.* the chemical shift difference between A and AD,

$\Delta = (\delta_A - \delta)$  *ie.* the chemical shift difference between A and the observed shift,

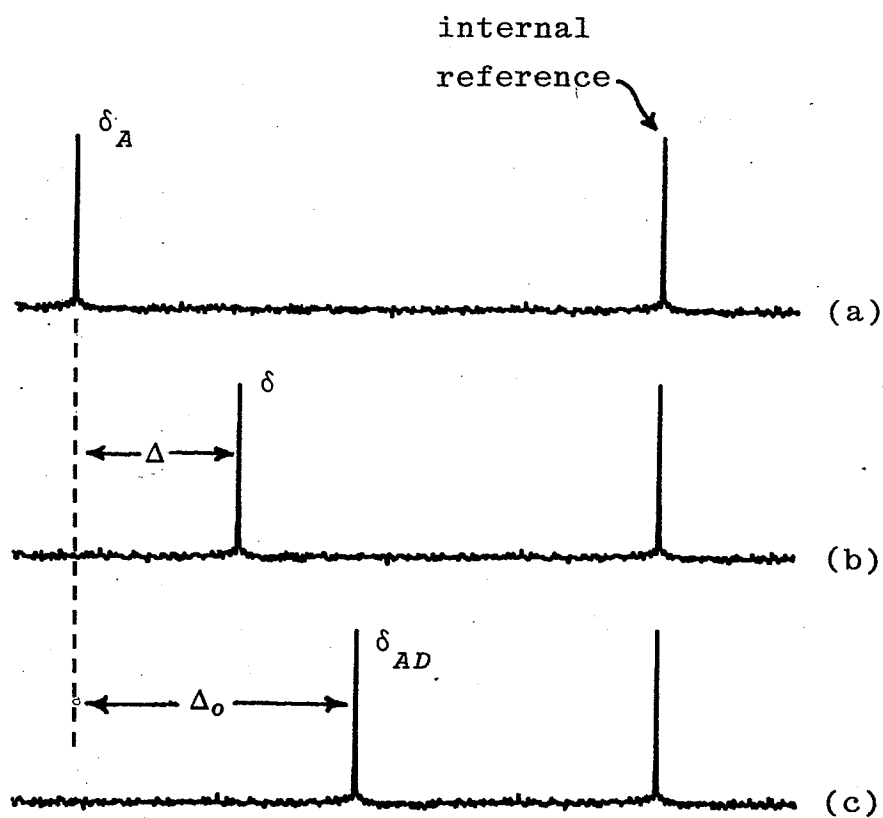


FIGURE 3. Nmr spectra showing the relationship between  $\delta$ ,  $\delta_A$ ,  $\delta_{AD}$ ,  $\Delta$  and  $\Delta_0$ . (a) The spectrum of A in the absence of D. (b) The spectrum of the equilibrium mixture. (c) The spectrum of the pure complex in solution (not measureable).



then the mole fraction (here of A) complexed can be written as

$$[16] \quad P_{AD} = \frac{(\delta_A - \delta)}{(\delta_A - \delta_{AD})} = \frac{\Delta}{\Delta_0} = \frac{[AD]}{[A]_0}$$

Making appropriate substitutions for  $[AD]/[A]_0$  in [13] one obtains the nmr analogue of the Benesi-Hildebrand equation (26) which is used in the optical absorption measurements of charge-transfer complexes,

$$[17] \quad \frac{1}{\Delta} = \frac{1}{K\Delta_0[D]_0} + \frac{1}{\Delta_0}$$

A plot of  $1/\Delta$  vs.  $1/[D]_0$  gives a slope of  $-1/K\Delta_0$  and y-intercept of  $1/\Delta_0$ .

The method, originally used in a study of hydrogen-bonded interactions (27, 28), was first applied to a recognized donor-acceptor system by Hanna and Ashbaugh (29).

A disadvantage of this method is that an extrapolation to high concentration is necessary to determine the intercept with the ordinate ( $\Delta_0$ ) before the equilibrium constant can be evaluated from the slope. This will be particularly crucial for systems where K is small.

Rearrangement of [17] to the well-known Hanna-Ashbaugh-Foster-Fyfe (HAFF) equation

$$[18] \quad \Delta/[D]_0 = -K\Delta + K\Delta_0$$

allows K to be determined directly from the slope of a plot of  $\Delta/[D]_0$  against  $\Delta$  for a series of solutions where  $[D]_0 \gg [A]_0$ .

The disadvantage of both of these methods is that one component must be in large excess.

(b) Methods Not Requiring a Large Excess of One Component

Substitution of  $[AD] = (\Delta/\Delta_o)[A]_o$  into [12] yields

$$[19] \quad K = \frac{\Delta}{(\Delta_o - \Delta) \left\{ [D]_o - (\Delta/\Delta_o) [A]_o \right\}}$$

which can be rearranged to

$$[20] \quad \frac{1}{K} = \frac{\Delta_o}{\Delta} [D]_o - [A]_o - [D]_o + \frac{\Delta}{\Delta_o} [A]_o$$

This equation is the nmr analogue of the Rose-Drago equation used in optical experiments (24). All quantities are known except  $K$  and  $\Delta_o$  which are obtained by solving a set of simultaneous equations, either graphically as discussed by Wachter and Fried (36) or by computer methods.

Association constants may also be determined from [15] by varying  $K$  until the  $P_{AD}$  values calculated from it vary linearly with  $\delta$  (37).

(c) Application to EDA Equilibria

The equilibrium constants which have been reported for EDA interactions have been evaluated largely by application of the HAFF equation [18]. Foster and Fyfe applied this method in determining  $K$  and  $\Delta_o$  for several benzoquinone-alkylbenzene complexes by  $^1\text{H}$  nmr.  $^1\text{H}$  nmr chemical shift studies on various indoles complexed to 1,3,5-trinitro-

benzene have been reported (31, 32, 38). The results have indicated (31) that complex formation (with TNB) is somewhat localized over the C(2)-C(3) region of the indole.  $K$  and  $\Delta_o$  values for different protons of the indole have allowed for speculation about the relative orientation of TNB and the indole in the complex (32).

$^{19}\text{F}$  nmr, which has several advantages over  $^1\text{H}$  nmr in such a study, has been used to study certain fluoranil complexes (33). In general,  $^{19}\text{F}$  chemical shift changes will be larger resulting in more accurate  $K$  values. Furthermore, the problem of overlap from solvent or other resonances in the acceptor or donor will be less than in  $^1\text{H}$  work.

When this particular research was initiated (1974) there were, to the best of this author's knowledge, no reports in the literature on the use of  $^{13}\text{C}$  nmr in the determination of equilibrium constants. Subsequently,  $K$  and  $\Delta_o$  have been obtained from  $^{13}\text{C}$  chemical shifts for a hydrogen-bonded system (34) as well as for recognized EDA complexes between several aromatic donors and trinitrobenzene (35) and *o*-chloranil (39).

Proton nmr studies have shown that both donors and acceptors shift upfield on complex formation, but that donors shift upfield by a smaller amount (32). Although, as has been mentioned previously, the interpretation of chemical shifts is difficult, several factors have been postulated to account for present observations. These diamagnetic shifts are generally attributed to the predominance of the ring current effects of one component on the nuclei of the other (32). If the

effects of charge migration were predominant in EDA complex formation, then the donor protons should shift downfield and the acceptor protons should shift upfield as the complexes become stronger. Since such observations are not made it appears that  $^1\text{H}$  nmr is not sensitive to the effects of charge migration(32).

With the greater sensitivity of  $^{13}\text{C}$  nmr to electronic factors (40), the effects of charge migration are expected to be greater than in  $^1\text{H}$  nmr. Recent studies on TNB and chloranil complexes with various aromatic donors show that the acceptor carbons experience upfield shifts, again attributed to the ring current effect of the donors on the carbon atoms of the acceptor. However, several donors contain carbon atoms which have experienced paramagnetic (downfield) shifts. These observations have been reported for C-2 of naphthalene and anthracene complexed to TNB (35) and for C-2 of naphthalene, C-1 and C-2 of anthracene and the ring carbons of mesitylene all complexed to *o*-chloranil (39). These downfield shifts are best ascribed to the predominance of charge-transfer effects at these carbons in the molecule.

Therefore,  $^{13}\text{C}$  nmr is in fact much more sensitive to the effects of charge migration in EDA interactions than are proton shifts.

(d) Criticism of the Method

Although the methods discussed above have been widely used to study EDA interactions, the number of assumptions made will lead to uncertainties in the results obtained.

(i) Deviations from ideality of any of the solute species over the concentration range used means that the term  $(\gamma_{AD}/\gamma_D\gamma_A)$  is not unity. In this case the equilibrium quotient is not a measure of the thermodynamic equilibrium constant.

(ii) Presence of several isomeric 1:1 complexes means that  $K_{exp} = \sum K_i$  where  $K_i$  is the association constant of the  $i$ th 1:1 complex.

(iii) Contact charge-transfer, transfer of charge which supposedly takes place during random collisions of D and A, may affect the value of K.

(iv) Presence of termolecular complexes such as  $AD_2$ , may lead to small deviations in K.

(v) Specific solvation of one or more of the solute species in the equilibrium may affect the measured K.

## D. CARBON-13 SPIN LATTICE RELAXATION

### 1. INTRODUCTION

#### (a) General (41-44)

When a sample, which can be considered as an ensemble of nuclear magnetic spins, is placed in an external magnetic field  $\bar{H}_0$ , a Boltzmann distribution of spins will result as the sample comes to thermal equilibrium. This results in a net magnetization  $\bar{M}_0$  in the field direction (the z-axis in the rotating frame) since alignment with the field is preferred over alignment against  $\bar{H}_0$ . However, since the spins are precessing about the z-axis at random, there is no net magnetization in the xy-plane, *ie.*  $\bar{M}_{xy}=0$  and  $\bar{M}_z=\bar{M}_0$  (see Figure 4a).

In pulsed Fourier transform (PFT) nmr (41, 42) all nuclei are excited simultaneously by a short burst of radio frequency (rf) radiation. The rf excitation, applied along the x-axis (43), deflects the net magnetization vector  $\bar{M}_0$  towards the y-axis by an amount determined by the duration of the pulse. The resulting nuclear transitions change the relative populations in the two energy levels causing a decrease in the net magnetization in the field direction, *ie.*  $\bar{M}_z$  decreases. However, all nuclei are forced to precess in phase giving rise to transverse magnetization,  $\bar{M}_{xy}$  (see Figure 4b).

After this perturbation, relaxation processes tend to restore the system to equilibrium again (43, 44). The exponential decay of the transverse magnetization with time con-

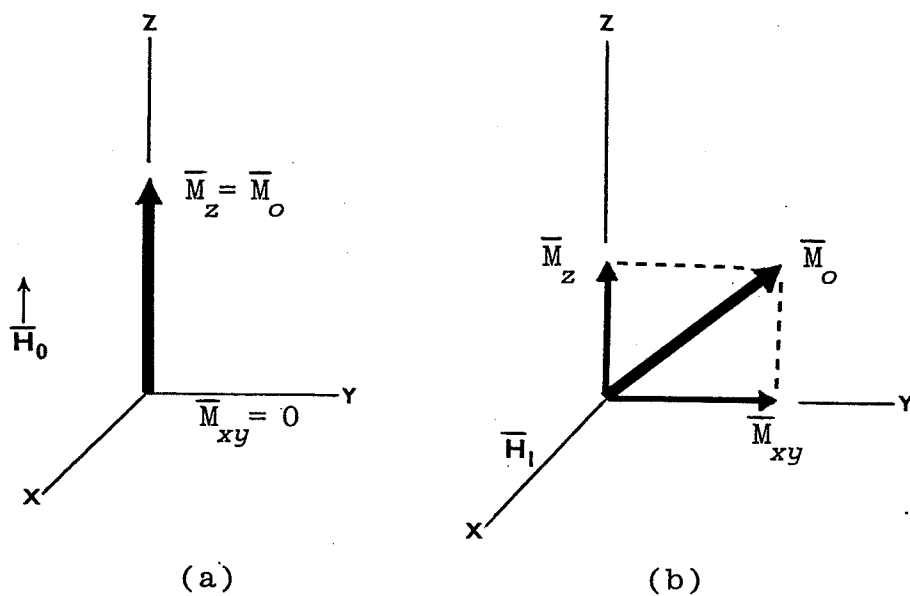


FIGURE 4. (a) The net magnetization of the sample at equilibrium in an external field  $\vec{H}_0$ . (b) The interaction of  $\vec{M}_0$  with a rf excitation applied along the x-axis.

stant  $T_2$  is known as spin-spin relaxation. (Since this decay is affected by field inhomogeneity, the time constant  $T_2^*$  is used to represent the overall decay). This gives rise to the free induction decay (FID) which, on Fourier transformation, yields the spectrum in the frequency domain. This process can be thought of as a dephasing of the magnetic vectors in the  $xy$ -plane, *ie.*  $\overline{M}_{xy} \rightarrow 0$ .

Reestablishment of the Boltzmann distribution of spins (*ie.* the recovery of the full longitudinal magnetization in the field direction,  $\overline{M}_z = \overline{M}_0$ ) takes place by spin-lattice relaxation according to a time constant  $T_1$ .

Both relaxation processes, which take place simultaneously but independently, can be described by first-order kinetics according to the Bloch equations (43)

$$[21] \quad \frac{dM_z}{dt} = - \frac{(M_z - M_0)}{T_1}$$

$$[22] \quad \frac{dM_{xy}}{dt} = - \frac{M_{xy}}{T_2} .$$

#### (b) Free Induction Decay and Fourier Transformation

The free induction decay (FID) for a single type of nucleus in a perfectly homogeneous field, in which the excitation pulse is applied right at the resonance frequency of the nucleus, would be perfectly exponential (see Figure 5a) since the magnetization vector  $\overline{M}_{xy}$  is stationary relative to the frame which is rotating at the radio frequency  $\overline{H}_1$ , *ie.*  $\overline{M}_{xy}$  is in phase with  $\overline{H}_1$ .

If the rf field or pulse is applied slightly off the



resonance frequency of the nucleus, then  $\bar{M}_0$  will rotate relative to the rotating frame (or  $\bar{H}_1$ ) and a "beating" pattern is produced as  $\bar{M}_{xy}$  and  $\bar{H}_1$  alternately come in and out of phase (42, 45). This "beating" pattern decays exponentially as shown in Figure 5b. As the rf pulse is applied farther from the resonance frequency of the nucleus, the rate of "beating" increases considerably (45) as shown in Figure 5c.

Since most compounds have a number of different nuclei, each giving rise to a characteristic "beating" pattern or wave form, most FID's are very complicated superpositions of wave forms (see Figure 5d) which are virtually impossible to analyze (42), even though all the information on chemical shifts, coupling constants, etc. is contained in this decay pattern.

Fourier transformation, a mathematical technique for separating the wave forms, converts the spectrum from the time domain into the frequency domain. The Fourier transform of a function  $f(t)$  can be represented by

$$[23] \quad F(\omega) = \int_{-\infty}^{\infty} f(t) e^{i\omega t} dt$$

where  $\omega$  = the angular frequency

$t$  = time

$$e^{i\omega t} = \cos(\omega t) + i\sin(\omega t)$$

In practice the Fourier transformation is usually evaluated by the algorithm developed by Cooley and Tukey, as described in Becker and Farrar (45).

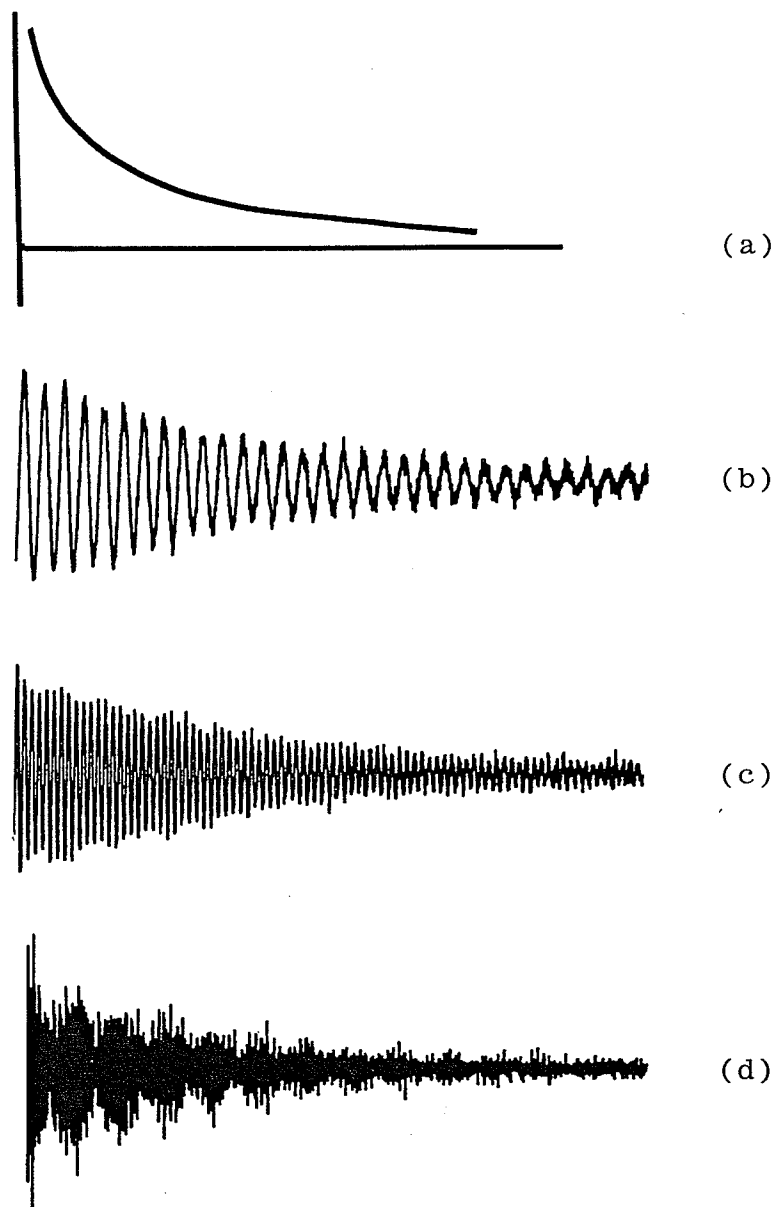


FIGURE 5. Free induction decay patterns for a single type of nucleus with the pulse applied (a) at the resonance frequency, (b) slightly off resonance, and (c) further off resonance, and for a molecule with a number of nonequivalent nuclei (d).

## 2. SPIN-LATTICE RELAXATION

### (a) The Origin of Magnetic Relaxation

In order to reestablish equilibrium after rf excitation some nuclei must lose energy and undergo a transition to the lower energy state. This takes place through the interaction of the nuclear spins with their environment or lattice, hence the process is known as spin-lattice relaxation.

Spin-lattice relaxation depends on a time-dependent magnetic field acting on the magnetic moments of the nuclei being relaxed (46). The time dependence (or fluctuation) of these local fields ( $\bar{H}_{loc}$ ) must be of the proper frequency -that of the transition frequency of the nucleus (47)- in order for energy to be transferred from the spin to the lattice.

In liquids the time dependence which produces appropriate fluctuations of  $\bar{H}_{loc}$  arises from the random Brownian motion of the molecules as they tumble (by rotation and diffusion) through the fluid.

Although  $^{13}\text{C}$  nuclei can be relaxed by different mechanisms they all depend on the interaction of the  $^{13}\text{C}$  spin with  $\bar{H}_{loc}$  produced by the particular mechanism. The measured spin-lattice relaxation time ( $T_1$ ) will be an indication of the time taken for the energy transfer from the spin to the lattice and hence of the relative efficiency of the relaxation process.

(b) The Dipole-Dipole Relaxation Mechanism (47)

The major source of relaxation of  $^{13}\text{C}$  nuclei in organic molecules free of paramagnetic impurities is the internuclear dipole-dipole (DD) interaction, usually with bonded protons. The instantaneous local field produced at the  $^{13}\text{C}$  nucleus  $j$  by a neighboring magnetic nucleus  $i$  is given (47) by

$$[24] \quad \bar{H}_{loc} = \pm \bar{\mu}_i \frac{3 \cos^2 \theta_{ij} - 1}{r_{ij}^2}.$$

The strength of the DD interaction depends on the magnetic moment of the neighboring nucleus,  $\bar{\mu}_i$ , and the internuclear separation,  $\bar{r}_{ij}$ . The rotational motion of the molecules imparts a time-dependence to  $\bar{H}_{loc}$  by changing  $\theta_{ij}$ , the angle of  $\bar{r}_{ij}$  relative to the external field,  $\bar{H}_o$ .

Assuming Brownian motion (46), *ie.* small-step displacements or short times between collisions, a time-dependent correlation function  $G(\tau)$ , which describes the persistence of  $\bar{H}_{loc}$  before being averaged to zero by molecular motion, can be written

$$[25] \quad G(\tau) = \left\langle \bar{H}_{loc}(0) \cdot \bar{H}_{loc}(\tau) \right\rangle_o$$

at a reference time  $t=0$ . (The reader is referred to (47) and the references therein for full details).

If the decay of  $G(\tau)$  is described by an appropriate exponential function, Fourier transformation converts it into the frequency domain (46, 47) according to

$$[26] \quad J(\omega) = \left\langle \bar{H}_{1oc}^2(0) \right\rangle_o \frac{2\tau_c}{1 + \omega^2\tau_c^2}.$$

$J(\omega)$ , the spectral density, represents the efficiency of relaxation at a particular frequency of fluctuation,  $\omega$ , and  $\tau_c$ , the molecular correlation time, represents molecular reorientation. If the latter provides fluctuations close to the  $^{13}\text{C}$  resonance frequency,  $\omega_o$ , then the DD relaxation will be most efficient. Motions which are much faster or slower will not be as effective in relaxing the nuclei. This means that  $T_1$  goes through a minimum as illustrated in Figure 6.

Increasing correlation times, corresponding to slower motion, will decrease  $T_2$  (see Figure 6) and consequently cause line-broadening since  $T_2$  is related to the line-width at half-height (24),  $\Delta\nu_{\frac{1}{2}} \sim 1/T_2$ . If the frequency of the fluctuations of  $\bar{H}_{1oc}$  produced by the molecular motion exceeds  $\omega_o$ ,  $T_2$  increases and sharp lines are observed (43). Molecules which are not too large ( $MW < 300$ ) tumble very fast in nonviscous solutions and therefore fall into this region of "motional narrowing".

Since spin-lattice relaxation involves nuclear spin transitions, the transition probabilities (which can be derived quantum-mechanically by treating  $\bar{H}_{1oc}$  by perturbation theory (46)) must be worked out to get an expression for  $T_1$ . For dipolar relaxation by a bonded proton, the pertinent transition probabilities,  $W_i$ , (see Figure 7) are (48, 50)

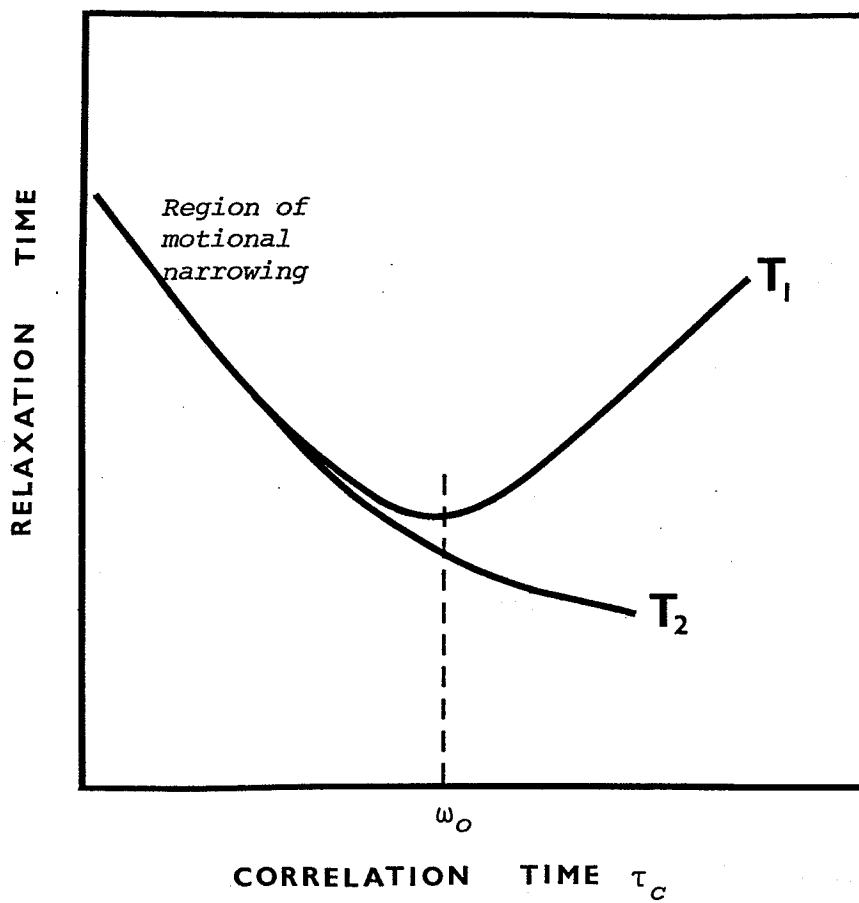


FIGURE 6. The dependence of  $T_1$  and  $T_2$  on the effective molecular correlation time.

$$[27a] \quad W_o = \frac{1}{20} \hbar^2 \gamma_C^2 \gamma_H^2 J_o(\omega_H - \omega_C)$$

$$[27b] \quad W_{1C} = \frac{3}{40} \hbar^2 \gamma_C^2 \gamma_H^2 J_1(\omega_C)$$

$$[27c] \quad W_2 = \frac{3}{10} \hbar^2 \gamma_C^2 \gamma_H^2 J_2(\omega_H + \omega_C).$$

Note that the transition probabilities are dependent on the spectral density or the efficiency of relaxation at the particular fluctuation frequency,  $\omega_i$ .

Under conditions of complete proton decoupling the  $T_1$  expression, which represents the time rate of change of  $\bar{M}_z$ , can be written (49)

$$[28] \quad \frac{1}{T_1} = W_o + 2W_{1C} + W_2.$$

Substitution of [27] into [28] gives

$$[29] \quad \frac{1}{T_1} = \frac{1}{20} \hbar^2 \gamma_C^2 \gamma_H^2 \left[ J_o(\omega_H - \omega_C) + 3J_1(\omega_C) + 6J_2(\omega_H + \omega_C) \right].$$

If we assume that the reorientation of the molecule can be described by a single effective molecular correlation time,  $\tau_c$ , then (48)

$$[30] \quad J(\omega) = \frac{2\tau_c}{(1 + \omega^2 \tau_c^2) r_{CH}^6}.$$

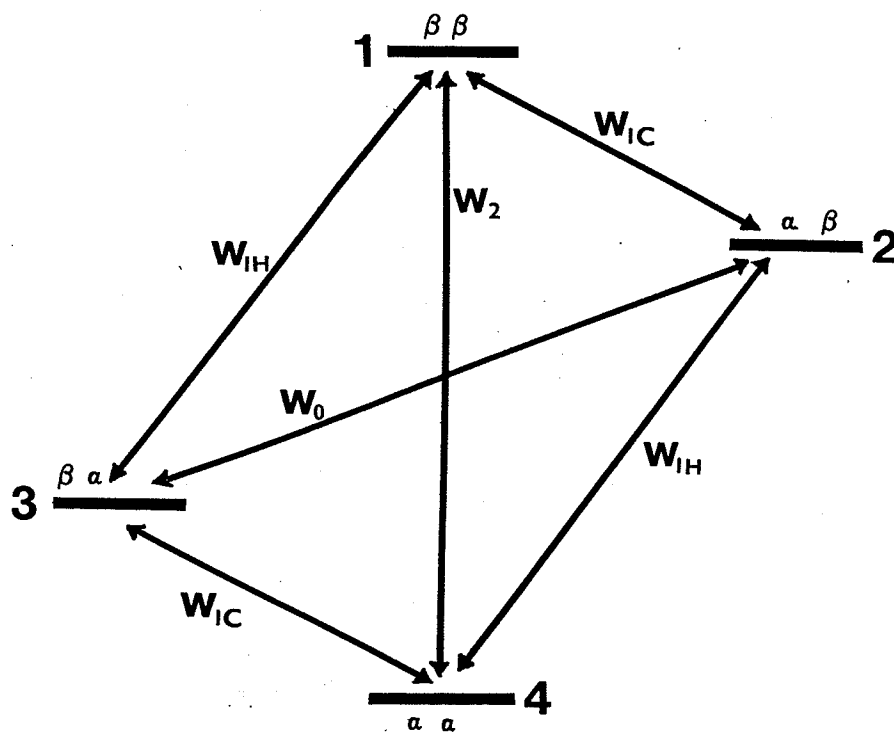


FIGURE 7. Transition probabilities,  $W_i$ , for the  $^{13}\text{C}$ - $^1\text{H}$  two-spin system. The carbon spin is given first, followed by the proton spin, eg.  $\alpha\beta$ . (After (47)).





Substitution into [29] gives

$$[31] \quad \frac{1}{T_1} = \frac{1}{10} \frac{\hbar^2 \gamma_C^2 \gamma_H^2}{r_{CH}^6} \left[ \frac{\tau_c}{1 + (\omega_H - \omega_C)^2 \tau_c^2} + \frac{3\tau_c}{1 + \omega_C^2 \tau_c^2} + \frac{6\tau_c}{1 + (\omega_H + \omega_C)^2 \tau_c^2} \right]$$

In the region of motional narrowing (50)  $\omega\tau_c \ll 1$  (therefore  $\omega^2 \tau_c^2 \ll 1$ ) and the expression simplifies to

$$[32] \quad \frac{1}{T_1} = \frac{\hbar^2 \gamma_C^2 \gamma_H^2}{r_{CH}^6} \tau_c$$

for the relaxation due to one bonded proton. For N bonded protons this equation is simply multiplied by N.

Due to the  $r^{-6}$  dependence, relaxation due to dipolar interactions with nonbonded protons is generally negligible.

### (c) Other Relaxation Mechanisms

Although dipole-dipole interaction usually dominates  $^{13}\text{C}$  relaxation, for certain molecules under certain conditions other mechanisms lead to fluctuations in  $\bar{H}_{1oc}$  and give rise to a correlation time of their own.

In addition to the effects of rotational diffusion discussed above, significant fluctuations of  $\bar{H}_{1oc}$  can arise from rapid rotation of small molecules or freely rotating  $\text{CH}_3$  groups by the spin rotation (SR) mechanism. This mechanism may dominate the relaxation of nonprotonated carbons and will become increasingly important as the temperature rises.

Other  $^{13}\text{C}$  nuclei may be relaxed by the fluctuations in  $\bar{H}_{1oc}$  arising from fast relaxation of a quadrupolar nucleus to which it is coupled. This scalar coupling (SC) mechanism is

important only for  $^{13}\text{C}$  bonded to  $^{79}\text{Br}$ .

If the tumbling molecule causes large enough changes in the components of anisotropic shielding constants, then relaxation by chemical shift anisotropy (CSA) may be important. This is rare for  $^{13}\text{C}$  nuclei at normal magnetic fields.

Finally, for nuclei with spin  $I \geq 1$ , interaction of the quadrupole moment with the fluctuating electric field gradient of the tumbling molecule leads to nuclear quadrupole relaxation.

(d) Determination of  $T_1$  by Inversion Recovery (43,44,45)

The most frequently used procedure for the determination of spin-lattice relaxation times is the inversion recovery method. This method utilizes the pulse sequence

$$180^\circ - t_i - 90^\circ - AT - PD \dots$$

where AT = the acquisition time

PD = the pulse delay

$t_i$  = the time interval between the  $180^\circ$  and  $90^\circ$  pulses.

After a  $180^\circ$  pulse inverts the magnetization vector  $\bar{M}_0$  onto the  $-z$  axis, longitudinal relaxation proceeds to restore  $\bar{M}_z$  back to its equilibrium value,  $\bar{M}_0$ . After a certain time delay,  $t_i$ , a  $90^\circ$  pulse rotates  $\bar{M}_z$  to the  $+y$  or  $-y$  axis (see Figure 8) for observation. The acquisition of data begins immediately after the  $90^\circ$  pulse, giving rise to the FID. A pulse delay of at least  $5T_1$  allows the system to return to equilibrium prior to the next pulse. This pulse sequence is repeated until adequate signal-to-noise is obtained. Fourier transformation of the FID then gives the spectrum.

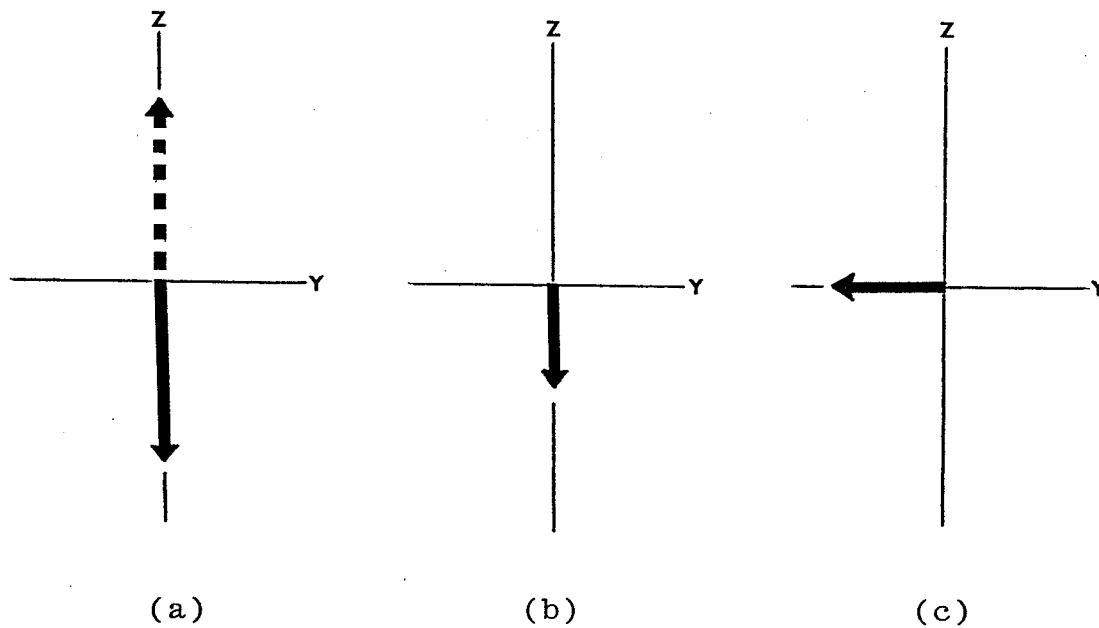


FIGURE 8. The  $180^\circ-t_i-90^\circ$  pulse sequence used to determine  $T_1$ . (a) Inversion of magnetization by a  $180^\circ$  pulse. (b) Partial recovery during a short time delay,  $t_i$ . (c) Effect of the  $90^\circ$  or observation pulse applied along the positive x-axis.

The time delay,  $t_i$ , is now varied over a wide range to obtain a series of spectra in which the peak intensity changes from the equilibrium value  $\bar{M}_0$ , passing through zero and becoming inverted. The strongest inverted peak will come from the  $180^\circ-0-90^\circ$  pulse sequence.

The peak areas, which are a measure of the magnetization immediately after the  $90^\circ$  pulse, can be used to determine the rate of recovery of the longitudinal magnetization. Peak heights which have been found to be proportional to peak areas are commonly used in these measurements.

The rate at which  $\bar{M}_z$  returns to equilibrium is given by the Bloch equation

$$[21] \quad \frac{dM_z}{dt} = - \frac{(M_z - M_0)}{T_1}.$$

This recovery process is illustrated in Figure 9.

Rearrangement of this equation to

$$[33] \quad \frac{dM_z}{(M_z - M_0)} = - \frac{dt}{T_1}$$

followed by integration, yields

$$[34] \quad \ln(M_z - M_0) = -t/T_1 + c.$$

When  $t=0$ ,  $\bar{M}_z = -\bar{M}_0$  and the integration constant is  $c = \ln(-2M_0)$ .

The equation for the recovery of the longitudinal magnetization may now be written

$$[35] \quad \ln(M_0 - M_z) = -t/T_1 + \ln(2M_0).$$

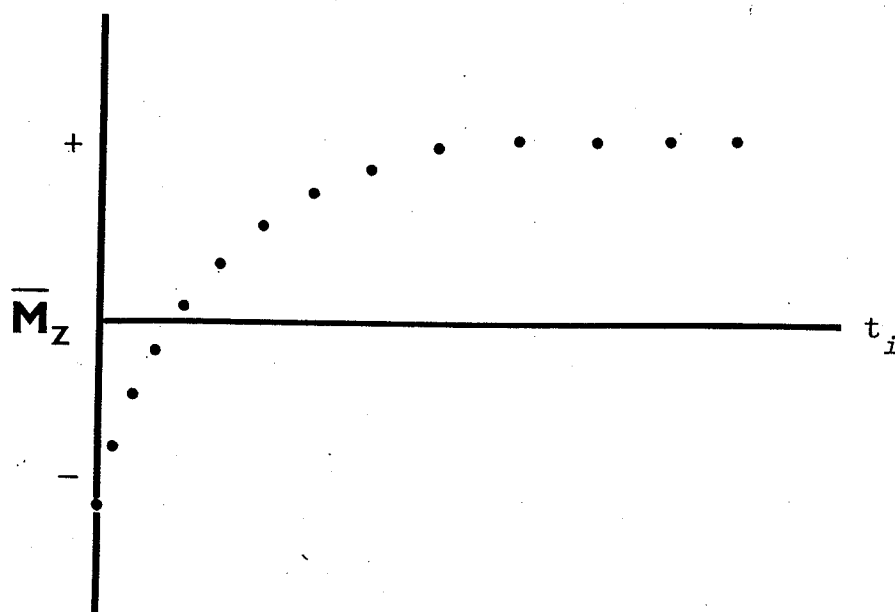


FIGURE 9. The recovery of  $\bar{M}_z$  as a function of the time delay,  $t_i$ , in the inversion recovery determination of  $T_1$ . Note that the peaks will pass from negative intensity through zero to positive intensity.

A plot of  $\ln(A_0 - A_z)$ , where  $A_0$  is the peak height for  $t_i = \infty$  and  $A_z$  is the peak height for any other time delay  $t_i$ , versus  $t_i$  will yield the spin-lattice relaxation time as the reciprocal slope, *ie.* slope =  $-1/T_1$ .

### 3. RELAXATION AND NUCLEAR OVERHAUSER ENHANCEMENT

#### (a) The Nuclear Overhauser Effect

The intensities of carbon resonances measured under conditions of complete proton noise decoupling are frequently greater than expected from collapse of the multiplet of the coupled spectrum. This effect, observable for many nuclei, is referred to as the nuclear Overhauser effect (nOe).

Maintaining a strong rf field at the Larmor frequency of the protons throughout the experiment saturates the proton spin energy levels, *ie.* the populations in energy levels 2 and 4 are equalized as are the populations in levels 1 and 3 (see Figure 7).

After a weak rf excitation at the carbon Larmor frequency, spin-lattice relaxation tends to restore the  $^{13}\text{C}$  spins to equilibrium. The saturation of the proton spins will not affect the net transition probabilities  $W_{1C}$  since the probability for the  $2 \rightarrow 1$  transition is increased but the  $4 \rightarrow 3$  transition probability is decreased proportionately. However, the saturation forces cross relaxation,  $W_2$ , increasing the population in level 4 and thereby providing the enhancement of the  $^{13}\text{C}$  signal intensity.

The signal enhancement or nOe obtained by saturating

the proton spin levels in the  $^{13}\text{C}-^1\text{H}$  system has been shown (51) to be given by

$$[36] \quad nOe = \frac{W_2 - W_o}{W_o + 2W_{1C} + W_2} \cdot \frac{\gamma_H}{\gamma_C} .$$

$\gamma_H$  and  $\gamma_C$  being the magnetogyric ratios of hydrogen and carbon.

(b) Differentiation of Relaxation Mechanisms

The  $nOe$  will be a maximum when the dipole-dipole interaction overwhelmingly dominates the relaxation of the carbon under observation since it is the only mechanism, other than a seldomly encountered scalar coupling (47), which gives rise to cross relaxation.

In the region of motional narrowing the ratio of transition probabilities  $W_o : W_{1C}^{DD} : W_2$  for the  $^{13}\text{C}-^1\text{H}$  two-spin system under proton decoupling conditions has been worked out (47) to be  $1/6 : 1/4 : 1$ . Under these conditions [36] becomes

$$[37] \quad nOe = \frac{\gamma_H}{2\gamma_C}$$

and the maximum observable  $nOe$  is 1.988.

When other relaxation mechanisms are contributing, additional  $W_{1C}$  terms must be added to the denominator in [36], and the  $nOe$  is decreased.

The observed relaxation rate is then written (44) as a sum of all contributing factors

$$[38] \quad R_1^{OBS} = R_1^{DD} + R_1^{SR} + R_1^{CSA} + R_1^{SC} + R_1^{other} .$$

In terms of relaxation times this equation can be written

$$[39] \quad \frac{1}{T_1^{OBS}} = \frac{1}{T_1^{DD}} + \frac{1}{T_1^{SR}} + \frac{1}{T_1^{CSA}} + \frac{1}{T_1^{SC}} + \frac{1}{T_1^{other}}$$

When the nOe is a maximum, only DD relaxation is operative and  $T_1^{OBS} = T_1^{DD}$ . When the nOe < 1.988 then the DD contribution to relaxation is given by (43, 44)

$$[40] \quad \%DD = \frac{nOe}{1.988} \times 100$$

and the dipolar spin-lattice relaxation time is calculated as

$$[41] \quad T_1^{DD} = T_1^{OBS} \frac{1.988}{nOe}$$

#### 4. MOLECULAR REORIENTATION IN LIQUIDS

##### (a) Introduction

The molecular correlation time,  $\tau_c$ , which can be calculated from  $T_1^{DD}$  according to [32] contains information about the rotational dynamics of the molecule in solution. However, an interpretation of the molecular motion may be difficult since from [32] only one  $\tau_c$  is calculated. This  $\tau_c$  is a measure of the overall reorientation of the molecule. In order to get a good physical picture of the molecular motion several models of molecular reorientation should be tested to see how compatible they are with the experimental results.



(b) Isotropic Reorientation

If one assumes that the molecules in a liquid are undergoing rotational Brownian motion (rotation proceeding by a large number of small, random jumps continually being interrupted by molecular collisions) the reorientation time may be expressed in terms of a rotational diffusion coefficient (46),  $\theta$ , as

$$[42] \quad \tau_c = \frac{1}{6\theta}.$$

The diffusion coefficient itself may be expressed in terms of a rotational friction coefficient,  $\zeta$ , derived from hydrodynamics, by

$$[43] \quad \theta = \frac{kT}{\zeta}$$

where  $\zeta = 8\pi a^3 \eta$  for a spherical particle of radius  $a$  moving uniformly through a continuous fluid of viscosity  $\eta$ , at a temperature  $T$ ,  $k$  being the Boltzmann constant. The result, [44], known as the Stokes-Einstein equation (52) assumes that the fluid at the surface of the sphere is carried along with the rotating surface.

$$[44] \quad \theta = \frac{kT}{8\pi a^3 \eta}$$

Therefore, the reorientation time predicted by the Stokes-Einstein equation is given (53) as

$$[45] \quad \tau_c = \frac{4\pi a^3 \eta}{3kT} = \frac{V\eta}{kT}$$

where  $V$  is the molecular volume.

Although this hydrodynamical model has severe limitations (54) it may be applicable to molecules which are fairly spherical and which are interacting strongly with the solvent (eg. by hydrogen-bonding). These spherical molecules undergo isotropic reorientation since the motion about each principal axis is the same. However, since most molecules are nonspherical, the calculated reorientation time will not be meaningful unless the equations reflect the geometry of the molecule.

### (c) Anisotropic Reorientation

For nonspherical molecules the rotational diffusion and friction coefficients are tensor quantities and must be broken down into components along each of the molecular axes in order to get information on molecular motion.

The simplest case to consider are the symmetric top molecules which can be approximated as oblate or prolate spheroids in the hydrodynamical description. For this geometry the motion about two of the molecular axes is the same. Again assuming that the fluid at the surface of the spheroid has the same velocity as the surface, the components of the rotational friction tensor have been worked out (55, 56) to be

$$[46a] \quad \zeta_1 = \zeta_2 = \frac{32\pi\eta(c^4 - a^4)}{3[(2c^2 - a^2)S - 2c]}$$

$$[46b] \quad \zeta_3 = \frac{32\pi\eta a^2(c^2 - a^2)}{3(2c - a^2S)}$$

where  $a$  is the major axis and  $c$  is the minor axis, and

$$[47a] \quad S = 2(a^2 - c^2)^{-\frac{1}{2}} \tan^{-1} [(a^2 - c^2)^{\frac{1}{2}}/c]$$

for oblate spheroids (where  $a > c$ ), or

$$[47b] \quad S = 2(c^2 - a^2)^{-\frac{1}{2}} \ln[c + (c^2 - a^2)^{\frac{1}{2}}/c]$$

for prolate spheroids (where  $a < c$ ).

The correlation time can now be expressed in terms of the components of the rotational diffusion tensor (56,57)

$$[48] \quad \tau_c = \frac{1}{24\theta_1} + \frac{3}{8(\theta_1 + 2\theta_3)}$$

or in terms of the components of the rotational friction tensor

$$[49] \quad \tau_c = \frac{\zeta_1}{24kT} + \frac{3\zeta_1}{8kT(1 + 2\zeta_1/\zeta_3)}$$

Equations have been derived for planar asymmetric top molecules (57), for which  $\zeta_1 \neq \zeta_2 \neq \zeta_3$ . These equations become yet more complex and will not be considered here.

(d) Boundary Conditions

The equations shown above are derived on the assumption that the solvent at the surface of the particle rotates with the particle. This "sticking" boundary condition often leads to  $\tau_c$  values which are much larger than the experimental  $\tau_c$  values. It appears that this model predicts too much friction and may only apply in cases where the solvent strongly hydrogen-bonds to the solute.

A change to the "slipping" boundary condition, in which the solvent is considered to slip past the surface of the rotating particle, has brought the calculated  $\tau_c$  values into better agreement with experimental results. The slip condition has also been much more successful in accounting for the experimental viscosity dependence (53, 58) of  $\tau_c$ , given by the constant C in

$$[50] \quad \tau_c = C\eta/T.$$

For spherical molecules rotating under slipping boundary conditions, the rotational friction coefficient  $\zeta=0$  since the molecule is rotating in its own volume and does not disturb any solvent. However, nonspherical molecules will have rotations which move solvent even under slip conditions. Hu and Zwanzig (59) have calculated friction coefficients for rotation of the symmetry axis of oblate and prolate spheroids under slip conditions as a function of the geometry of the spheroid, with the geometry ranging from a perfect sphere to the extreme limits of compression -a disk (for the oblate

geometry) and a needle (for the prolate geometry).

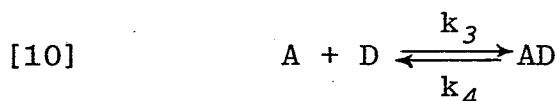
Bauer *et.al.* (60) have shown that the correlation time for rotation about the symmetry axis of the symmetric top molecules benzene and mesitylene is virtually independent of the viscosity of the medium. On the other hand, rotation of the symmetry axis moves more solvent and has a greater viscosity dependence as expected under slip boundary conditions.

## 5. MOLECULAR DYNAMICS OF COMPLEX FORMATION

### (a) Effect of Chemical Exchange on Relaxation

Any changes in the environment of the molecule being observed which affect its overall motion, will have an effect on the dipolar relaxation time. This is a consequence of the dipolar relaxation mechanism which arises out of the rotational motion of the molecule.

Consider, for example, the equilibrium



where  $k_1$  is the rate constant for the reorientation of free D,

$k_2$  is the rate constant for the reorientation of complexed D (*ie.* AD),

$k_3$  is the rate constant for association of A and D,

$k_4$  is the rate constant for dissociation of AD,

and where  $k_1$  and  $k_2$  are related to the correlation times for free and complexed D respectively by  $k_i = (\tau_i)^{-1}$ .

If the spin-lattice relaxation time of a nucleus in D is being measured, the  $T_1$  will depend on the rate constant for the reorientation of the free D molecule,  $k_1$ . When D is complexed the reorientation rate constant  $k_2$  will normally be slower. Therefore the observed  $T_1$  will depend not only on the reorientation rates of the molecule in the free and complexed environments, but also on the rate at which the molecule exchanges between these environments since the reorientational behaviour will vary with time as a result of the exchange.

Anderson and Fryer (61) show that the relaxation behaviour of a molecule D is very dependent on the relative rates of chemical exchange and molecular rotation. For intramolecular dipolar relaxation, they show that the  $T_1$  can be expressed as

$$[51] \quad \frac{1}{T_1} = \frac{B}{5} \left[ \frac{Q_+/\lambda_+}{1+(\omega_o/\lambda_+)^2} + \frac{(4Q_+/\lambda_+)}{1+(2\omega_o/\lambda_+)^2} + \frac{Q_-/\lambda_-}{1+(\omega_o/\lambda_-)^2} + \frac{(4Q_-/\lambda_-)}{1+(2\omega_o/\lambda_-)^2} \right]$$

where B is a constant which depends on the nmr method used (*ie.*  $^1\text{H}$ ,  $^2\text{H}$ ,  $^{13}\text{C}$ , ...),

$\omega_o$  is the nmr frequency of the nucleus under observation, and

$Q_{\pm}$  and  $\lambda_{\pm}$  are expressions which introduce the rate constants,  $k_1$ ,  $k_2$ ,  $k_3$ ,  $k_4$ , the fraction of D molecules complexed,  $\alpha$ , and the concentration of the other component, A, at equilibrium, (see (61) for complete details).

In the region of motional narrowing,  $k_1, k_2 \gg \omega_0$ , this expression simplifies to

$$[52] \quad \frac{1}{T_1} = B \left[ \frac{Q_+}{\lambda_+} + \frac{Q_-}{\lambda_-} \right].$$

When the rate of chemical exchange is slow relative to the rates of molecular reorientation, *ie.*  $k_3, k_4 \ll k_1, k_2$ , the observed spin-lattice relaxation rate,  $R_1$  or  $1/T_1$ , is a weighted average of the spin-lattice relaxation rates of the free and complexed molecules,  $1/T_D$  and  $1/T_{AD}$  respectively,

$$[53] \quad \frac{1}{T_1} = \frac{1}{T_D} (1-\alpha) + \frac{1}{T_{AD}} (\alpha).$$

When the rates of exchange are fast relative to the reorientation rates, *ie.*  $k_3, k_4 \gg k_1, k_2$ , then

$$[54] \quad T_1 = T_D(1-\alpha) + T_{AD}(\alpha).$$

Anderson and Fryer (61) have generated theoretical curves illustrating the effects of different exchange rates,  $k_4$ , relative to the rate of reorientation of the complex,  $k_2$ , on the relaxation time. In these calculations they assume  $k_4/k_3 = 10$ ,  $k_1/k_2 = 100$  and then compute  $T_1$  as a function of  $\alpha$  for various ratios of  $k_4/k_2$ . Their results are qualitatively illustrated in Figure 10.

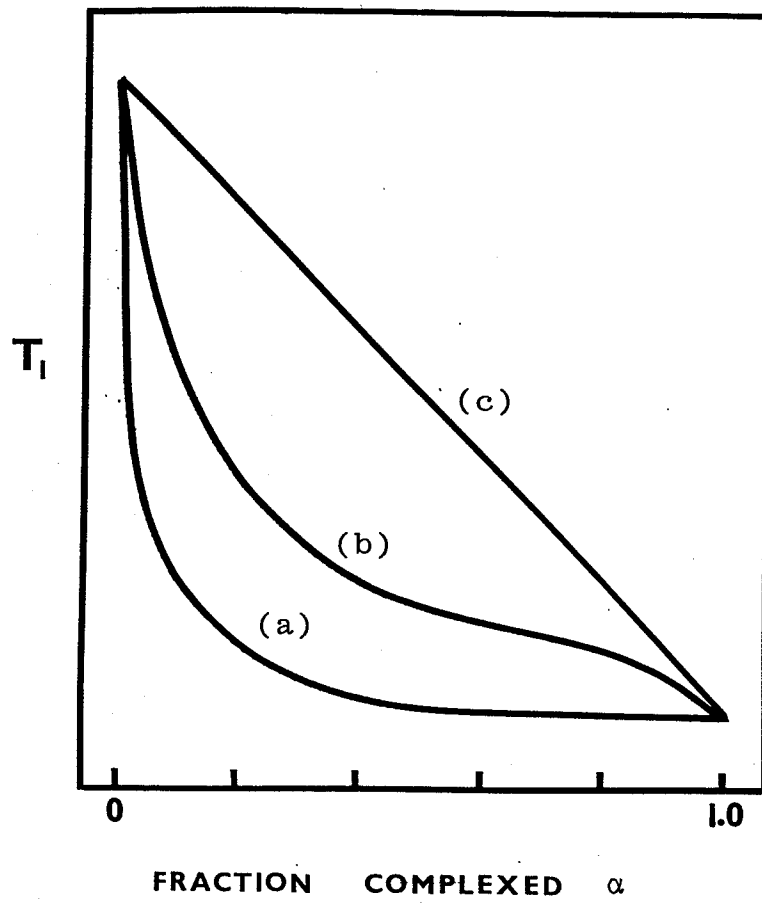


FIGURE 10. Theoretical curves showing the effect of (a) slow ( $k_4/k_2=10^{-4}$ ), (b) intermediate ( $k_4/k_2=10$ ), and (c) fast ( $k_4/k_2=10^6$ ) chemical exchange on the relaxation behaviour. (After Anderson and Fryer (61)).



(b) Evaluation of the Rate Constants(i) Determination of Relative Exchange Rates

The  $T_1$  ratio as used by Anderson and Fryer ( $T_1$  of the donor in a complexing environment relative to the  $T_1$  of the free donor where  $\alpha=0$ ) may be useful in some cases to establish whether the system being studied can be classified under slow exchange or fast exchange. Figure 10 shows that this  $T_1$  ratio may provide insight into exchange rates particularly in the region where  $\alpha$  is small. Their data examined in this manner indicated that the iodine complexes of dimethylsulfoxide and t-butylamine fall into the slow or intermediate exchange category. However, the iodine complexes of benzene and p-dioxane, for example, definitely fall into the fast exchange category since the  $T_1$ 's of these donors are hardly affected by this complex formation. This is consistent with dielectric relaxation studies which have shown (62) that the iodine:benzene and iodine:p-dioxane complexes have lifetimes which are comparable to or less than their reorientation times, i.e. fast exchange is taking place. These studies also demonstrated that the trinitrobenzene complexes of triethylamine and tributylamine undergo slow exchange.

Behr and Lehn (63) rearrange the  $T_1$  expression for slow exchange [53] to

$$[55] \quad \frac{1}{T_1} = \left( \frac{1}{T_{AD}} - \frac{1}{T_D} \right) \alpha + \frac{1}{T_D} .$$

The equilibrium constant for a given system, determined by any of the standard methods, allows calculation of the fraction complexed,  $\alpha$ . The measured relaxation rate,  $1/T_1$ , is then plotted versus  $\alpha$ . Linearity of the plot is taken as an indication that slow exchange is a valid conclusion. The  $\alpha=1$  intercept gives  $1/T_{AD}$ , allowing the molecular correlation time and the rate constant for reorientation to be calculated for the pure complex.

### (ii) Curve Fitting

The first study of the molecular dynamics of EDA complex formation was reported by Brevard and Lehn (64) who investigated the complex formation of trinitrobenzene with the donors, fluorene- $d_1$ , methylfluorene- $d_2$ , and methylenefluorene- $d_1$ , using deuterium  $T_1$  values. They used the general expression of Anderson and Fryer [52] with  $B = 3/8(e^2qQ/\hbar)^2$ , where  $(e^2qQ/\hbar)$  is the quadrupolar coupling constant of the  $^2\text{H}$  nucleus.

This expression was simplified to contain only two unknowns,  $k_2$  and  $k_4$ , by introducing the experimental equilibrium constant,  $K=k_3/k_4$  (see [10]), and the reorientation rate of the pure donor,  $k_1$ . The authors then fit their  $T_1$  data to [52] using their computer program QUADDEX. In QUADDEX  $T_1$  values are expressed as a function of  $\alpha$ , with  $k_2$  and  $k_4$  being varied until the best fit to the experimental data is obtained. This yields the values for  $k_2$  and  $k_4$  and thus allows a complete description of the dynamics of the system.

Their results indicate that the rates of dissociation of these complexes are slow relative to the rate of reorientation of the free donor but comparable to the rate of reorientation of the complexed donor.

III. EXPERIMENTALA. MATERIALS

1,4-Benzoquinone - practical grade (Matheson, Coleman & Bell), was recrystallized from ethanol, mp 111.5-113°.

Hexamethylbenzene - reagent grade (Aldrich), was recrystallized from ethanol, mp 163-164°.

Pentamethylbenzene - reagent grade (Aldrich), was recrystallized from methanol, mp 52-54°.

Carbon tetrachloride - certified ACS (Fisher), was freshly distilled.

Deuterium oxide - 99.7 atom % D (Merck, Sharp & Dohme), was used without further purification.

Phenylhydrazine - Baker grade (J.T.Baker) was used without further purification.

Acetone-1,3-<sup>13</sup>C<sub>2</sub> - 90 atom % <sup>13</sup>C (Merck, Sharp & Dohme), Lot no. E-508, was used without further purification.

Acetone-2-<sup>13</sup>C - 90 atom % <sup>13</sup>C (Merck, Sharp & Dohme), Lot no. E-1027, was used without further purification.

Methanol - absolute, reagent grade (Fisher), was used without further purification.

Benzene - certified ACS (Fisher), was used without further purification.

Mesitylene - reagent grade (Fisher), was dried over anhydrous CaSO<sub>4</sub> and then distilled.

Zinc chloride - Baker analyzed reagent (J.T.Baker), was freshly fused, ground up and desiccated over  $P_2O_5$ .

n-Pentane - pesticide grade (Fisher), was used without further purification.

1,2-Dichloroethane - certified ACS (Fisher), was washed successively with concentrated sulfuric acid, water, sodium bicarbonate, water, and then dried over anhydrous  $MgSO_4$  and distilled.

1,2-Dichloroethane- $d_4$  - 99 atom % D (Merck, Sharp & Dohme), Lot nos. E-998 and E-142, was used without further purification.

1,1,2,2-Tetrachloroethane - reagent grade (Aldrich), was washed with concentrated sulfuric acid, water, and then dried over anhydrous  $CaCl_2$  and distilled.

1,3,5-Trinitrobenzene - (BDH), was recrystallized from ethanol, mp 122-123°.

2-methylindole-(methyl,3)- $^{13}C_2$  - was synthesized by the *Fischer indole synthesis* (7).

Acetone-1,3- $^{13}C_2$  phenylhydrazone was prepared by refluxing a slight excess of phenylhydrazine (1.5g) with 90 atom % acetone-1,3- $^{13}C_2$  (0.63g) in absolute methanol (18ml) for forty minutes. The methanol was then distilled off carefully. Addition of benzene (15ml) allowed the last traces of methanol and water to be distilled out as azeotropes.

Dry mesitylene (4.8g) and freshly fused zinc chlo-

ride (1.7g) were added to the warm acetone phenylhydrazine (theoretical yield 1.6g). The mixture was then refluxed vigorously for 1 hour.

After decanting the supernatant into a clean flask, the mesitylene was removed with a rotary evaporator leaving crude 2-methylindole. The tarry residue was refluxed for 1 hour in 0.2N HCl (15ml) to dissolve inorganic material. The solution was filtered through glass wool, cooled and extracted with ether. The ethereal solution was dried over  $\text{Na}_2\text{SO}_4$  and the ether carefully removed on the rotary evaporator leaving a small amount of crude 2-methylindole as a very viscous oil.

The combined crude 2-methylindole was purified by soxhlet extraction with *n*-pentane for approximately 3 hours. The extracted product and solvent were then refrigerated. The 2-methylindole which crystallized out was filtered, dried and weighed. Yield 0.67g (47%).

The product was further purified by sublimation. It was found that slow sublimation using a water aspirator to evacuate the apparatus resulted in the collection of the whitest crystals on the cold finger. During the sublimation the cold finger was packed with crushed ice and the sample compartment was immersed in a paraffin bath maintained at approximately  $50^\circ$ .

The purified 2-methylindole-(methyl,3)- $^{13}\text{C}_2$  had a mp of  $58-59^\circ$ .

2-methylindole-2-<sup>13</sup>C - was synthesized from 0.58g of acetone-2-<sup>13</sup>C using the same ratio of reagents and the procedure described above. Purification was also by soxhlet extraction and sublimation. Yield 0.71g (55%), mp 58-59°.

2-methylindole - technical grade (Aldrich), was soxhlet extracted and sublimed as above, mp 58-59.5°.

#### B. NMR SAMPLE PREPARATION

For the chemical shift study of the *p*-benzoquinone:hexamethylbenzene and *p*-benzoquinone:pentamethylbenzene systems in carbon tetrachloride, all components were weighed into a 2-ml volumetric flask on an analytical balance. After dissolving, the samples were transferred into 10mm nmr tubes and a coaxial tube containing D<sub>2</sub>O was inserted for nmr lock purposes.

The same procedure was followed in preparing samples for the chemical shift studies of the 2-methylindole:1,3,5-trinitrobenzene system in 1,2-dichloroethane.

The samples used for the spin-lattice relaxation time study of C-3 of 2-methylindole-(methyl,3)-<sup>13</sup>C<sub>2</sub> as a function of the concentration of added TNB were also weighed out as described above. In these experiments 50% by volume of the 1,2-dichloroethane solvent was of the deuterated type in order to provide a deuterium lock signal. These solutions were transferred into 8mm nmr tubes to a depth of 27-28mm, attached to the vacuum rack (see Figure 11) and slowly frozen in

liquid nitrogen (bp  $-195.8^{\circ}$ ). With the oxygen trap also immersed in liquid nitrogen the sample was slowly evacuated. The stopcock leading to the nmr tube was then closed, the liquid nitrogen was removed and the sample was allowed to thaw slowly to release dissolved oxygen. The sample was then frozen and evacuated again. This freeze-pump-thaw cycle was repeated four times. After the fourth freezing the tube was sealed by heating with a medium flame from an oxygen-propane torch just above the constriction. The seal was made as symmetrical as possible to facilitate smooth spinning of the sample. Finally, a hot flame was used to fire-polish the seal. The sample was then thawed and placed in hot water to test the seal under pressure.

The sample used for a  $T_1$  study of 2-methylindole as a function of temperature (viscosity) was prepared by weighing out 2-methylindole-(methyl,3)- $^{13}\text{C}_2$  in 1,2-dichloroethane, 50% of which was 1,2-dichloroethane- $d_4$ . The sample was degassed by four freeze-pump-thaw cycles and then sealed in an 8mm nmr tube.

The samples used for the  $T_1$  study of 2-methylindole as a function of viscosity at a constant temperature were prepared by weighing out 2-methylindole-(methyl,3)- $^{13}\text{C}_2$ , 1,2-dichloroethane and 1,1,2,2-tetrachloroethane. The viscosity was varied by changing the ratio of dichloroethane and tetrachloroethane over the series. Approximately 0.1ml of the dichloroethane in each sample was of the deuterated type. An additional sample was prepared by weighing out the 2-methylindole in pure 1,1,2,2-tetrachloroethane to extend the vis-



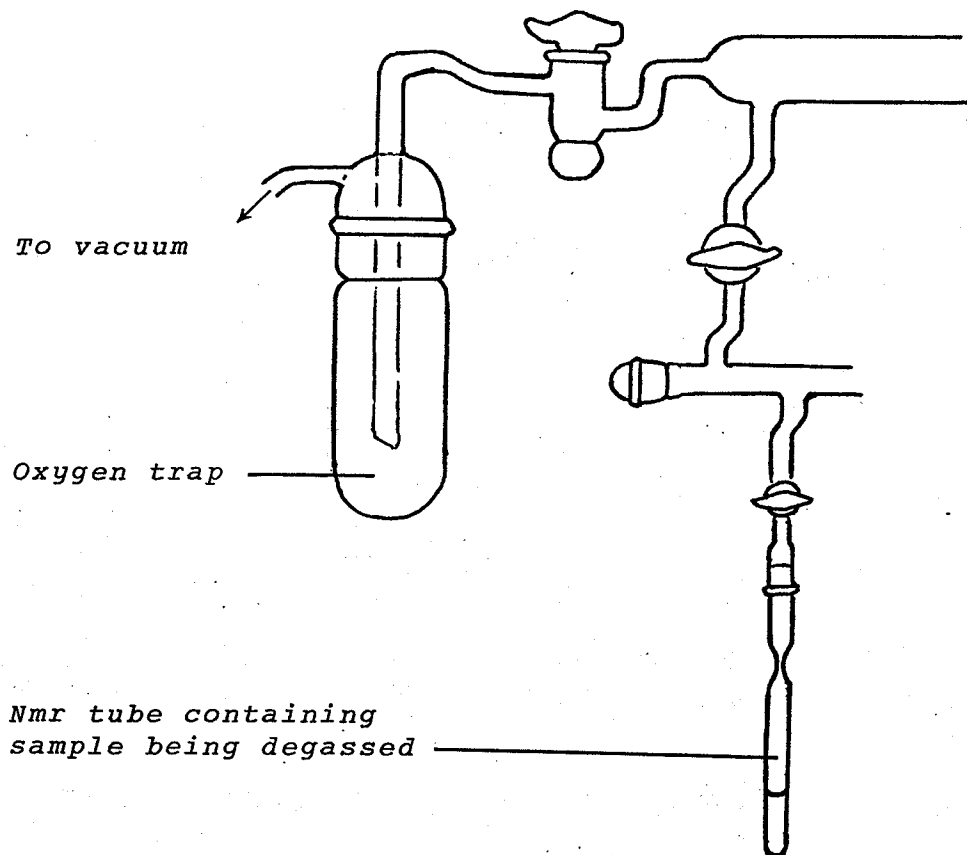


FIGURE 11. Section of the vacuum rack used to degas and seal nmr samples.

cosity range. Since this sample did not contain a deuterium lock nucleus, a coaxial tube containing  $D_2O$  was added. The  $T_1$  of this viscous sample was expected to be sufficiently small so that dissolved oxygen would not appreciably affect the results. Nevertheless, the sample was degassed by bubbling dry nitrogen through for about 3 minutes.

### C. HIGH RESOLUTION CARBON-13 NMR SPECTRA

Carbon-13 nmr spectra were obtained on a Varian CFT-20 pulse Fourier transform spectrometer operating at 20.0 MHz (magnetic field strength 18.682 kG) with field stabilization via internal deuterium lock. The spectra were obtained under conditions of complete proton noise decoupling.

Probe temperatures, measured before and after obtaining each spectrum, were maintained to within a  $1^\circ$  range by maintaining a constant SCFH (standard cubic feet per hour) air flow through the probe body. The probe temperature was measured with a thermometer in a water sample set into the probe to the same depth as the samples used for the nmr studies. With the interlock system inactivated and the decoupler going continuously the temperatures could be measured while the instrument was pulsing.

Each sample was allowed approximately 15 minutes for equilibration in the probe prior to accumulation of data. The field homogeneity was optimized before each sample was run.

The spectral width (SW) was set just wide enough to include the solute peak being monitored and the solvent peak

used as the reference. The maximum number of data points (DP) available was always used. Consequently, the acquisition time (AT) for each experiment was set by the following relationship:  $DP = 2 \times SW \times AT$ . The flip angle, as determined by the pulse width, was set small enough so that the magnetization could return to equilibrium during the AT between pulses. Consequently no pulse delay (PD) was used.

The accumulation of data was continued until adequate signal-to-noise (S/N) was obtained. The FID was then weighted to enhance the S/N further and Fourier transformed as illustrated in Figure 12.

#### D. SPIN-LATTICE RELAXATION TIMES

The observed carbon-13 spin-lattice relaxation times were determined by the inversion recovery method using the  $(180^\circ - t_i - 90^\circ - AT - PD)$  pulse sequence. By varying  $t_i$ , the delay time between the  $180^\circ$  and the  $90^\circ$  observation pulse, a series of spectra, showing the rate of recovery of the longitudinal magnetization after the  $180^\circ$  pulse, are obtained (see Figure 9). A pulse delay of at least  $6T_1$  was used for all samples.

The probe temperature was measured before and after each  $T_1$  determination using a thermometer immersed in 1,2-dichloroethane following the technique described earlier. For the constant temperature  $T_1$  studies the probe temperature was maintained at  $35.0 \pm 0.5^\circ$  with a Varian CFT-20 Variable Temperature Accessory. For the study of the  $T_1$  as a function

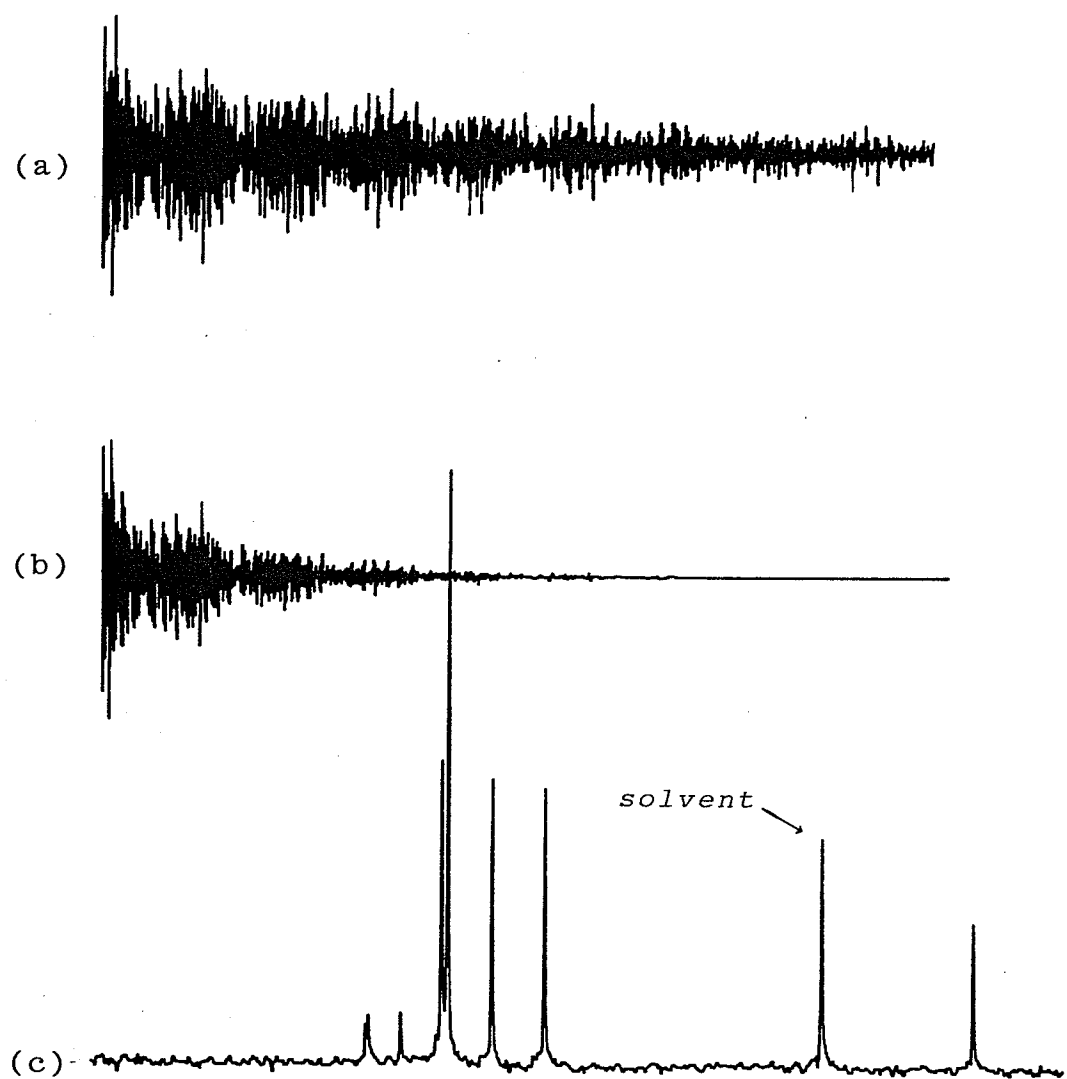


FIGURE 12. Obtaining a  $^{13}\text{C}$  nmr spectrum of 2-methylindole in 1,2-dichloroethane with  $\text{D}_2\text{O}$  in a coaxial tube for lock purposes. (a) the FID, (b) the FID after sensitivity enhancement and (c) the weighted FID transformed into the frequency spectrum.

of temperature, the probe body was cooled with  $N_2$  gas which was passed through the heat exchanger coils immersed in either crushed ice-water, dry ice-acetone, or liquid nitrogen depending on the temperature required. The Variable Temperature Accessory was again used to maintain a constant temperature.

Field homogeneity was again optimized prior to each determination.

The pulse widths corresponding to the  $90^\circ$  and  $180^\circ$  pulses were determined for use in the inversion recovery sequence.

A total of 40 to 50 pulses was sufficient to obtain good S/N on Fourier transformation. The FID was weighted to broaden the lines, otherwise seen as a doublet due to  $^{13}C$ - $^{13}C$  coupling in this compound, 2-methylindole-(methyl,3)- $^{13}C_2$ . This made phasing easier.

For each  $T_1$  determination 10-12  $t_i$  values were used.

#### E. NUCLEAR OVERHAUSER ENHANCEMENTS

The nOe factors were measured before and after each  $T_1$  determination. First, a spectrum showing the nOe was obtained by running the sample with continuous proton decoupling. Next, a fully decoupled spectrum without nOe was obtained using pulse-modulated proton decoupling. This was accomplished by gating the decoupler on during the observation pulse and data acquisition but gating it off during the pulse delay. The pulse delays were never less than  $6T_1$ .

## F. VISCOSITY DETERMINATIONS

The viscosities of the 2-methylindole-trinitrobenzene solutions in 1,2-dichloroethane and the solutions of 2-methylindole in various mixtures of 1,2-dichloroethane and 1,1,2,2-tetrachloroethane were determined with an Ostwald viscometer and density bottle at 35°. The solutions were allowed to equilibrate in the water bath, maintained at 35.00±0.01° for at least 15 minutes prior to removal for weighing. The density bottle containing the sample was then weighed at 4 minute intervals, allowing an extrapolation back to the time at which the sample was removed from the bath, i.e. the weight at 35°.

Drop times were measured with 3ml volumes in the viscometer which was clamped in the constant temperature bath.

#### IV. RESULTS AND DISCUSSION

##### A. SYNTHESIS OF CARBON-13 ENRICHED 2-METHYLINDOLES

###### 1. DIFFICULTIES IN THE SYNTHESIS

Although the synthesis of 2-methylindole via the *Fischer indole synthesis* is well documented in the literature (7, 10, 11), reported yields were difficult to reproduce for small scale syntheses.

Preliminary experiments, using nonenriched acetone as the starting material, were carried out to gain familiarity with the procedure and to identify critical points in the synthesis.

Originally the acetone phenylhydrazone was synthesized by refluxing a mixture of acetone (0.5g), phenylhydrazine (1g), absolute ethanol (12.5ml) and 1 drop of glacial acetic acid for 20 minutes. Basically this is the method reported in Pasto and Johnson (65) with the exception that absolute ethanol was used as the solvent in place of methanol. This allowed for removal of water from the system prior to indolization. This was accomplished with the addition of an excess of benzene followed by distillation of the benzene-ethanol-water azeotrope (bp 64.6°). The acetone phenylhydrazone was then subjected to indolization following the method of Chapman, Clarke and Hughes (11), *ie.* addition of cumene (4ml) and ZnCl<sub>2</sub> (1g) followed by 1 hour of refluxing. This resulted in extensive tar formation. However, evaporation of cumene from the supernatant did result in a small amount of

viscous oily material, shown to be impure 2-methylindole by  $^{13}\text{C}$  nmr. Attempts to purify the product by recrystallization from cyclohexane failed to yield a crystalline product. After other attempts by this method yielded the same unsatisfactory result a series of syntheses were performed in order to improve the quantity and quality of the product.

First, methanol was used in place of ethanol in the synthesis of acetone phenylhydrazone. After refluxing for 20 minutes the methanol was distilled off and the indolization carried out as described above. Although there was still extensive tar formation the oil obtained on evaporation of the cumene did solidify in the cold. Soxhlet extraction of this material with pentane provided solid 2-methylindole with yields of 18-26%.

Several other factors which were tested did not affect the yield appreciably. A change in the inert solvent used in the indolization from cumene to mesitylene resulted in a 24% yield. The use of freshly fused  $\text{ZnCl}_2$  did not appear to increase the yield (30%) significantly. Finally, the removal of methanol and water as azeotropes with benzene (bp  $58.3^\circ$  and  $69.4^\circ$  respectively) prior to indolization only increased the yield to 33%.

Several other methods were used (10, 13, 66) in an attempt to improve the yield but with no success. Therefore, attention was focused on the preparation of acetone phenylhydrazone since the indolization procedures all gave similar results.

A larger portion of the acetone phenylhydrazone was



synthesized following the method of Posvic *et.al.* (67), by refluxing acetone with phenylhydrazine in methanol without acid catalyst. After purification of the phenylhydrazone by vacuum distillation, indolization by the usual method (addition of  $ZnCl_2$  and mesitylene) gave yields of 54-70% 2-methylindole with essentially no tar formation. Therefore, it appeared to be crucial that the phenylhydrazone be pure prior to indolization. Although a satisfactory yield had been achieved it was desirable to develop a method that did not require distillation of the acetone phenylhydrazone for use in the synthesis of labelled 2-methylindole where very small amounts would be used. Therefore it was necessary to determine whether traces of acid or of methanol or both caused the low yields during the indole synthesis.

The next synthesis was carried out by preparing the acetone phenylhydrazone without the use of the solvent (methanol) or the acid catalyst by simply refluxing equimolar amounts of acetone and phenylhydrazine. Indolization resulted in a yield of 29% (the presence of water produced by the reaction may have contributed to this low yield). However, when the phenylhydrazone was prepared in methanol without the acid catalyst (as in Posvic *et.al.*), indolization after removal of water as the benzene azeotrope resulted in a 60% yield.

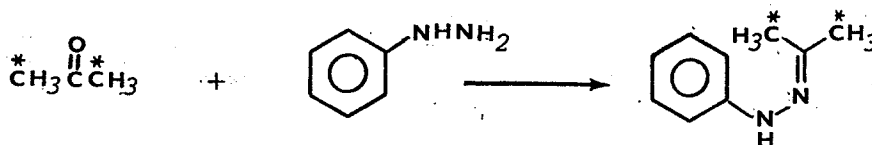
These results indicate that preparation of the acetone phenylhydrazone in methanol (without an acid catalyst) followed by removal of the methanol and water by distillation

as their benzene azeotropes gives material suitable for the indolization step.

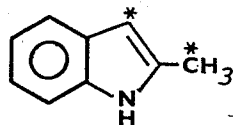
## 2. POSITION OF ENRICHMENT

### (a) Consideration of the Mechanism

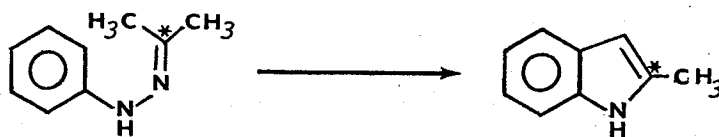
When acetone-1,3- $^{13}\text{C}_2$  is used to synthesize acetone phenylhydrazone, the enrichment takes place as follows:



Indolization of the acetone phenylhydrazone according to the accepted mechanism for the *Fischer indole synthesis* (14, 15) would yield 2-methylindole-(methyl,3)- $^{13}\text{C}_2$ .



When acetone-2- $^{13}\text{C}$  is used as the starting material, the enriched acetone phenylhydrazone produces 2-methylindole-2- $^{13}\text{C}$  according to the mechanism.



(b) Carbon-13 Nmr Spectra

Parker and Roberts (68) have resolved all of the carbon resonances of 2-methylindole and assigned them to specific carbon atoms with the help of off-resonance proton decoupling. When the chemical shifts, which they report relative to  $\text{CS}_2$ , are referenced to TMS at 0.00 ppm, the carbon resonances appear as summarized in Table 3.

In the spectrum of 2-methylindole in 1,2-dichloroethane, several carbon resonances are not resolved. However, assignments can be made as indicated in Figure 13c on the basis of the data cited above.

Thus, the products obtained (see Figures 13a and 13b) on the basis of the peak assignments of Parker and Roberts, show enrichment at C-3 and the methyl carbon in the first instance and at C-2 in the second.

Although there is some discrepancy in the literature regarding the assignments of C-5 and C-6 of indole (69), this does not affect the C-2, C-3 and methyl carbons of 2-methylindole.

TABLE 3. Chemical shifts of the carbons of 2-methylindole relative to TMS at 0.00 ppm.

CARBON ATOM	CHEMICAL SHIFT ( $\delta$ )
C-2	135.7
C-3	100.4
C-4	120.0
C-5	121.1
C-6	119.9
C-7	111.7
C-8	129.9
C-9	137.1
Methyl	13.4

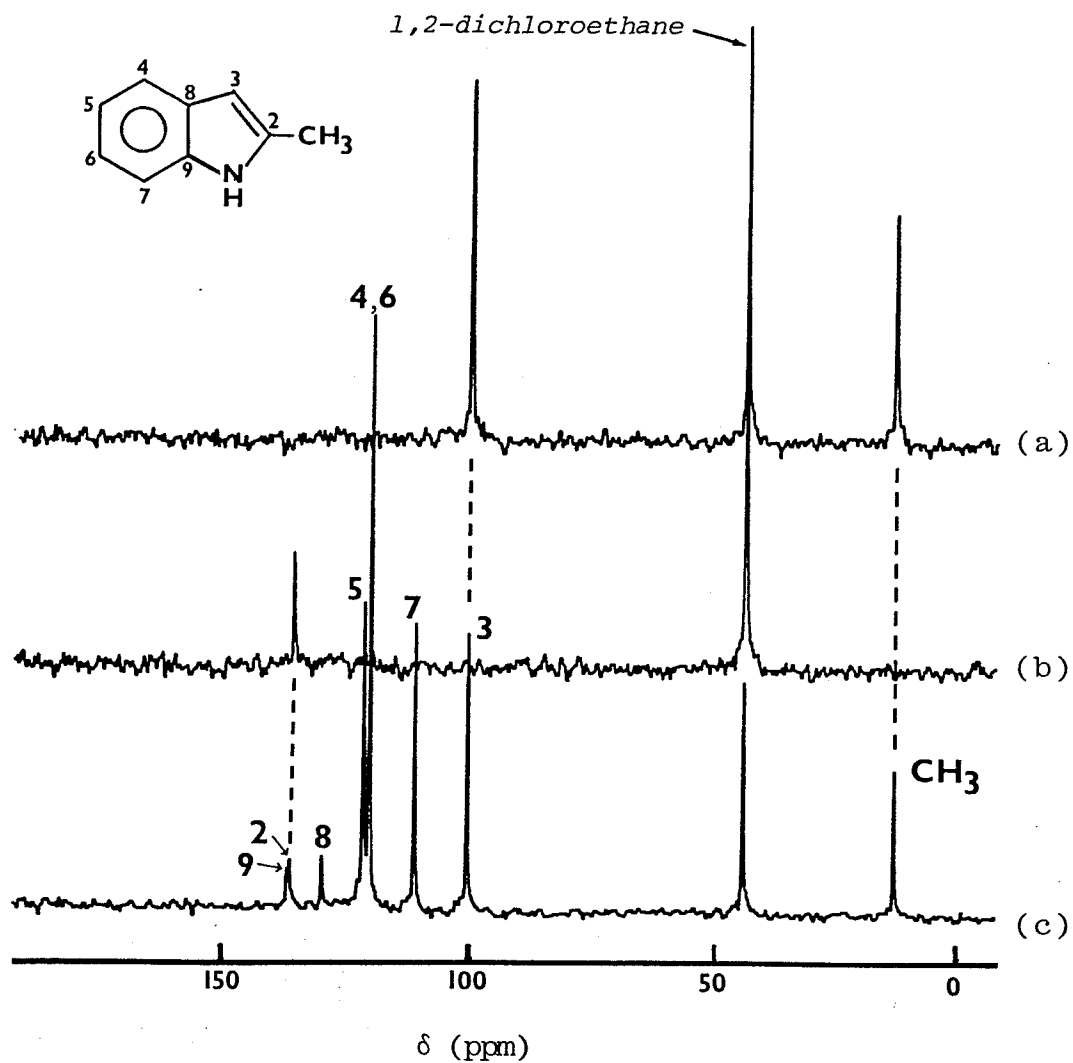


FIGURE 13. Carbon-13 nmr spectra of (a) 2-methylindole-(methyl,3)- $^{13}\text{C}_2$ , (b) 2-methylindole-2- $^{13}\text{C}$ , and (c) nonenriched 2-methylindole in 1,2-dichloroethane.

B. CARBON-13 CHEMICAL SHIFT STUDIES OF SEVERAL  
EDA INTERACTIONS

1. METHOD OF ANALYSIS

Although the HAFF equation [18] is frequently used to evaluate equilibrium constants, this method requires that one component be kept in large excess.

$$[18] \quad \Delta/[D]_o = -K\Delta + K\Delta_o, \quad \text{for } [D]_o \gg [A]_o.$$

As long as the large excess is maintained, the equilibrium concentration of the major component,  $[D]_{eq}$ , is approximately equal to its initial concentration. However, because of the high concentrations of the minor component required in  $^{13}\text{C}$  nmr studies, it was not feasible to have a large excess of one component over the other. Therefore, the HAFF method (or any other method requiring a large excess) is not applicable.

Determination of K by the Rose-Drago method was found to be too subjective. The other method (discussed in section II.C.) appeared too awkward.

Therefore, the following approach was developed. The data were evaluated by a method of successive approximations using  $[D]_{eq}$  values in the HAFF equation

$$[56] \quad \Delta/[D]_{eq} = -K\Delta + K\Delta_o.$$

This is an exact equation which does not require the large excess of one component.

The exact form of the equilibrium constant expression can be written as

$$[57] \quad K = \frac{[AD]}{[D]_{eq}([A]_o - [AD])}$$

This can be rearranged to

$$[58] \quad [AD] = \frac{K[D]_{eq}[A]_o}{1 + K[D]_{eq}}$$

An expression for  $[D]_{eq}$  was obtained by substituting [58] into

$$[59] \quad [D]_{eq} = [D]_o - [AD]$$

resulting in

$$[60] \quad [D]_{eq} = [D]_o - \frac{K[D]_{eq}[A]_o}{1 + K[D]_{eq}}$$

The equilibrium constant was obtained to a first approximation by a first-order least-squares-fit of  $\Delta$  vs  $\Delta/[D]_o$  (the HAFF method). Using this value of  $K$ , a series of  $[D]_{eq}$  values were calculated by substituting  $[D]_o$  for  $[D]_{eq}$  in the right hand side of [60]. These approximate  $[D]_{eq}$  values were then used in [60] to calculate a new set of  $[D]_{eq}$  values. This iterative procedure was continued until the  $[D]_{eq}$  values converged. (It was felt that this procedure was easier to program than solving by a quadratic equation where instructions for selecting the correct root must be included). A

better approximation for K was then obtained from the least-squares-fit of  $\Delta$  vs  $\Delta/[D]_{eq}$ .

The iterative process used to calculate  $[D]_{eq}$  values was again applied, using the new value of K. With these  $[D]_{eq}$  values a still better approximation for K was obtained. The entire process was continued until K converged to some value.

The APL\360 computer program 'SHIFT' (see Appendix A) was written to perform the calculations and iterations.

## 2. HYDROCARBON COMPLEXES OF *p*-BENZOQUINONE

Since at the outset of this work there were no publications on the application of  $^{13}\text{C}$  nmr to the study of EDA interactions, systems which had been studied by  $^1\text{H}$  nmr were investigated in order to determine the suitability of  $^{13}\text{C}$  nmr for this type of study. In this regard complex formation of *p*-benzoquinone (PBQ) with the donors hexamethylbenzene (HMB) and pentamethylbenzene (PMB) in  $\text{CCl}_4$  were chosen.

In each of these systems a series of solutions were prepared in which the chemical shift of the protonated carbon of PBQ was measured as a function of the concentration of the donor. The PBQ concentration was maintained at *ca.* 0.07 molal while the donor concentrations ranged from *ca.* 0.2 molal to an upper limit of *ca.* 0.5 molal for HMB and *ca.* 0.8 molal for PMB (determined by the solubility in  $\text{CCl}_4$ ). The chemical shifts were measured in hertz relative to the  $^{13}\text{C}$  resonance of  $\text{CCl}_4$ . Reproducibility of line positions was experimentally



determined to be  $\pm 0.06$  Hz. All spectra in this study were run such that Fourier transformation provided 1 real data point every 0.25 Hz.

The data are summarized in Tables 4 and 5 for HMB and PMB respectively. Plots of  $\Delta$  vs  $\Delta/[D]_{eq}$  (after convergence of K) are presented in Figures 14 and 15.

A standard first-order least-squares-fit of the data provided the equilibrium constant as the negative slope. Values of  $K = 0.62$  (kg solvent) $\text{mol}^{-1}$  and  $K = 0.49$  (kg solvent) $\text{mol}^{-1}$  were obtained for the PBQ:HMB and PBQ:PMB systems respectively, in  $\text{CCl}_4$  at  $34.5^\circ$ . The correlation coefficient for both sets of data was 0.990.

Foster and Fyfe (30) have determined equilibrium constants for these two systems in  $\text{CCl}_4$  at  $33.5^\circ$  using  $^1\text{H}$  nmr. The values reported for the PBQ:HMB and PBQ:PMB equilibria are  $K = 0.66$  (kg solution) $\text{mol}^{-1}$  and  $K = 0.49$  (kg solution) $\text{mol}^{-1}$  respectively. When the  $^{13}\text{C}$  data were evaluated using this concentration scale, corresponding K values of 0.44 and 0.34 (kg solution) $\text{mol}^{-1}$  were calculated for these systems at  $34.5^\circ$ .

When the variations frequently encountered in investigating the same EDA system by different methods are considered, this agreement is quite good suggesting that  $^{13}\text{C}$  nmr shifts are useful for this type of study.

The y-intercept obtained in the least-squares-fit of the data to [56] corresponds to the value  $K\Delta_0$ . The values of both K and  $\Delta_0$  obtained for the systems under consideration

TABLE 4.  $^{13}\text{C}$  nmr chemical shifts for ca. 0.07m PBQ as a function of the HMB concentration.

$[\text{PBQ}]_0^a$	$[\text{HMB}]_0^a$	$\delta(\text{Hz})^b$	$\Delta(\text{Hz})$
0.0636	—	799.76	—
0.0679	0.203	793.75	6.01
0.0691	0.274	791.86	7.90
0.0707	0.358	789.95	9.81
0.0707	0.428	788.26	11.50
0.0725	0.513	786.72	13.04

TABLE 5.  $^{13}\text{C}$  nmr chemical shifts for ca. 0.07m PBQ as a function of the PMB concentration.

$[\text{PBQ}]_0^a$	$[\text{PMB}]_0^a$	$\delta(\text{Hz})^b$	$\Delta(\text{Hz})$
0.0636	—	799.76	—
0.0677	0.274	794.60	5.16
0.0689	0.368	793.09	6.67
0.0706	0.456	791.63	8.13
0.0729	0.581	789.93	9.83
0.0755	0.807	787.37	12.39

<sup>a</sup> Initial concentrations of all components in mol (kg solvent)<sup>-1</sup>.

<sup>b</sup> The observed chemical shifts of the PBQ resonance relative to the  $\text{CCl}_4$  peak.

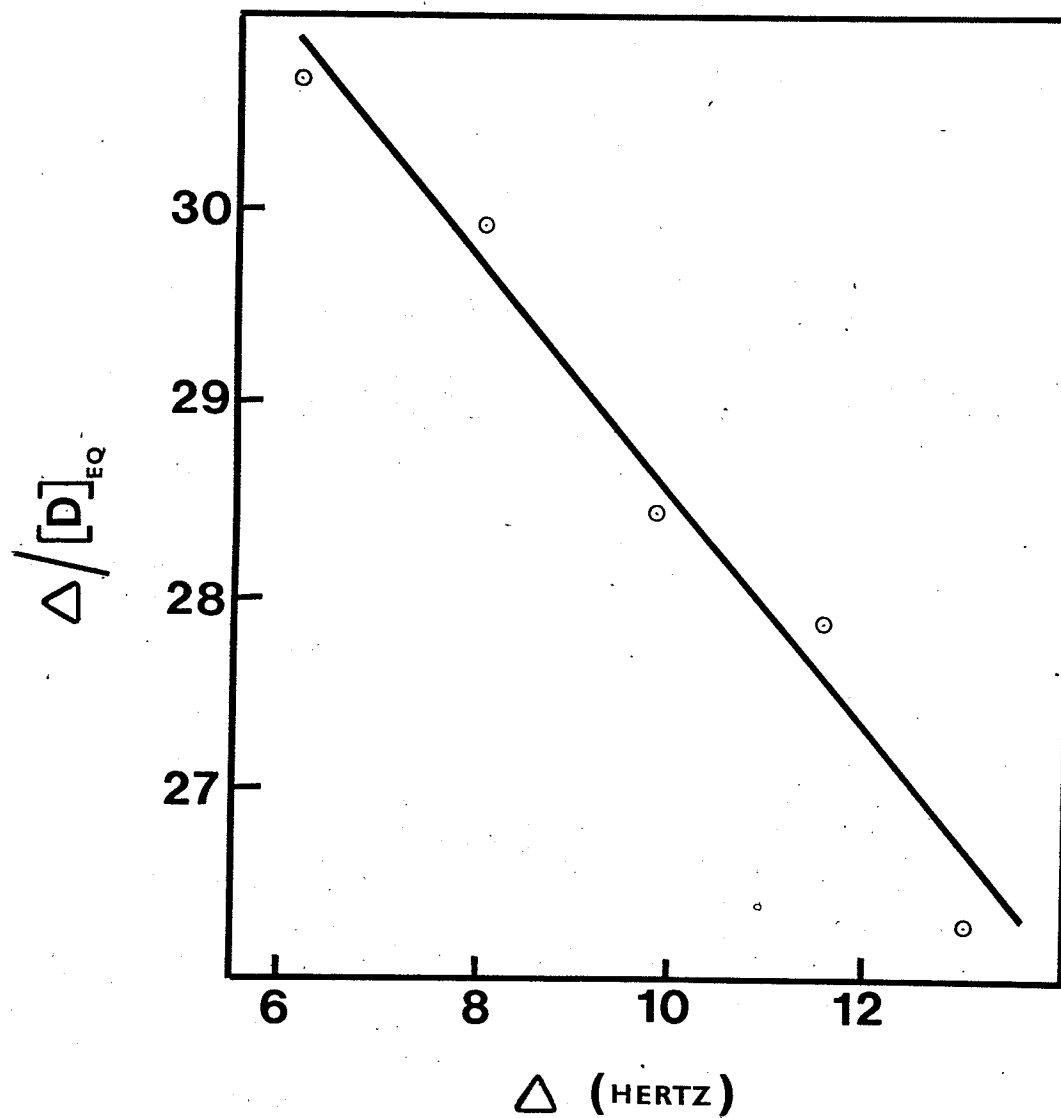


FIGURE 14. Plot of  $\Delta$  vs  $\Delta/[D]_{eq}$  (after convergence of K) for the system PBQ:HMB in  $CCl_4$  at  $34.5 \pm 0.5^\circ$ .

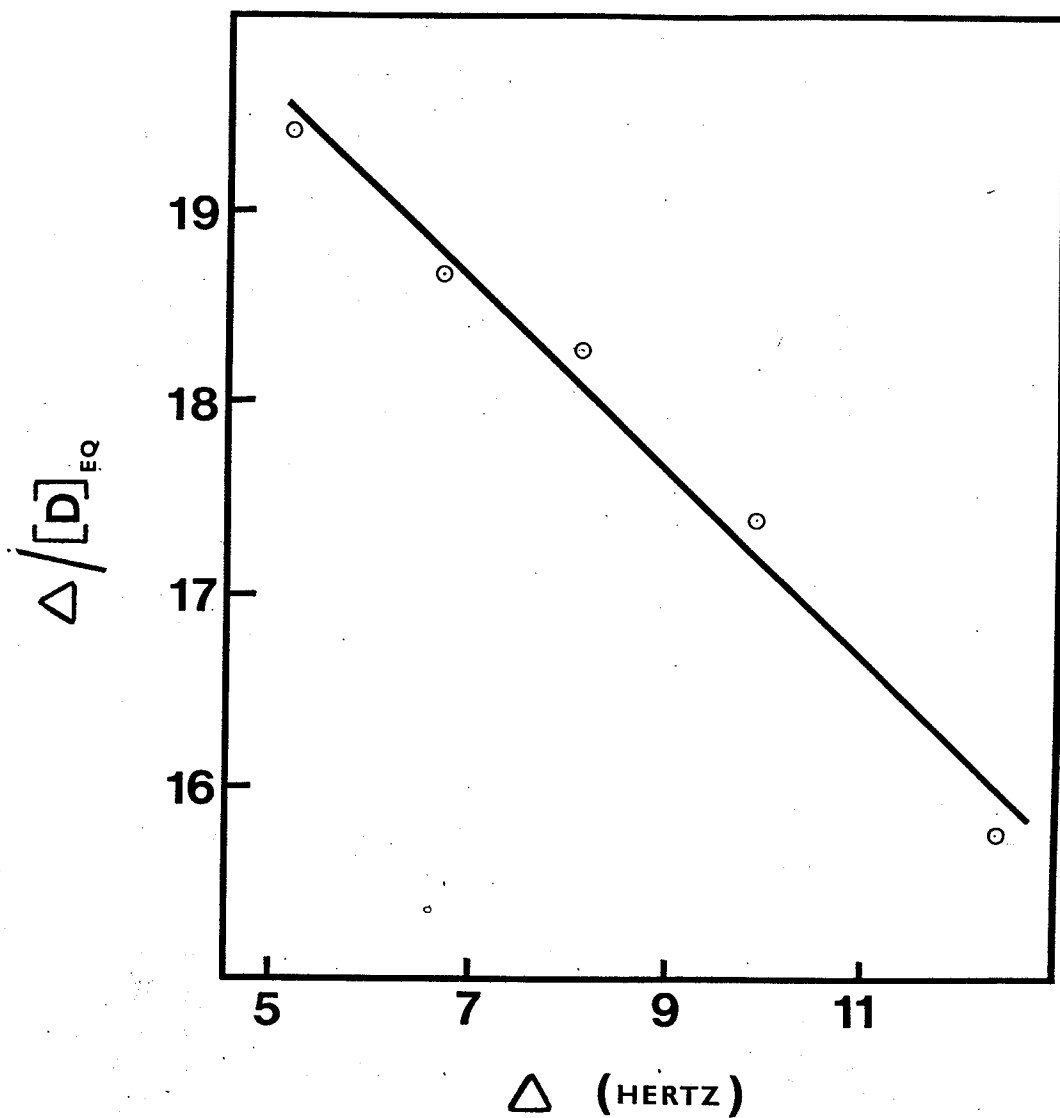


FIGURE 15. Plot of  $\Delta$  vs  $\Delta/[D]_{eq}$  (after convergence of K) for the system PBQ:PMB in  $\text{CCl}_4$  at  $34.5 \pm 0.5^\circ$ .

TABLE 6. Comparison of K and  $\Delta_o$  values for PBQ:HMB and PBQ:PMB in  $\text{CCl}_4$  from  $^1\text{H}$  and  $^{13}\text{C}$  nmr<sup>a</sup>.

	K (kg solution) $\text{mol}^{-1}$	$\Delta_o$ (ppm)
PBQ:HMB	0.44 (0.66)	3.9 (1.4)
PBQ:PMB	0.34 (0.49)	3.3 (1.5)

<sup>a</sup>  $^1\text{H}$  measurements (in brackets) reported at  $33.5^\circ$ ,  $^{13}\text{C}$  measurements at  $34.5^\circ$ .

are compared with the published  $^1\text{H}$  nmr results in Table 6.

The observed upfield shifts may be accounted for by ring current and/or charge migration effects.

### 3. THE 2-METHYLINDOLE:1,3,5-TRINITROBENZENE COMPLEX

The synthesis of two  $^{13}\text{C}$  enriched 2-methylindoles provided a considerable time saving in the study of the EDA interaction of this donor with 1,3,5-trinitrobenzene. Since the chemical shifts of the labelled carbons were monitored, 2-methylindole was used as the minor component. The solvent 1,2-dichloroethane allowed the trinitrobenzene (TNB) concentration to be varied over a fairly wide range (0.3-2.4 molal), while the 2-methylindole (2-MeI) concentration was maintained in the region of 0.05-0.10 molal. The equilibrium constants were determined from the methyl shifts in 2-methylindole-(methyl,3)- $^{13}\text{C}_2$  and from the C-2 shifts in 2-methylindole-2- $^{13}\text{C}$  as a function of the TNB concentration, using the method of successive approximations described previously. All chemical shifts were again referenced to the solvent peak. Where 2-methylindole-2- $^{13}\text{C}$  was used, a large SW (2500 Hz) was necessary so that both the solvent peak and C-2 of this donor appeared in the spectrum. Fourier transformation provided 1 real data point *ca.* every 0.6 Hz. Where 2-methylindole-(methyl,3)- $^{13}\text{C}_2$  was used, a SW of 1000 Hz was sufficient, providing 1 real data point *ca.* every 0.3 Hz.

The data for the two studies are summarized in Tables 7 and 8. The data obtained from the C-2 shifts of 2-methylindole-2- $^{13}\text{C}$  at  $35.0 \pm 0.5^\circ$  gave an equilibrium constant of 1.61 (kg solvent) $\text{mol}^{-1}$ . The correlation coefficient for this data, plotted in Figure 16, was 0.976. When methyl shifts of 2-methylindole-(methyl,3)- $^{13}\text{C}_2$  were used, an equilibrium

TABLE 7.  $^{13}\text{C}$  nmr chemical shifts for C-2 of 2-methylindole-2- $^{13}\text{C}$  as a function of the TNB concentration.

$[\text{2-MeI}]_0^a$	$[\text{TNB}]_0^a$	$\delta(\text{Hz})^b$	$\Delta(\text{Hz})$
0.0521	—	1822.33	—
0.0550	0.393	1825.53	-3.20
0.0552	0.611	1826.38	-4.05
0.0591	0.949	1827.26	-4.93
0.0643	1.440	1828.49	-6.16
0.0715	2.360	1828.71	-6.38

TABLE 8.  $^{13}\text{C}$  nmr chemical shifts for the methyl carbon of 2-methylindole-(methyl,3)- $^{13}\text{C}_2$  as a function of the TNB concentration.

$[\text{2-MeI}]_0^a$	$[\text{TNB}]_0^a$	$\delta(\text{Hz})^b$	$\Delta(\text{Hz})$
0.0991	—	615.21	—
0.0977	0.334	621.30	6.09
0.0978	0.741	625.60	10.39
0.0970	1.229	629.20	13.99
0.0959	1.550	630.48	15.28
0.0965	2.215	633.08	17.87

<sup>a</sup>Initial concentrations of all components in mol (kg solvent)<sup>-1</sup>.

<sup>b</sup>The observed chemical shifts of the labelled carbon of 2-methylindole relative to the 1,2-dichloroethane peak.

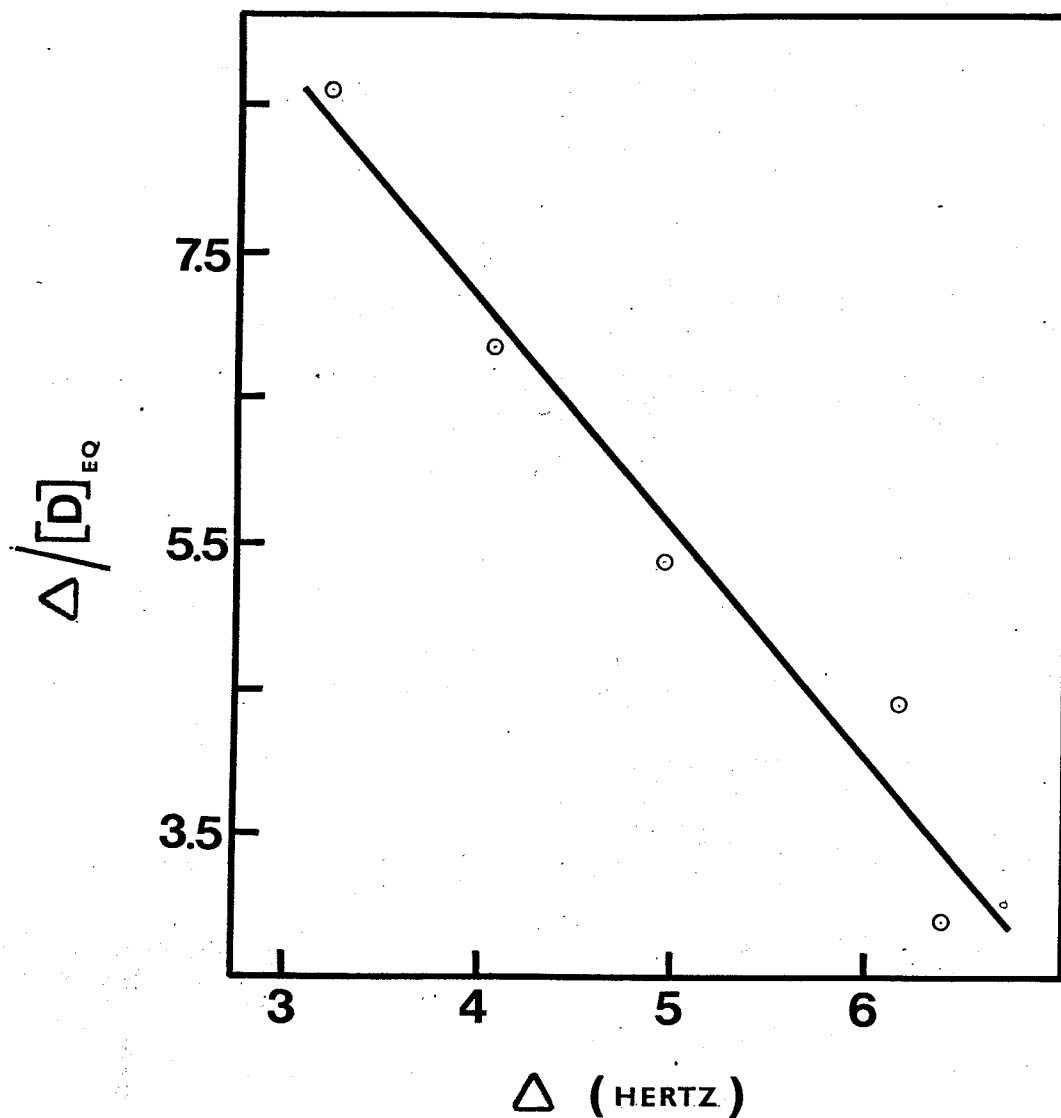


FIGURE 16. Plot of  $\Delta$  vs  $\Delta/[D]_{eq}$  (after convergence of K) for the system 2-MeI: TNB in 1,2-dichloroethane at  $35.0 \pm 0.5^\circ$ , using the C-2 shifts of 2-methylindole- $2-^{13}\text{C}$ .



constant of  $0.95 \text{ (kg solvent)mol}^{-1}$  was obtained. This data, with a correlation coefficient of 0.998, is plotted in Figure 17.

Although  $K$  for complex formation between 2-methylindole and TNB in 1,2-dichloroethane has not been determined by  $^1\text{H}$  nmr, Foster and Fyfe (31) have measured  $K$  for this system in chloroform at  $33.5^\circ$ . Using 2-methylindole as the major component and monitoring the proton shifts in TNB, a value of  $2.16 \text{ (kg solution)mol}^{-1}$  was reported. When the  $^{13}\text{C}$  data obtained in this study were evaluated in the corresponding concentration scale,  $K$  values of 1.39 and 0.73  $\text{(kg solution)mol}^{-1}$  were obtained from the C-2 and methyl shifts of 2-methylindole respectively.

Considering the decrease expected in  $K$  with the change to a solvent of higher dielectric constant (32), the  $^{13}\text{C}$  results are reasonable. A comparable decrease in  $K$ , from 1.65 to 0.85, has been reported (31) for the complex formation of indole with TNB on going from chloroform to 1,2-dichloroethane.

As indicated in Tables 7 and 8, upfield shifts were measured for the methyl resonance of 2-methylindole on complex formation with TNB, whereas downfield shifts were observed for C-2. Although downfield shifts were also observed for C-3, these were too small to be used for a determination of  $K$ .

The paramagnetic shifts observed for C-2 and C-3 suggest that the charge-transfer interaction makes a significant contribution. The greater sensitivity of C-2 over C-3 to the charge-transfer interaction is consistent with earlier work.

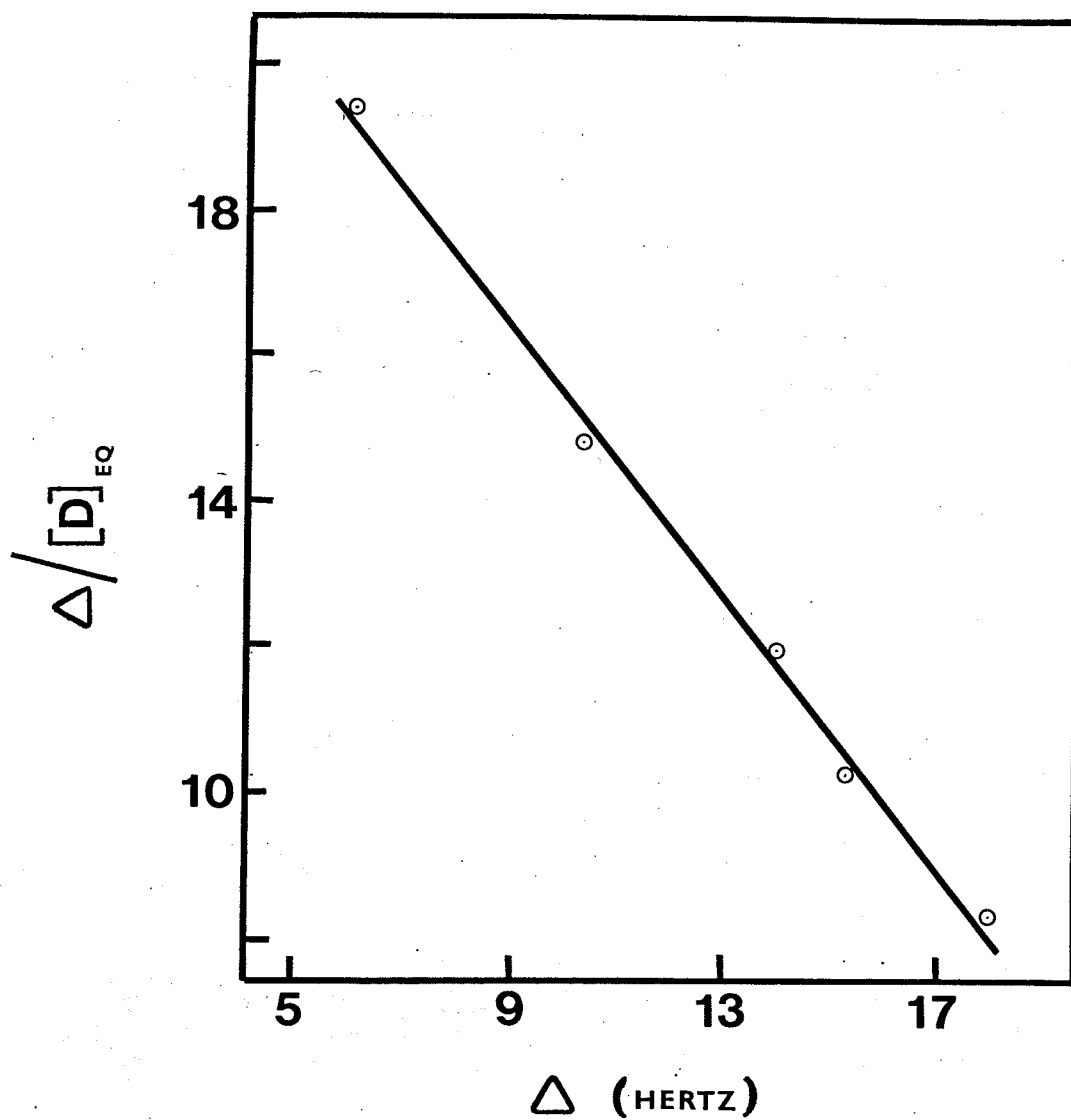


FIGURE 17. Plot of  $\Delta$  vs  $\Delta/[D]_{eq}$  (after convergence of K) for the system 2-MeI: TNB in 1,2-dichloroethane at  $35.0 \pm 0.5^\circ$ , using the methyl shifts of 2-methylindole-(methyl,3)- $^{13}\text{C}_2$ .

Foster and Fyfe (31) have shown that H-3 of indole experiences a greater upfield shift on complex formation with TNB than does H-2. A possible explanation is that the charge-transfer effect (deshielding for donors) is greater at H-2 than at H-3. As discussed in section II.C., paramagnetic  $^{13}\text{C}$  shifts have also been reported for C-2 of naphthalene and anthracene when complexed with TNB (35) and with *o*-chlor-anil (39). These shifts have also been interpreted in terms of the effects of charge migration.

The upfield shifts observed for the methyl carbon of 2-methylindole on complex formation suggests that the ring current effect predominates these  $^{13}\text{C}$  shifts.

Although the relative orientations of indole and TNB have been determined in the solid complex by X-ray crystallography (see (19) for example), there is not enough information in these  $^{13}\text{C}$  results to postulate a preferred orientation in solution. The orientations (in solution) postulated by Sung and Parker (32), although consistent with their  $^1\text{H}$  results are, at best, difficult to apply to these  $^{13}\text{C}$  results.

The  $^{13}\text{C}$  nmr results suggest that  $^{13}\text{C}$  chemical shifts are much more sensitive to the effects of charge migration in EDA interactions than are  $^1\text{H}$  shifts. Thus  $^{13}\text{C}$  shifts should provide a better insight into localization of charge-transfer in such interactions.

C. A CARBON-13 SPIN-LATTICE RELAXATION TIME STUDY OF THE EDA INTERACTION OF 2-METHYLINDOLE AND 1,3,5-TRINITROBENZENE

1. INTRODUCTION

Carbon-3 of 2-methylindole was expected to be overwhelmingly relaxed by the dipolar interaction with its bonded proton. Since the dipolar relaxation mechanism depends on the overall motion of the molecule, the  $T_1$  of this carbon should be sensitive to the change in the rate of molecular reorientation due to complex formation. Therefore, the  $T_1$  of C-3 of 2-methylindole was measured as a function of the concentration of added TNB.

Since the viscosity of the medium will also influence the overall reorientation rate of the molecule, the observed decreases in  $T_1$  (see Table 9) must be interpreted in terms of both complex formation and changes in viscosity. The viscosities of the solutions were determined from a plot of the variation of viscosity as a function of the TNB concentration.

The relaxation times were determined by the inversion recovery method which utilizes a  $(180^\circ - t_i - 90^\circ - \text{AT-PD})$  pulse sequence. Variation of  $t_i$  gave a series of spectra (see Figure 18) showing the rate of recovery of the longitudinal magnetization after the  $180^\circ$  pulse. The plots of  $\ln(A_0 - A_z)$  vs  $t_i$  (see Figure 19) illustrate the effect of addition of TNB on the recovery of the longitudinal magnetization of C-3 of 2-methylindole.

TABLE 9. Spin-lattice relaxation times for C-3 of 2-methylindole as a function of the TNB concentration in 1,2-dichloroethane at 35°.

$[2\text{-MeI}]_0^a$	$[\text{TNB}]_0^a$	$\eta(\text{cp})^b$	$T_1(\text{sec})^c$
0.100	—	0.68 <sub>6</sub>	6.6
0.099	0.101	0.72 <sub>0</sub>	5.2
0.100	0.360	0.81 <sub>1</sub>	3.8
0.102	0.365	0.81 <sub>4</sub>	3.6
0.100	0.555	0.88 <sub>3</sub>	3.1
0.100	1.153	1.13 <sub>0</sub>	2.1 <sub>5</sub>
0.103	1.588	1.34 <sub>6</sub>	1.7 <sub>2</sub>

<sup>a</sup>Initial concentrations in mol(kg solvent)<sup>-1</sup>.

<sup>b</sup>Viscosity in centipoise at 35.0°.

<sup>c</sup>The observed spin-lattice relaxation times for C-3 of 2-methylindole-(methyl,3)-<sup>13</sup>C<sub>2</sub>.

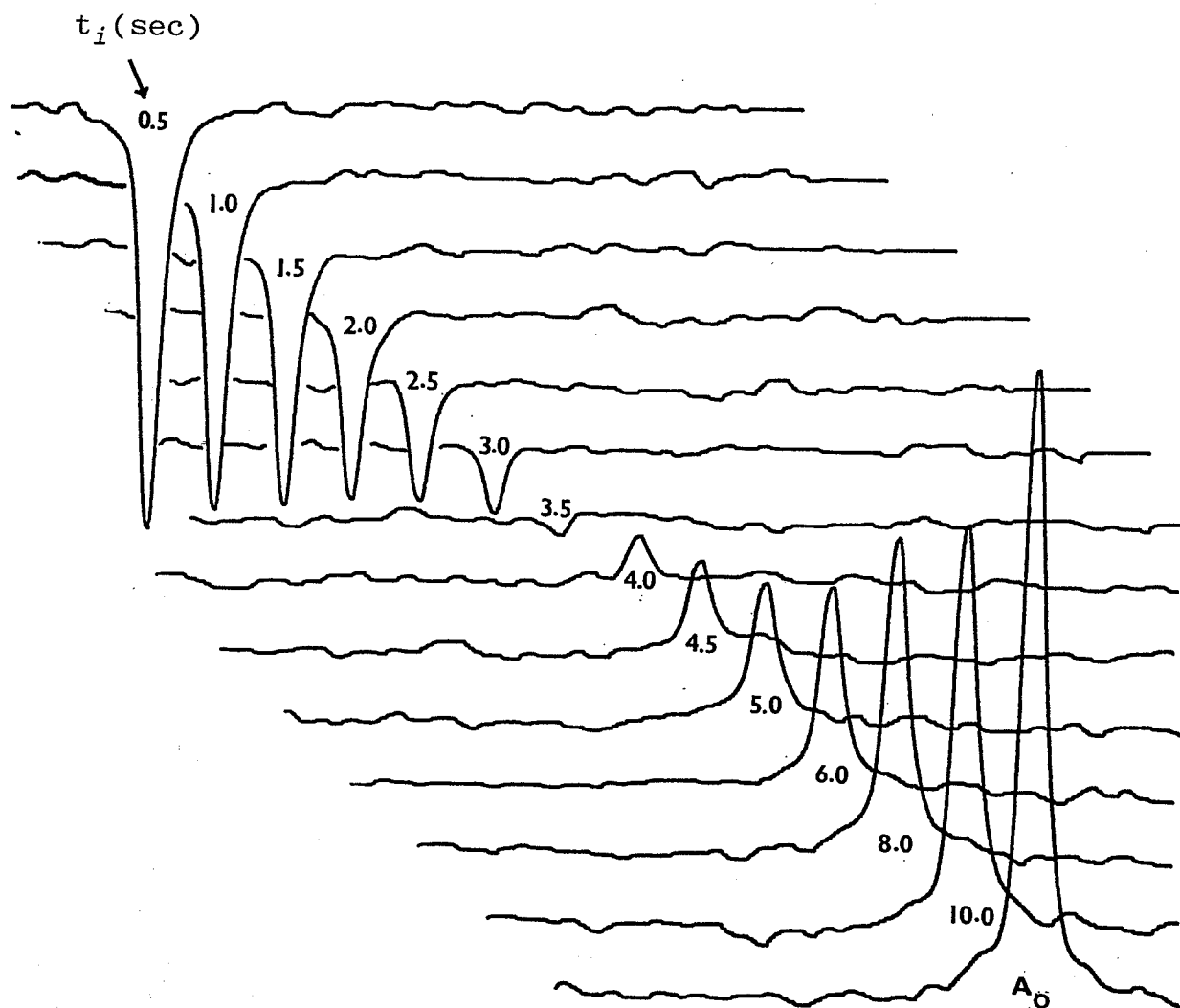


FIGURE 18. Spectra obtained by the inversion recovery method for the determination of  $T_1$  for C-3 of 2-methylindole-(methyl,3)- $^{13}\text{C}_2$  (0.100 molal) in 1,2-dichloroethane at  $35^\circ$ . Variation of  $t_i$  in the ( $180^\circ$ - $t_i$ - $90^\circ$ -AT-PD) pulse sequence give the series of spectra showing the rate of recovery of the longitudinal magnetization.

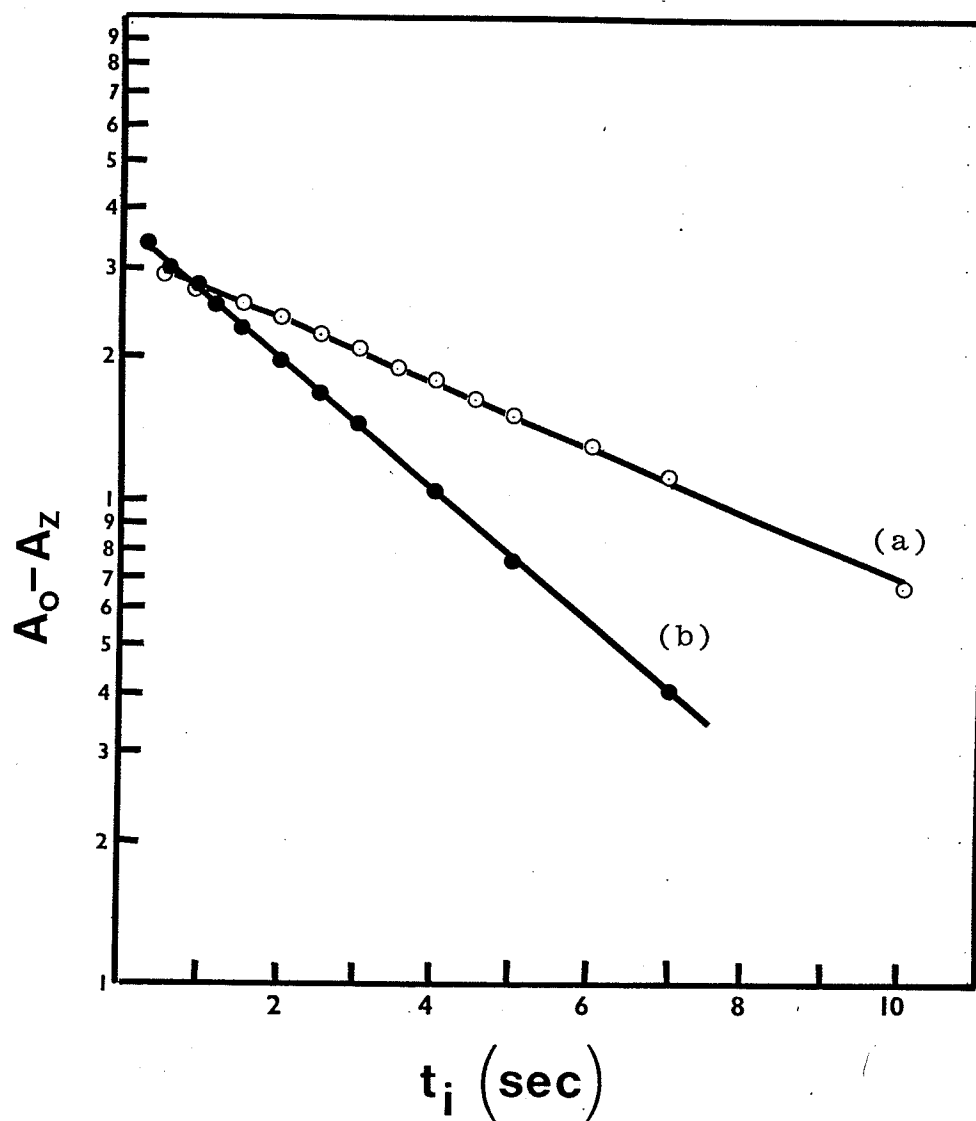


FIGURE 19. Plots of  $\ln(A_0 - A_z)$  vs  $t_i$  for C-3 of 2-methylindole-(methyl,3)- $^{13}\text{C}_2$  (0.100 molal) in 1,2-dichloroethane at  $35^\circ$ , (a) with no TNB and (b) with 0.555 molal TNB added.

The nOe factors (see Figure 20 for an example) measured for all solutions were within experimental error ( $\pm 0.2$ ) of the full nOe (1.988).

## 2. METHOD OF ANALYSIS OF K

Assuming that the rates of chemical exchange are slow relative to the rates of molecular reorientation, the observed spin-lattice relaxation rate,  $1/T_1$ , is a weighted average of the spin-lattice relaxation rates of the free and complexed molecules (61),  $1/T_D$  and  $1/T_{AD}$ . For the 1:1 complex

$$[53] \quad \frac{1}{T_1} = \frac{1}{T_D} (1-\alpha) + \frac{1}{T_{AD}} (\alpha) .$$

If the spin-lattice relaxation rates of the free and complexed molecules vary linearly with the macroscopic viscosity,  $\eta$ , at a constant temperature — as would be expected if  $T_1$  is dominated by dipolar relaxation — then they may easily be corrected to account for viscosity changes which are affecting the observed  $T_1$ . If  $\eta_o$  is the viscosity of the reference solution (the one containing no TNB), then

$$[61] \quad \frac{1}{T_1} = \left(1 - \frac{[AD]}{[D]_o}\right) \frac{\eta}{T_D \eta_o} + \frac{[AD]}{[D]_o} \frac{\eta}{T_{AD} \eta_o}$$

Rearrangement of the equilibrium constant expression

$$[62] \quad K = \frac{[AD]}{[A]_{eq} ([D]_o - [AD])}$$



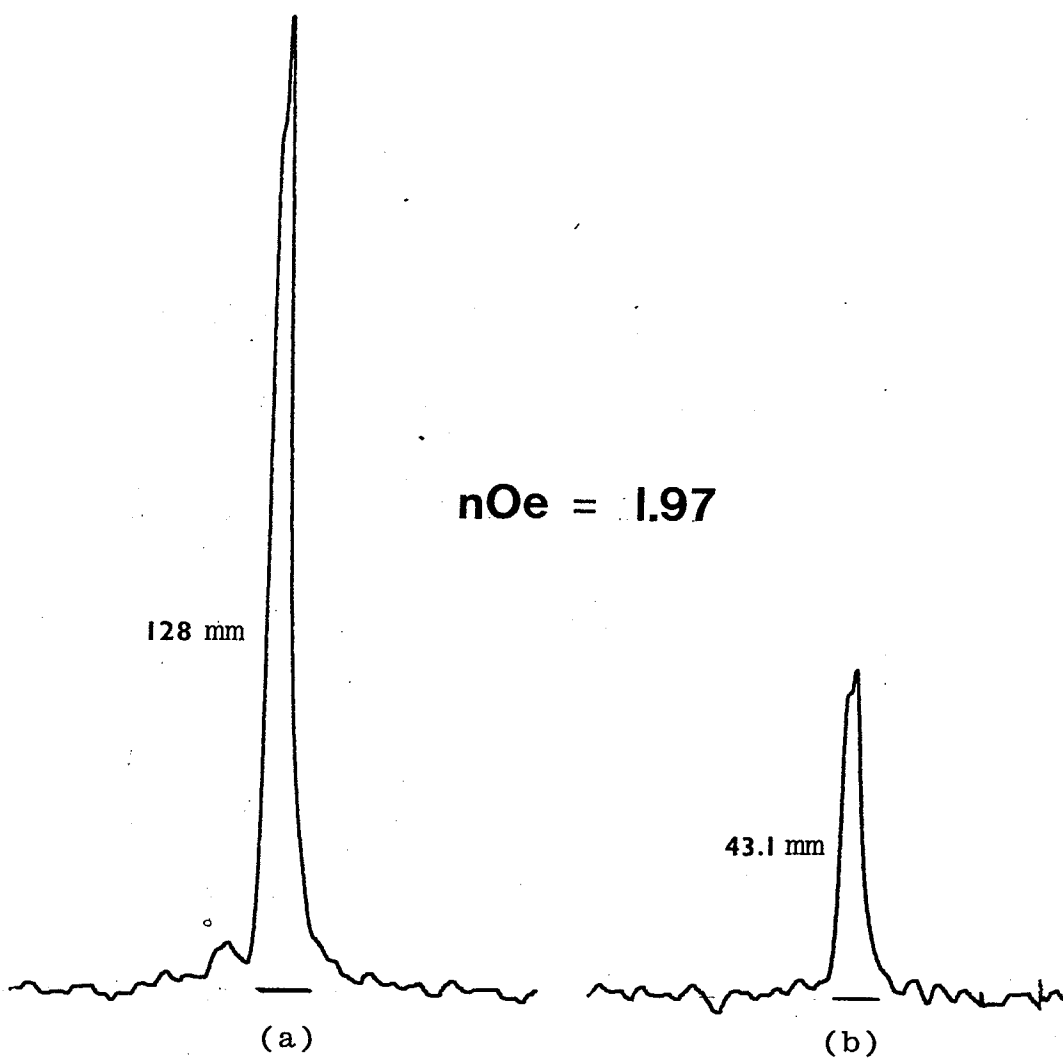


FIGURE 20. Determination of the  $nOe$  for C-3 of 2-methylindole-(methyl,3)- $^{13}C_2$  (0.100 molal) in 1,2-dichloroethane at  $35^\circ$ . Spectra were obtained with (a) continuous proton decoupling and (b) the decoupler gated on only during the observation pulse and data acquisition, using a pulse delay of  $ca. 10T_1$  in both cases.

yields

$$[63] \quad \frac{[AD]}{[A]_{eq}} = K[D]_o - K[AD] .$$

Solving for [AD] in [61] and substituting into [63], followed by simplification yields

$$[64] \quad \left( \frac{\eta_o}{\eta T_1} - \frac{1}{T_D} \right) \frac{1}{[A]_{eq}} = -K \frac{\eta_o}{\eta T_1} + K \frac{1}{T_{AD}}$$

A plot of the left hand side of [64] vs  $\eta_o/\eta T_1$  will give a straight line with a slope of  $-K$  and y-intercept of  $K/T_{AD}$ .

The equation

$$[65] \quad [A]_{eq} = [A]_o - \frac{K [A]_{eq} [D]_o}{1 + K[A]_{eq}}$$

is arrived at in the same manner as [60].

Equations [64] and [65] were used in the same way as [56] and [60] to obtain  $K$ , again using a method of successive approximations.

The APL\360 computer program 'EDA' (see Appendix B) was written to perform the iterations, calculations and least-squares-fit required in the above operation.

Analysis of the data yields a value for  $K$  of  $2.3_g$  (kg solvent) $\text{mol}^{-1}$  or  $2.1_3$  (kg solution) $\text{mol}^{-1}$ . The correlation coefficient for this data, plotted in Figure 21, was 0.965. Although the value of  $K$  is somewhat larger than the  $K$  determined by chemical shifts, it is reasonable considering the assumptions made in this treatment.

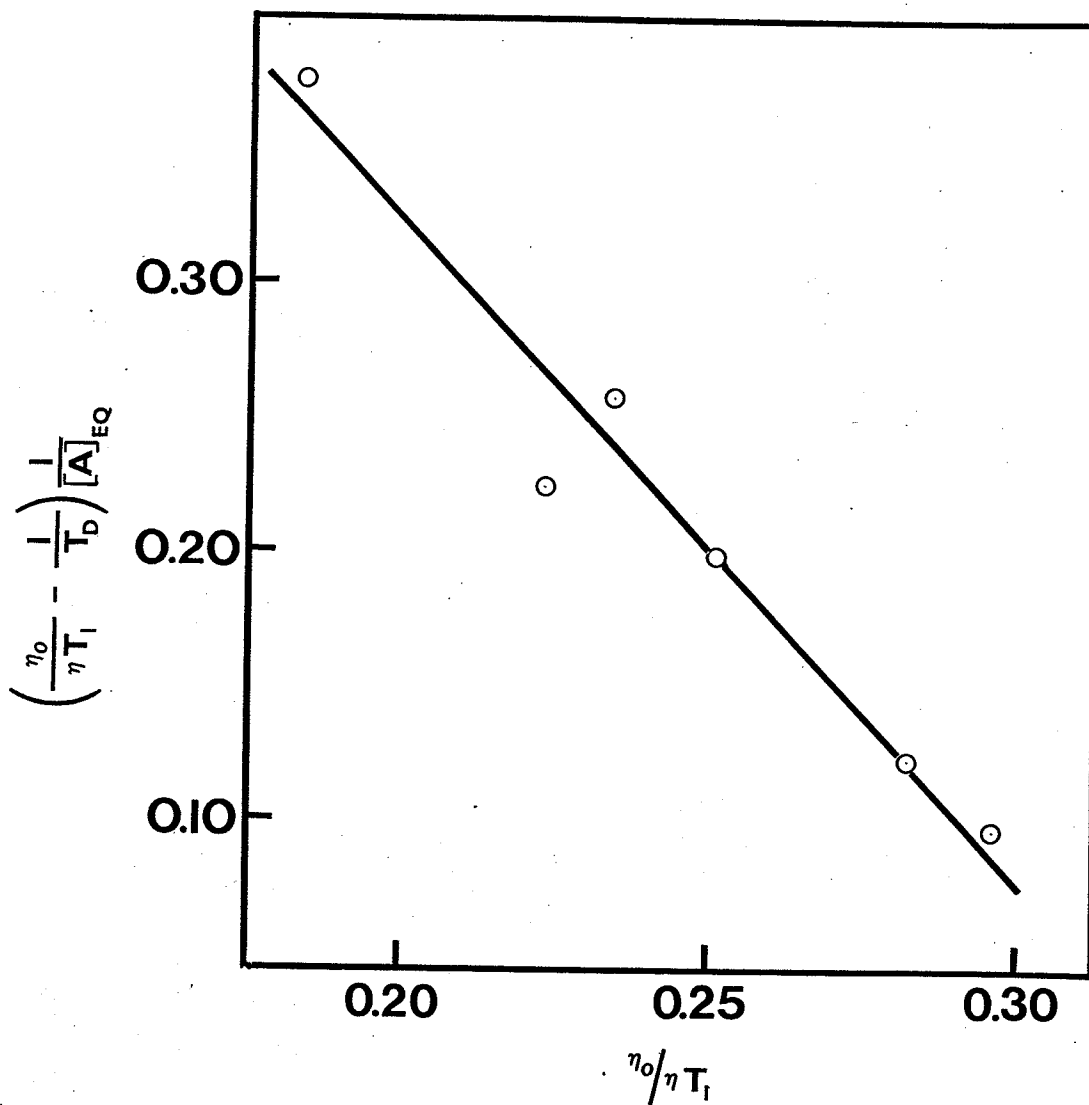


FIGURE 21. The data of Table 9 plotted according to equation [64] after convergence of K.

### 3. THE ASSUMPTIONS INVOLVED IN THE DETERMINATION OF K FROM $T_1$ DATA

Equation [64] has been derived on the assumption that the spin-lattice relaxation rates of both the free donor and its EDA complex,  $1/T_D$  and  $1/T_{AD}$ , are directly proportional to the macroscopic viscosity of the solution.

The spin-lattice relaxation rate of the pure complex,  $1/T_{AD}$ , would be virtually impossible to study as a function of viscosity since the complex would dissociate to some degree in the solvent. However, the spin-lattice relaxation rate of C-3 of free 2-methylindole,  $1/T_D$ , has been shown to vary directly with viscosity (to be discussed in section IV. E.). Therefore, the assumption that the spin-lattice relaxation rate of this same carbon in the pure complex,  $1/T_{AD}$ , would also vary linearly with viscosity seems reasonable.

For some systems, when one component is in large excess, termolecular complex formation has been detected (4); however, several studies (31, 32, 70) between indoles and TNB under these conditions have been interpreted successfully in terms of 1:1 complex formation. Since, on the average, a smaller excess of the major component was used in this study, a bimolecular treatment seems justifiable.

Finally, the entire treatment is based on the assumption of slow chemical exchange. The appropriateness of this assumption will be discussed fully in section IV.D.

#### 4. T<sub>1</sub> IN THE PURE COMPLEX

The y-intercept obtained in the plot of the data according to [64] gives  $K/T_{AD}$ . The spin-lattice relaxation time for C-3 of 2-methylindole in the pure complex (at the reference viscosity,  $\eta_0$ ) may be obtained without recourse to a doubtful extrapolated intercept by rearrangement of [64] to

$$[66] \quad [A]_{eq} = \frac{(1/T_{AD} - 1/T_D) [A]_{eq}}{(\eta_0/\eta T_1 - 1/T_D)} - \frac{1}{K}$$

which has a slope of  $(1/T_{AD} - 1/T_D)$ .

This equation is not sensitive to experimental error in  $K$  for the range of concentrations employed in this study. For example, when the calculations were performed manually using  $K$  values of 1.5, 2.0 and 2.5 (kg solvent) $\text{mol}^{-1}$  to solve for  $[A]_{eq}$ ,  $T_{AD}$  values of 2.95, 2.97 and 2.98 sec. were obtained on least-squares-fitting the data to [66].

#### 5. EFFECTIVE CORRELATION TIMES

Assuming that the overall reorientation of the molecule can be described by one effective molecular correlation time,  $\tau_c$ , [32] can be used to calculate correlation times in the motional narrowing region under conditions of complete proton decoupling.

Since the  $nOe$  is considered to be full,  $T_D = 6.6$  and  $T_{AD} = 3.0$  sec represent the dipolar spin-lattice relaxation times of free 2-methylindole and its TNB complex.

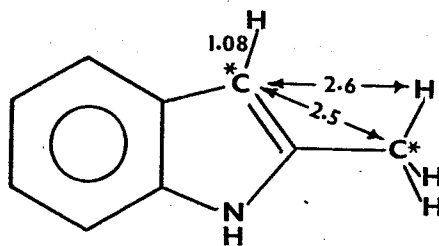
Using  $1.08\text{\AA}$  as a reasonable bond length for C(3)-H of 2-methylindole (71), values of  $6.7 \times 10^{-12}$  and  $14.7 \times 10^{-12}$  sec were calculated for the effective correlation times (at  $35^\circ$  and 0.686 centipoise) of 2-methylindole and its TNB complex respectively. As expected, the reorientation of the larger rotating unit (the complex) is substantially slower.

The semilog plots of  $T_1$  and  $T_2$  as a function of  $\tau_c$  for the CFT-20 nmr spectrometer (Figure 22) show that the "motional narrowing" assumption was valid. These plots, as well as that of  $nOe$  vs  $\tau_c$  (Figure 23) were obtained by using the expressions in Doddrell *et.al.* (48). The  $T_1$  expression is also given by [31] in this thesis.

## 6. DISCUSSION OF $T_1$ VALUES

Since the  $nOe$ 's measured are within experimental error of the full  $nOe$ , the dipolar relaxation mechanism completely dominates the relaxation of C-3 of 2-methylindole.

The approximate distances from C-3 to the nearest magnetic spins - the bonded proton, the methyl protons and the enriched methyl carbon - were determined from a scale diagram of 2-methylindole (see Figure 26).



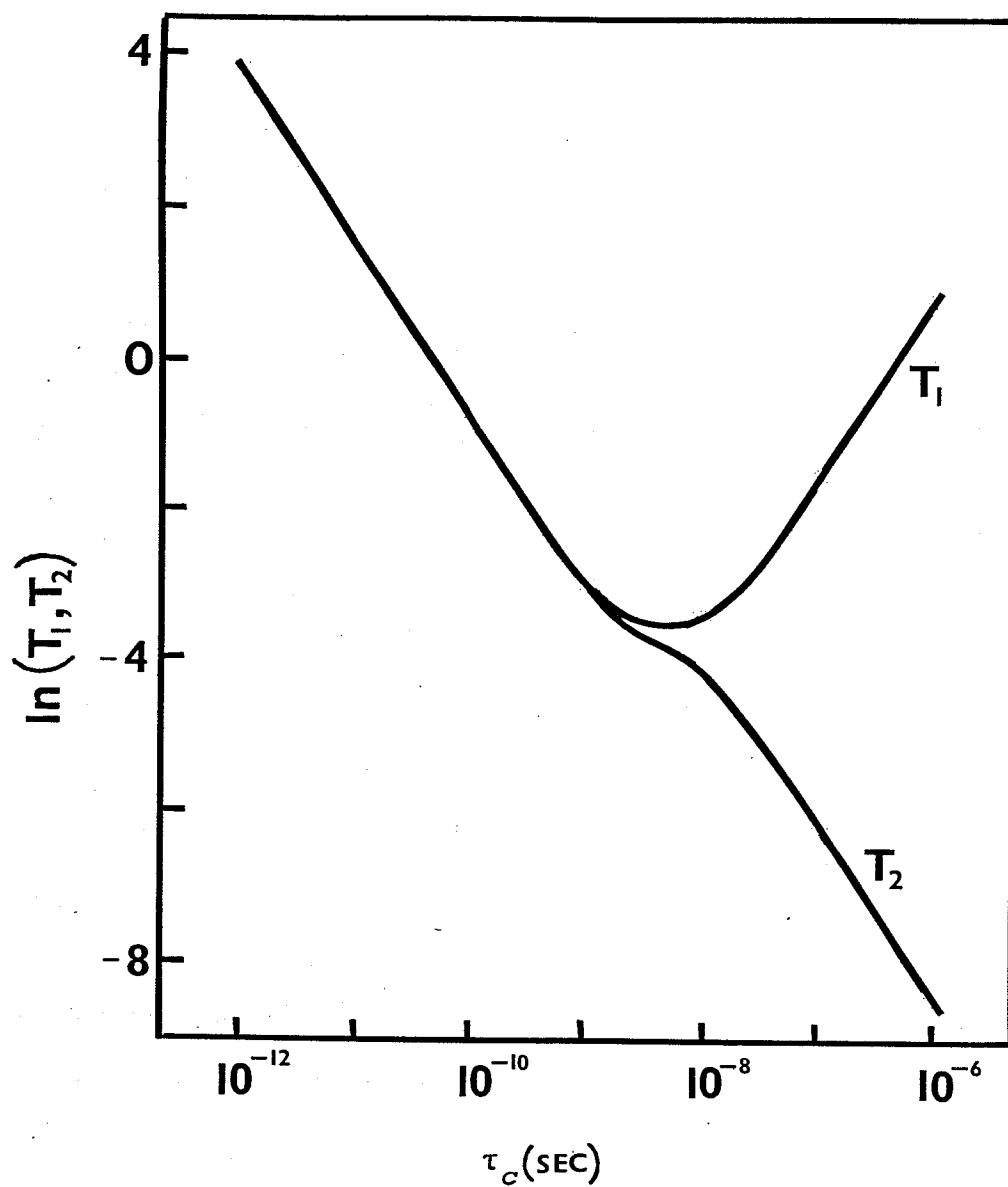


FIGURE 22. The dependence of  $T_1$  and  $T_2$  on  $\tau_c$  for the dipolar interaction between a  $^{13}\text{C}$  nucleus and its bonded proton (bond length  $1.08\text{\AA}$ ), under conditions of complete proton decoupling, where  $\omega_H = 79.54 \times 10^6$  rad/sec and  $\omega_C = 20.00 \times 10^6$  rad/sec at 18.682 kG.

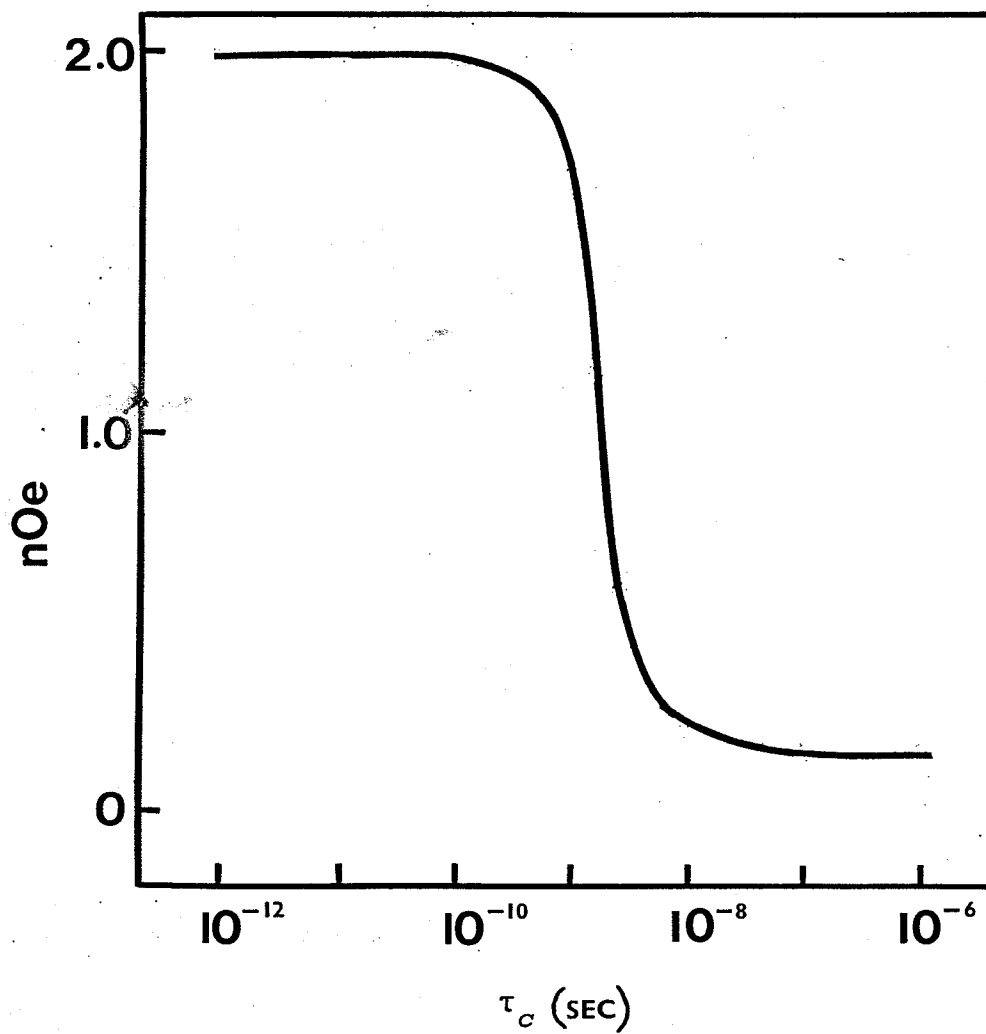


FIGURE 23. The dependence of the nOe on  $\tau_c$  for the CFT-20 nmr spectrometer (see the conditions given in Figure 22).



The contribution of the dipolar interaction of each of these nuclei with C-3 was then calculated as follows:

$$\begin{aligned}
 [67] \quad \frac{1}{T_1} &= \sum \frac{\hbar^2 \gamma_C^2 \gamma_H^2}{r_{C-H}^6} \tau_C + \left(\frac{3}{2}\right) \frac{\hbar^2 \gamma_C^4}{r_{C-C}^6} \tau_C \\
 &= 0.152 + 0.0078 + 0.000094 \text{ sec}^{-1}.
 \end{aligned}$$

Therefore, due to the  $r^{-6}$  dependence of the relaxation rates, the intramolecular nonbonded dipolar interactions may be ignored. It is reasonable to assume that intermolecular dipolar interactions will be insignificant as well.

The contribution due to dissolved oxygen (72),  $1/T_1^e \approx 0.01 \text{ sec}^{-1}$ , has been eliminated by vacuum degassing and sealing the nmr samples.

Although the inversion recovery method for determining  $T_1$  is not very sensitive to errors in the flip angle (72), the pulse width (PW) of the spectrometer was calibrated by observing the peak intensity as a function of PW (see Figure 24). Considering the peak height to be proportional to the magnetization, the  $t_{null}$  representing the  $360^\circ$  pulse was used to get the PW for the  $90^\circ$  and  $180^\circ$  pulses.

The drop-off in the pulse power for nuclei far off-resonance was not crucial in this study since the  $T_1$  of only one  $^{13}\text{C}$  nucleus was determined. Therefore, the transmitter was set near the resonance frequency of this nucleus to provide maximum pulse power.

Errors in peak height measurement, and therefore in  $T_1$ , will be reduced as the number of scans,  $N$ , increases, the S/N

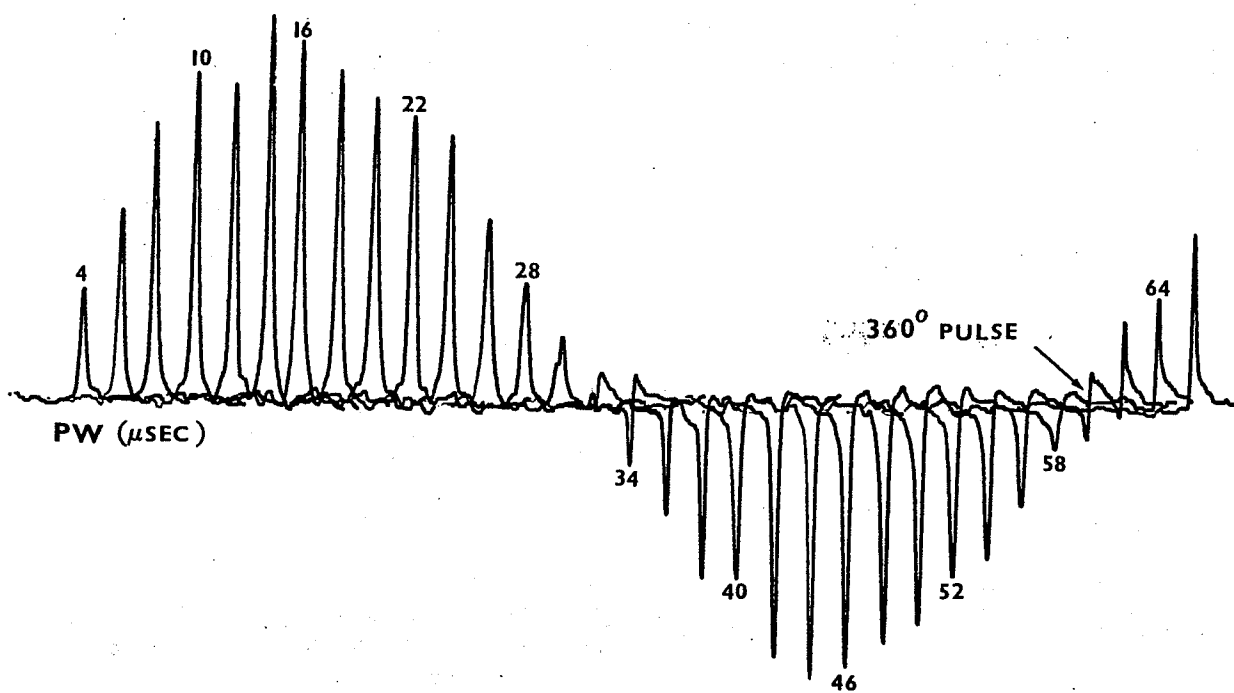


FIGURE 24. Pulse width calibration for the CFT-20 nmr spectrometer with neat *t*-butyl alcohol (locked onto  $D_2O$  in a coaxial tube).

increasing with  $\sqrt{N}$ . However, due to  $^{13}\text{C}$  enrichment, good S/N was obtained with a small number (fifty) of scans. The FID's were weighted to increase S/N further.

The  $T_1$ 's were determined to be reproducible to *ca.* 3% by running a particular sample several times. This, together with the fact that there was minimal scattering of the data as seen in the magnetization recovery plots (see Figure 19) is consistent with insignificant changes in instrument resolution, sensitivity, temperature, *etc.* over the course of the experiment.

Although the error in the  $T_1$ 's is not known, the values are probably no better than the usually reported accuracy of  $\pm 5$ -10% (72, 73, 74).

## 7. CRITICISM OF THE METHOD

It is impossible to estimate the error in K determined by the  $T_1$  method due to the uncertainty about the accuracy of the  $T_1$ 's. Due to the assumptions of this method and the large errors usually associated with  $T_1$ 's, determination of association constants by this method would generally not prove as reliable as a determination of K from more accurately measurable chemical shifts.

However, in certain cases where the nucleus under observation is in a small molecule being complexed to a much larger molecule, this method could be the method of choice.

D. MOLECULAR DYNAMICS OF 2-METHYLINDOLE:1,3,5-TRINITRO-  
BENZENE COMPLEX FORMATION

1. EXPERIMENTAL DEPENDENCE OF  $T_1$  ON FRACTION COMPLEXED

In the region of motional narrowing and under conditions of complete proton decoupling, the dipolar relaxation rate, which completely dominates the relaxation of C-3 of 2-methylindole, is given by

$$[68] \quad \frac{1}{T_1} = B_{dip} \tau_c$$

where  $B_{dip} = \frac{1}{2} \hbar^2 \gamma_C^2 \gamma_H^2 / r_{C-H}^6$  and is evaluated using  $r = 1.08 \text{ \AA}$  as the C-H bond length involved (see equation [32]).

The experimental dependence of  $T_1$  of C-3 on the fraction of 2-methylindole complexed (see Table 10) was determined by measuring the  $T_1$  as a function of the amount of TNB added. The fraction complexed,  $\alpha$ , was calculated from the original concentrations and the average equilibrium constant of  $1.3 \text{ (kg solvent) mol}^{-1}$ , obtained from the  $^{13}\text{C}$  chemical shift studies of C-3 and the methyl carbon of 2-methylindole.

The points in Figure 25 show the observed  $T_1$ , corrected to the reference viscosity, as a function of the fraction complexed. The reference viscosity chosen is that of the solution containing no TNB.

A  $T_1$  determination with a 0.18 molal solution of 2-methylindole containing no TNB indicated that a concentration change at these low concentrations does not affect  $T_1$ .

TABLE 10. Spin-lattice relaxation times for C-3 of 2-methylindole as a function of the fraction complexed.

$[2\text{-MeI}]_o^a$	$[\text{TNB}]_o^a$	$\eta(\text{cp})^b$	$T_1(\text{sec})^c$	$\alpha^d$
0.100	—	0.68 <sub>6</sub>	6.6 <sub>0</sub>	0.00
0.099	0.101	0.72 <sub>0</sub>	5.1 <sub>6</sub>	0.106
0.100	0.360	0.81 <sub>1</sub>	3.7 <sub>8</sub>	0.300
0.102	0.365	0.81 <sub>4</sub>	3.5 <sub>6</sub>	0.303
0.100	0.555	0.88 <sub>3</sub>	3.1 <sub>7</sub>	0.401
0.100	1.153	1.13 <sub>0</sub>	2.1 <sub>5</sub>	0.587
0.103	1.588	1.34 <sub>6</sub>	1.7 <sub>2</sub>	0.664

<sup>a</sup>Initial concentrations in mol(kg solvent)<sup>-1</sup>.

<sup>b</sup>Viscosity in centipoise at 35.0°.

<sup>c</sup>The  $T_1$  for C-3 of 2-methylindole-(methyl,3)-<sup>13</sup>C<sub>2</sub>.

<sup>d</sup>The fraction complexed as calculated by the program.

## 2. THEORETICAL DEPENDENCE OF DIPOLAR RELAXATION TIMES ON FRACTION COMPLEXED

As discussed in section II.D.5., the dipolar  $T_1$  of a nucleus undergoing exchange between the free and complexed state, will depend on the rate of reorientation of the free molecule,  $k_1$ , and the pure complex,  $k_2$ , as well as the rate of association,  $k_3$ , of the molecules and the rate of dissociation,  $k_4$ , of the complex.

Using the equations of Anderson and Fryer (see [52] and reference 61) the  $^{13}\text{C}$  dipolar relaxation rate can be written as a function of the rate constants and the fraction complexed,

$$[69] \quad \frac{1}{T_1} = B_{dip} f(k_1, k_2, k_3, k_4, \alpha).$$

Using this relationship, the  $T_1$  can be calculated as a function of the fraction complexed for a given set of rate constants.

The average equilibrium constant of 1.3 (kg solvent)  $\text{mol}^{-1}$ , determined from  $^{13}\text{C}$  chemical shifts for the 2-MeI:TNB system, allow a substitution to be made for  $k_3$ , since  $K = k_3/k_4$ . The rate of reorientation of the free 2-methylindole,  $k_1$ , was calculated from the correlation time which, in turn, was calculated from the  $T_1$  of 2-methylindole containing no TNB, *ie.*  $k_1 = (\tau_c)^{-1}$ . In this way the  $T_1$  expression has been reduced to an equation containing two unknowns,  $k_2$  and  $k_4$ .

The computer program 'QUADEX' (64, 75), modified for  $^{13}\text{C}$  dipolar relaxation and to take into account the effects

of viscosity on experimental  $T_1$ 's (see Appendix C), was used to generate a series of theoretical curves using [69], as described below. The theoretical curve (see the solid line in Figure 25) best fitting the experimental points was then determined, also as described below.

### 3. THE RATE CONSTANTS FOR THE 2-MeI:TNB SYSTEM

With the program 'QUADEX' the molecular correlation time of the pure complex,  $(\tau_c)_{AD}$ , is calculated for a given value of  $T_{AD}$  utilizing [68]. The rate of reorientation of the complex,  $k_2$ , is then calculated according to  $k_2 = (\tau_c)_{AD}^{-1}$ . A series of theoretical curves (see [69]) are now calculated for a given value of  $k_2$  (or  $T_{AD}$ ) by varying  $k_4$  to cover the range from slow chemical exchange relative to the rate of reorientation of the complex (i.e.  $k_4/k_2 = 10^{-5}$ ) to fast exchange ( $k_4/k_2 = 10^4$ ). The program selects the curve which best fits the experimental data.

As  $T_{AD}$  (or  $k_2$ ) is varied, a set of best-fitting theoretical curves are produced, one for each value of  $T_{AD}$ . A measure of the deviation (calculated by the program) of each of these curves from the experimental points indicates which value of  $T_{AD}$  provides the best fit without actually plotting any of the curves.

On plotting the best-fitting curves for  $T_{AD}$  values of 2.2, 2.3, ..., 3.2 sec, it was found that five of the theoretical curves were so similar that the selection of one of these over the others seemed arbitrary. Therefore, the pa-

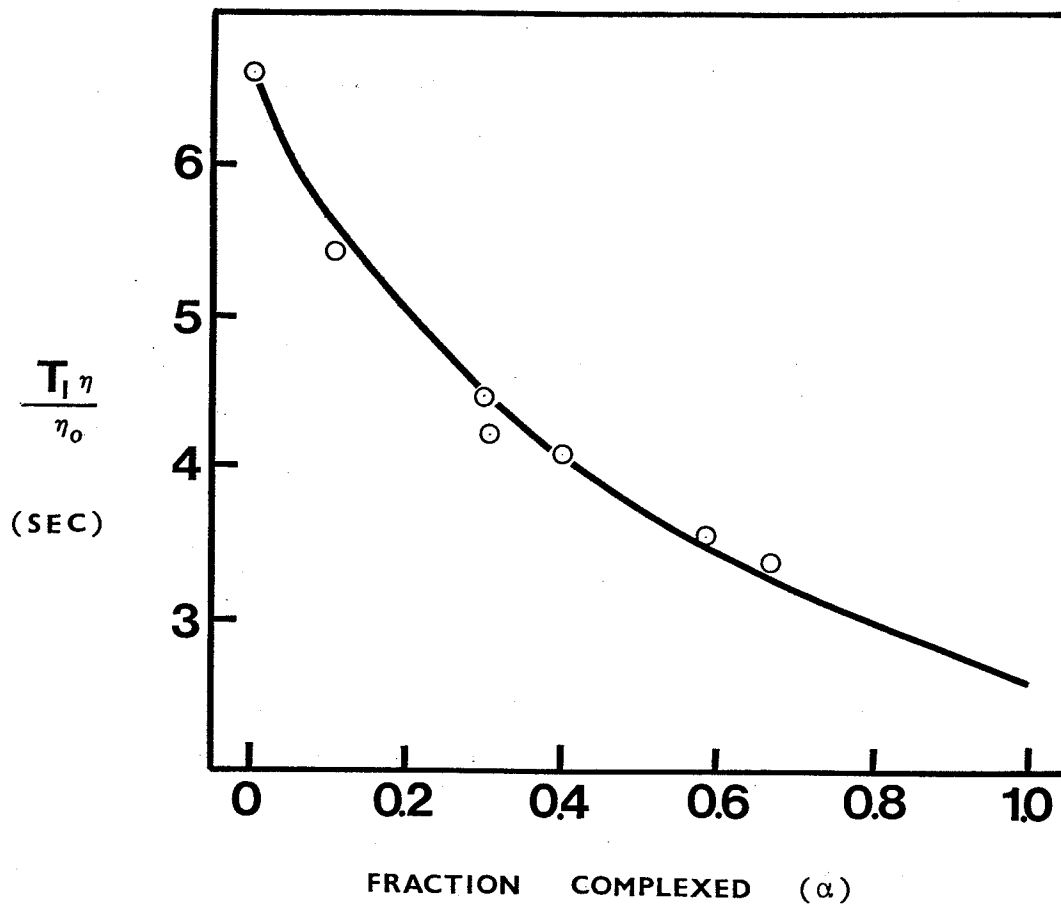


FIGURE 25. The dependence of  $T_1$  (corrected for the effects of viscosity) of C-3 of 2-methylindole on the fraction complexed, showing the experimental points and the theoretical curve providing the best fit.



rameters ( $k_2$ ,  $k_3$  and  $k_4$ ) obtained from these five curves were averaged. The data are summarized in Table 11.

TABLE 11. Relaxation times<sup>a</sup> and rate constants<sup>b</sup> for complex formation of 2-methylindole with 1,3,5-trinitrobenzene.

$T_D$	$T_{AD}$	$k_1$	$k_2$	$k_3$	$k_4$
6.6	2.4	150	55	18	14

<sup>a</sup>Relaxation times are reported in sec.

<sup>b</sup>All rate constants are reported in  $\text{nsec}^{-1}$ .

Several conclusions may be drawn from these results for the 2-MeI:TNB system. The overall rotational motion of 2-methylindole decreases considerably due to complex formation ( $k_1/k_2 \sim 3$ ). The rates of dissociation and association of the complex,  $k_4$  and  $k_3$ , are slower than the rate of reorientation of the complex,  $k_2$ , and consequently much slower than the rate of reorientation of free 2-methylindole,  $k_1$ .

The lifetime of the complex,  $(k_4)^{-1}$ , is therefore longer than the correlation time for rotational motion of the complex. This means that the complex experiences considerable rotational motion prior to dissociation.

Analysis of the theoretical curves shows that the best fits with the experimental data were obtained for an average exchange rate, relative to the rate of reorientation of the

complex, of  $k_4/k_2 \sim 10^{-1}$ . Comparison with the hypothetical curves presented by Anderson and Fryer (61) shows that the system under investigation is best approximated by an intermediate rate of exchange. This conclusion is substantiated by an examination of a series of theoretical curves. The curves for very slow exchange rates ( $k_4/k_2 = 10^{-5}$ ) generally give poor fits to the experimental data, as do curves where  $k_4/k_2 > 1.0$ .

In the limiting case ( $k_3, k_4 \ll k_1, k_2$ ) for slow exchange, the equation relating  $T_1$  to the fraction complexed simplifies to

$$[53] \quad \frac{1}{T_1} = \frac{1}{T_D} (1-\alpha) + \frac{1}{T_{AD}} (\alpha).$$

For the 2-MeI:TNB system  $k_3$  and  $k_4$  may not be small enough relative to  $k_2$  to allow such a simplification without introducing some error. Therefore, the use of the "slow exchange" approximation for this system may introduce some error into the determination of the equilibrium constant (see section IV.C.) by  $^{13}\text{C}$  spin-lattice relaxation times.

#### 4. $T_1$ IN THE PURE COMPLEX

As given in Table 11, the average value for  $T_1$  of C-3 of 2-methylindole in the pure complex, obtained by fitting the theoretical curves to the experimental data, is 2.4 sec.

From a previous treatment of the data under the assumption of slow exchange (see equation [66]), a value of 3.0 sec

was obtained. The reasonable agreement of the  $T_{AD}$  values indicates that a large error is not introduced in the latter treatment, even though the exchange rate,  $k_4/k_2$ , is ca.  $10^{-1}$ .

E. SPIN-LATTICE RELAXATION AND HYDRODYNAMICAL ROTATION  
OF 2-METHYLINDOLE

Several hydrodynamical models of molecular reorientation were investigated in order to provide some insight into the rotational behaviour of 2-methylindole in solution.

1. ISOTROPIC REORIENTATION

The simplest way of treating the reorientation of this molecule is through the application of the Stokes-Einstein model (53) which considers the molecule as an isotropically rotating sphere.

The sum of the van der Waals volume increments (54) of all the atoms in this molecule is  $126.8\text{\AA}^3$ . Assuming that this is a good approximation of the molecular volume,  $V$ , the radius of the sphere,  $a$ , was calculated to be  $3.12\text{\AA}$ . The Stokes-Einstein model then describes the effective molecular correlation time as

$$[45] \quad \tau_c = \frac{V\eta}{kT} = \frac{4\pi a^3 \eta}{3kT} = 20.5 \text{ psec},$$

Since there is a large disparity with the experimental value of  $\tau_c = 6.7$  psec. calculated from [32], this model is inadequate in approximating the reorientational behaviour of 2-methylindole in 1,2-dichloroethane.

## 2. ANISOTROPIC REORIENTATION

### (a) Determination of the Geometry

Since  $\tau_c$  is a function of the geometry of the molecule (in addition to the viscosity of the medium and the temperature), a better approximation of the molecular geometry is necessary to improve the theoretical  $\tau_c$  values. Construction of a space-filling model indicated that 2-methylindole may be approximated quite well by an oblate spheroid. Using the van der Waals radius of carbon,  $1.7\text{\AA}$ , as a good approximation of the minor axis,  $c$ , (19, 58) and assuming the molecular volume to be  $126.8\text{\AA}^3$ , the major axis,  $a$ , is calculated to be  $4.22\text{\AA}$ .

A scale diagram, using the bond lengths and angles of L-tryptophan hydrochloride (76) determined in the solid phase by X-ray crystallography, shows that  $4.22\text{\AA}$  may be somewhat small for the radius of the major axis. If the molecule is considered to extend one (proton) van der Waals radius ( $1.45\text{\AA}$ ) beyond the periphery of the methyl protons, then  $a=5.55\text{\AA}$  is an upper limit to this radius (58). Therefore,  $a=4.9\pm 0.5\text{\AA}$  was considered to be a good approximation.

### (b) Application of Boundary Conditions

Using this geometry for 2-methylindole, different boundary conditions were now applied for molecular reorientation of this molecule.

Under the stick boundary conditions - which assumes that the solvent sticks to the surface of the rotating solute and

rotates with the solute - the rotational friction coefficients are calculated (according to [46] and [47]) in terms of the geometry of the molecule and the viscosity of the medium. Rotation of the symmetry axis (see Figure 26) will produce a significant amount of friction as quite a large volume of solvent is being displaced. However, rotation about the symmetry axis produces less friction since little solvent is being moved. The effective molecular correlation times were calculated according to [49] at several viscosities. A least-squares-fit of this data to [50] gave a viscosity dependence,  $C_{stick}$ , of  $19.7 \text{ nsec}^\circ\text{K/cP}$ .

Under slip boundary conditions the solvent is considered to slip by the surface of the rotating molecule. For this condition  $\zeta_3 = 0$  (see [46]) since rotation about the symmetry axis of an oblate spheroid does not displace any fluid.  $\zeta_1 = \zeta_2 = \zeta_{slip}$  can be obtained for the particular geometry from the data provided by Hu and Zwanzig (59). The effective molecular correlation time for the slip condition becomes

$$[70] \quad \tau_{slip} = \frac{\zeta_{slip}}{kT}$$

since the second term of [49] becomes negligible. Calculation of  $\tau_{slip}$  for 2-methylindole at several viscosities gave a viscosity dependence,  $C_{slip}$ , of  $2.13 \text{ nsec}^\circ\text{K/cP}$ .

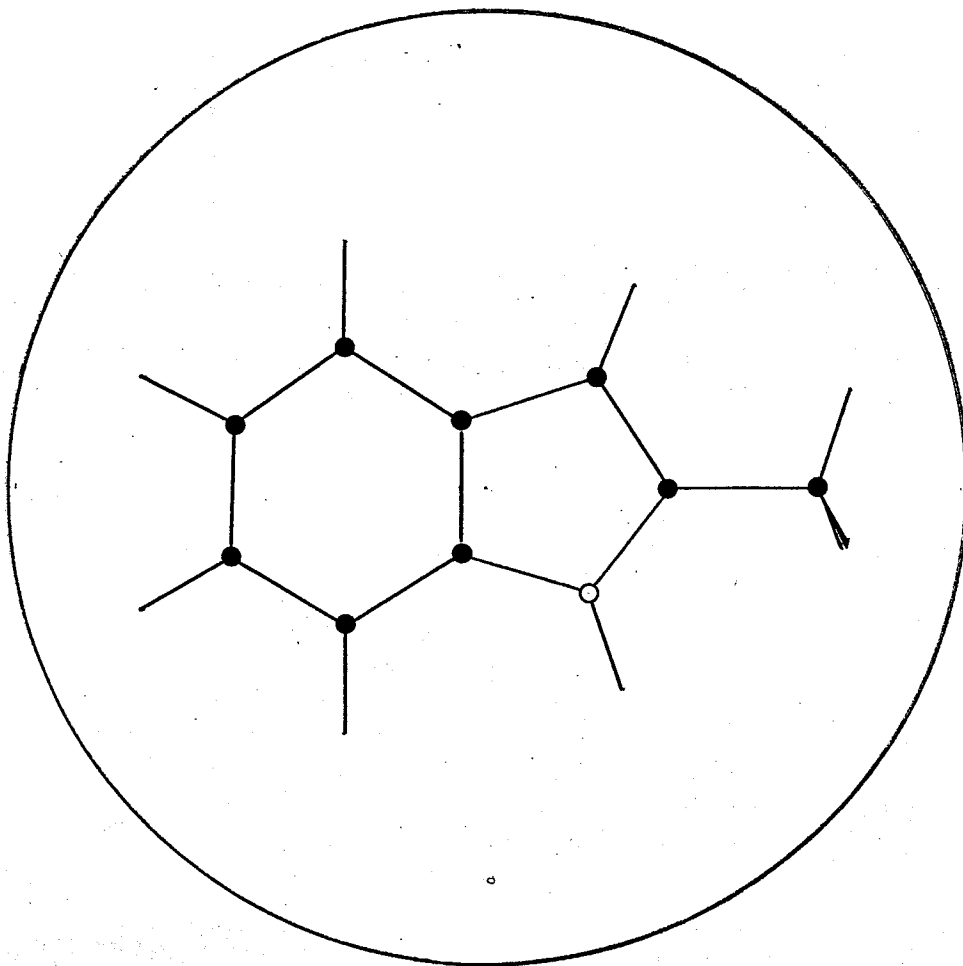


FIGURE 26. 2-methylindole within a circle of radius  $4.9\text{\AA}$ , ( $\bullet$  = carbon,  $\circ$  = nitrogen).

(c) Determination of the Experimental Viscosity  
Dependence of  $\tau_c$

(i) Variation of Temperature

Since the viscosity range in the study of complex formation of 2-methylindole with TNB (see Table 9) is 0.686-1.346 centipoise, the viscosity study had to be made over this range to check whether  $1/T_1 \propto \eta$  as assumed in [64].

The  $T_1$  data obtained for C-3 of 2-methylindole as a function of the temperature are summarized in Table 12. A linear relationship between  $1/T_1$  and  $\eta$  was obtained as shown in Figure 27.

The viscosities of the solutions were obtained from the literature viscosity data for 1,2-dichloroethane at various temperatures (77). It is assumed that the small amount of 2-methylindole (0.100 molal) and the use of 50% 1,2-dichloroethane- $d_4$  in the solvent (for nmr lock purposes) would not significantly affect the results.

The effective molecular correlation times were calculated from

$$[32] \quad \frac{1}{T_1} = \frac{\hbar^2 \gamma_C^2 \gamma_H^2}{r_{C-H}^6} \tau_c$$

using  $1.08\text{\AA}$  as the C-H distance.

A least-squares-fit of the data to  $\tau_c = C\eta/T$  gives the experimental viscosity dependence of  $\tau_c$  as  $C_{exp} = 3.46 \text{ nsec}^\circ\text{K}/\text{cP}$ , with a correlation coefficient of 0.995.



TABLE 12. The viscosity dependence of  $T_1$  (and therefore  $\tau_c$ ) of C-3 of 2-methylindole determined by temperature variation.

Temp( °C)	$\eta$ (cP)	$T_1$ (sec) <sup>a</sup>	$\tau_c$ (psec)
35.0	0.68 <sub>6</sub>	6.3 <sub>7</sub>	6.92
24.2	0.79 <sub>3</sub>	5.1 <sub>5</sub>	8.56
10.5	0.95 <sub>2</sub>	4.3 <sub>0</sub>	10.25
- 1.5	1.14 <sub>0</sub>	3.1 <sub>2</sub>	14.13
-12.1	1.36 <sub>0</sub>	2.4 <sub>4</sub>	18.06
-22.0	1.62 <sub>0</sub>	2.1 <sub>0</sub>	20.99

<sup>a</sup>Spin-lattice relaxation times for C-3 of 2-methylindole-(methyl,3)-<sup>13</sup>C<sub>2</sub> determined with a 0.100 molal solution in 1,2-dichloroethane, 50% of which was 1,2-dichloroethane-*d*<sub>4</sub>.

## (ii) Variation of the Solvent System

Variation of the viscosity (determined experimentally) over the desired range was also accomplished by using different mixtures of 1,2-dichloroethane and 1,1,2,2-tetrachloroethane as the solvent.

1,1,2,2-tetrachloroethane was the solvent chosen since its dielectric constant ( $\epsilon=7.83$  at  $25^\circ$ ) matched that of 1,2-dichloroethane ( $\epsilon=10.13$  at  $25^\circ$ ) reasonably well (78), it provided the necessary range in viscosity (77) ( $\eta=1.389$  cP at  $35^\circ$  for this solvent), and it is structurally similar to 1,2-dichloroethane. The changes in the solvent should therefore be minimal due to mixing of this component with 1,2-dichloroethane.

The  $T_1$ 's of C-3 of 2-methylindole determined in various mixtures of the two solvents at  $35^\circ$  are summarized in Table 13. A linear relationship between  $1/T_1$  and  $\eta$  was obtained as shown in Figure 27.

The correlation times, calculated as in the previous section, show a viscosity dependence of  $C_{exp} = 3.96 \text{ nsec}^\circ \text{K/cP}$  with a correlation coefficient of 0.996.

## (d) Comparison of Experimental Data with Theory

Comparison of the experimentally determined viscosity dependence of the molecular correlation time with the results of the slip and stick treatments (see Table 14 and Figure 28) indicates that 2-methylindole rotates with near slip conditions in 1,2-dichloroethane. This reorientation will disturb the least amount of solvent and will therefore show a smaller

TABLE 13. The viscosity dependence of  $T_1$  (and therefore  $\tau_c$ ) of C-3 of 2-methylindole determined by variation of the solvent system at 35°.

[2-MeI] <sup>a</sup>	$X_{tetra}^b$	$\eta$ (cP)	$T_1$ (sec) <sup>c</sup>	$\tau_c$ (psec)
0.100	0.00	0.69 <sub>6</sub>	6.3 <sub>7</sub>	6.92
0.096	0.24 <sub>5</sub>	0.86 <sub>3</sub>	4.8 <sub>1</sub>	9.16
0.098	0.49 <sub>5</sub>	1.04 <sub>7</sub>	3.7 <sub>1</sub>	11.88
0.091	0.71 <sub>1</sub>	1.21 <sub>8</sub>	3.1 <sub>0</sub>	14.22
0.097	0.98 <sub>4</sub>	1.44 <sub>8</sub>	2.6 <sub>9</sub>	16.39

<sup>a</sup>Molal concentration of 2-methylindole-(methyl,3)-<sup>13</sup>C<sub>2</sub>.

<sup>b</sup>Mole-fraction of 1,1,2,2-tetrachloroethane.

<sup>c</sup>Spin-lattice relaxation times for C-3 of 2-methylindole in various mixtures of 1,2-dichloroethane and 1,1,2,2-tetrachloroethane.

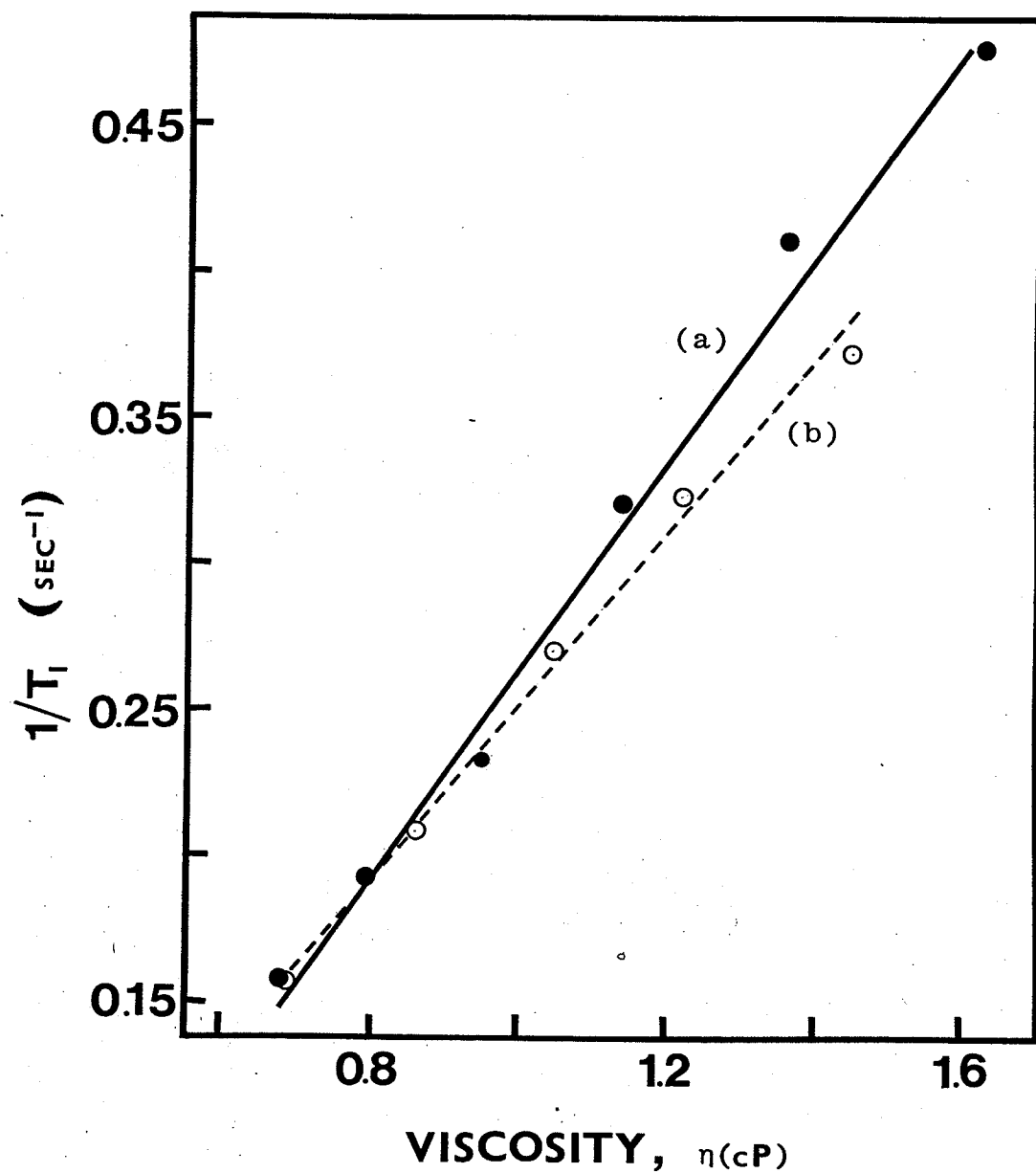


FIGURE 27. Viscosity dependence of  $1/T_1$  of C-3 of 2-methylindole determined by (a) variation of the temperature and (b) the use of mixed solvents at a constant temperature of  $35^\circ$ .

TABLE 14. Summary of the viscosity dependence,  $C$ , of  $\tau_c$  of 2-methylindole.

	$C$ (nsec °K/cP)	$\tau_c$ (psec) <sup>a</sup>
Stick	19.7	43.8
Exp <sup>b</sup>	3.71	6.7
Slip	2.13	4.8

<sup>a</sup>Correlation times at 0.686 cP. and 35°C.

<sup>b</sup>The average  $C_{exp}$  obtained by the two methods.

viscosity dependence and faster rate of reorientation. The stick boundary condition predicts too much friction to rotation and therefore shows a very high viscosity dependence. The solvent, 1,2-dichloroethane, is not expected to interact strongly with 2-methylindole since it will not hydrogen-bond to the solute. Therefore, the amount of "stick" is expected to be minimal, which is in agreement with what is observed.

(e) Application to the TNB complex of 2-methylindole

If the interplanar distance of the components in the complex is similar to that reported (19) for the 3-methylindole:TNB complex, *ie.* 3.30Å, then the minor axis can be calculated to be *ca.* 1.7 + 1.65 = 3.35Å. Assuming the same relative orientation of donor and acceptor as reported (19) for the 3-methylindole:TNB complex, 4.9Å is still a reason-

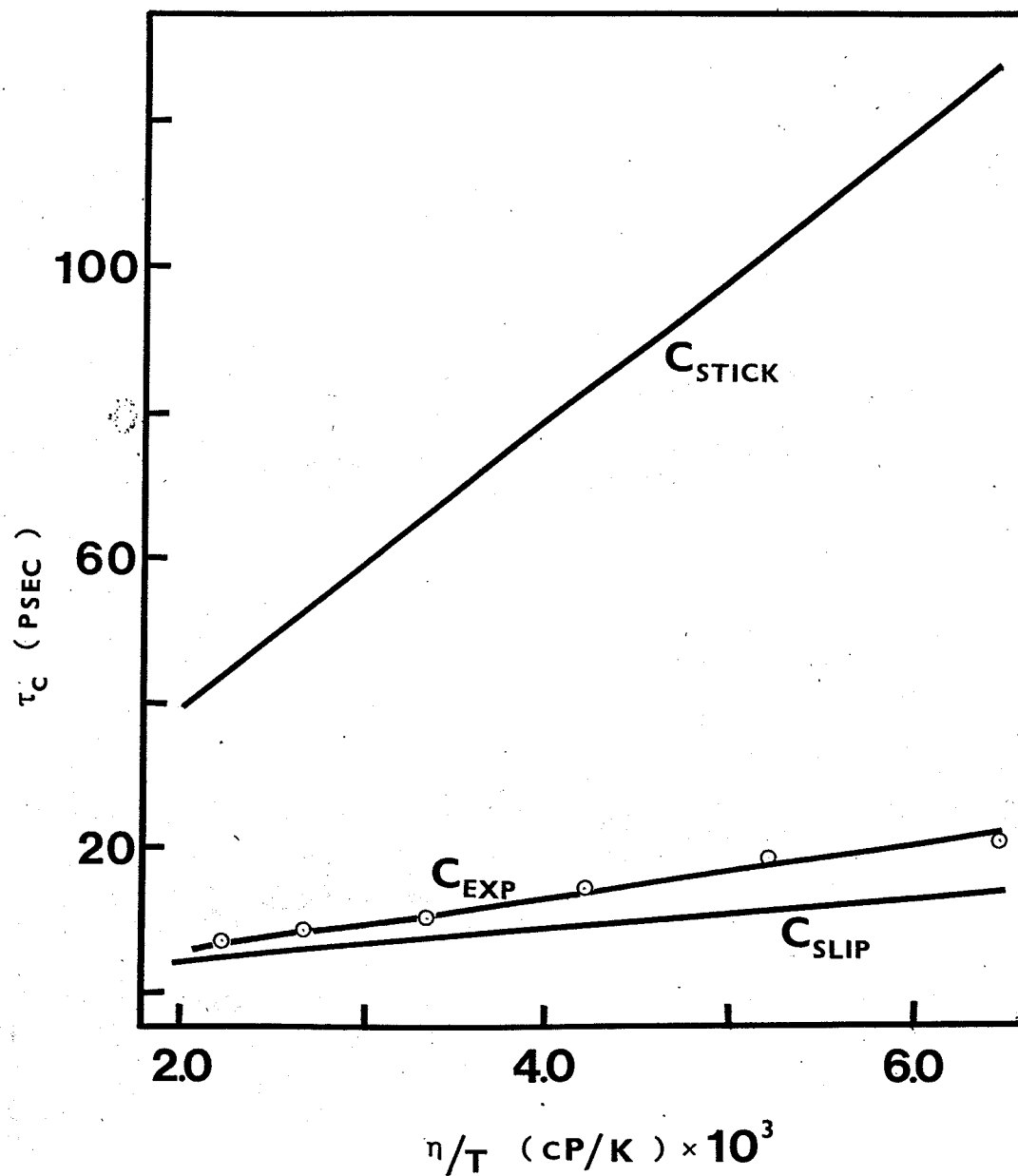


FIGURE 28. Comparison of theoretical viscosity dependence ( $C_{slip}$  and  $C_{stick}$ ) with the experimental ( $C_{exp}$ ) for 2-methylindole.

able approximation for the major axis.

With this geometry, the slip and stick boundary conditions were applied to the hydrodynamical rotation of the tight complex. The theory predicts viscosity dependences of  $26.7 \text{ nsec}^\circ\text{K/cP}$  for  $C_{stick}$  and  $0.53 \text{ nsec}^\circ\text{K/cP}$  for  $C_{slip}$  (see Table 15). Thus, the theory predicts less viscosity dependence for the pure complex than for the free 2-methylindole under slip conditions. This is expected since the rotation of the symmetry axis of the complex (approximated as an oblate spheroid) will not move as much solvent as will the same reorientation in the free 2-methylindole, since the complex is approaching "sphericity" in comparison to the free donor.

TABLE 15. Comparison of data, theoretical and experimental, for hydrodynamical rotation of the 2-MeI:TNB complex.

	$C$ (nsec $^\circ\text{K/cP}$ )	$\tau_c$ (psec) <sup>a</sup>
Stick	26.7	59.4
Exp	—	14.7
Slip	0.53	1.2

<sup>a</sup>Correlation times at 0.686 cP. and 35°C.

Although, as mentioned previously, the experimental viscosity dependence of the pure complex cannot be determined, the effective molecular correlation time for the pure complex has been obtained experimentally. The correlation times (see Table 15) show that the theory does not check very well with the experimental result. This may be due to errors in the assumed geometry of the complex. In any case, further work is necessary in this area.



V. BIBLIOGRAPHY

1. R. Foster, "Organic Charge-Transfer Complexes", Academic Press, London (1969).
2. M. A. Slifkin, "Charge-Transfer Interactions in Biomolecules", Academic Press, London (1971).
3. "Molecular Associations in Biology", edited by B. Pullman, Academic Press, New York (1968).
4. "Molecular Complexes", Vol. 2, edited by R. Foster, Crane Russak, New York (1974).
5. R. Foster and C. A. Fyfe in "Progress in Nuclear Magnetic Resonance Spectroscopy", Vol. 4, edited by J. W. Emsley, J. Feeney and L. H. Sutcliffe, Pergamon Press, Oxford (1969).
6. R. M. Lynden-Bell and R. K. Harris, "Nuclear Magnetic Resonance Spectroscopy", Thomas Nelson and Sons, Don Mills (1969).
7. B. Robinson, Chem. Rev. 63, 373 (1963).
8. E. Fischer and F. Jourdan, Ber. 16, 2241 (1883).
9. E. Fischer and O. Hess, Ber. 17, 559 (1884).
10. L. Marion and C. W. Oldfield, Can. J. Res. 25B, 1 (1947).
11. N. B. Chapman, K. Clarke and H. Hughes, J. Chem. Soc. 1424 (1965).
12. H. M. Kissman, D. W. Farnsworth and B. Witkop, J. Am. Chem. Soc. 74, 3948 (1952).
13. J. Shukri, S. Alazawe and A. S. Al-Tai, J. Ind. Chem. Soc. 47, 123 (1970).

14. G. M. Robinson and R. Robinson, J. Chem. Soc. 113, 639 (1918).
15. J. March, "Advanced Organic Chemistry", 2nd edition, McGraw-Hill, New York (1977).
16. L. N. Ferguson, "Organic Molecular Structure", Willard Grant Press, Boston (1975).
17. R. S. Mulliken, J. Am. Chem. Soc. 74, 811 (1952).
18. A. Streitwieser and C. H. Heathcock, "Introduction to Organic Chemistry", MacMillan Pub. Co., New York (1976).
19. C. K. Prout and J. D. Wright, Angew. Chem. Int. Ed. 7, 659 (1968).
20. R. Foster, Chem. Br. 12, 18 (1976).
21. M. J. S. Dewar and A. R. Lepley, J. Am. Chem. Soc. 83, 4560 (1961).
22. J. A. Pople, W. G. Schneider and A. J. Bernstein, "High Resolution Nuclear Magnetic Resonance", McGraw-Hill, New York (1959).
23. J. W. Emsley, J. Feeney and L. H. Sutcliffe, "High Resolution Nuclear Resonance Spectroscopy", Vol. 1, Pergamon Press, New York (1966).
24. R. S. Drago, "Physical Methods in Chemistry", W. B. Saunders, Toronto (1977).
25. G. E. Maciel in "Topics in Carbon-13 NMR Spectroscopy", Vol. 1, edited by G. C. Levy, J. Wiley and Sons, New York (1974).
26. H. A. Benesi and J. H. Hildebrand, J. Am. Chem. Soc. 71, 2703 (1949).

27. R. Mathur, E. D. Becker, R. B. Bradley and N. C. Li,  
J. Phys. Chem. 67, 2190 (1963).
28. P. J. Berkeley, Jr. and M. W. Hanna, J. Phys. Chem.  
67, 846 (1963).
29. M. W. Hanna and A. L. Ashbaugh, J. Phys. Chem. 68, 811  
(1964).
30. R. Foster and C. A. Fyfe, Trans. Fara. Soc. 62, 1400  
(1966).
31. R. Foster and C. A. Fyfe, J. Chem. Soc. (B), 926 (1966).
32. M. T. Sung and J. A. Parker, Proc. Nat. Acad. Sci. USA  
69, 1196 (1972).
33. N. M. D. Brown, R. Foster and C. A. Fyfe, J. Chem. Soc.  
(B), 406 (1967).
34. A. A. S. Bright, R. Foster and J. A. Chudek, J. Chem.  
Soc. Perkin II, 64 (1975).
35. R. C. Griffith, D. M. Grant and J. D. Roberts, J. Org.  
Chem. 40, 3726 (1975).
36. H. N.° Wachter and V. Fried, J. Chem. Educ. 51, 798 (1974).
37. C. J. Creswell and A. L. Allred, J. Phys. Chem. 66,  
1469 (1962).
38. B. Sabourault and J. Bourdais, Tetrahedron 33, 1739  
(1977).
39. I. Prins, J. W. Verhoeven and Th. J. de Boer, Org. Mag.  
Res. 9, 543 (1977).
40. G. L. Levy and G. L. Nelson, "Carbon-13 Nuclear Magnet-  
ic Resonance for Organic Chemists", Wiley, New York  
(1972).

41. E. Breitmaier, G. Jung and W. Voelter, *Angew. Chem. Int. Ed.* 10, 673 (1971).
42. E. D. Becker and T. C. Farrar, *Science* 178, 361 (1972).
43. E. Breitmaier, K.-H. Spohn and S. Berger, *Angew. Chem. Int. Ed.* 14, 144 (1975).
44. G. C. Levy, *Accounts Chem. Res.* 6, 161 (1973).
45. T. C. Farrar and E. D. Becker, "Pulse and Fourier Transform NMR", Academic Press, New York (1971).
46. A. Carrington and A. D. McLachlan, "Introduction to Magnetic Resonance", Harper and Row, New York (1967).
47. J. R. Lyerla, Jr. and G. C. Levy in "Topics in Carbon-13 NMR Spectroscopy", Vol. 1, edited by G. C. Levy, J. Wiley and Sons, New York (1974).
48. D. Doddrell, V. Glushko and A. Allerhand, *J. Chem. Phys.* 56, 3683 (1972).
49. I. Solomon, *Phys. Rev.* 99, 559 (1955).
50. F. W. Wehrli in "Topics in Carbon-13 NMR Spectroscopy", Vol. 2, edited by G. C. Levy, J. Wiley and Sons, New York (1976).
51. J. H. Noggle and R. E. Schirmer, "The Nuclear Overhauser Effect", Academic Press, New York (1971).
52. A. Einstein, "Investigations on the Theory of Brownian Movement", Dover, New York (1956).
53. D. R. Bauer, J. I. Brauman and R. Pecora, *J. Am. Chem. Soc.* 96, 6840 (1974).
54. J. T. Edward, *J. Chem. Educ.* 47, 261 (1970).
55. F. Perrin, *J. Phys. Radium* 7, 1 (1936).

56. D. E. Woessner, *J. Chem. Phys.* 37, 647 (1962).
57. W. T. Huntress, Jr., *J. Chem. Phys.* 48, 3524 (1968).
58. R. E. Wasylishen, B. A. Pettitt and W. Danchura, *Can. J. Chem.* 55, 3602 (1977).
59. C. Hu and R. Zwanzig, *J. Chem. Phys.* 60, 4354 (1974).
60. D. R. Bauer, G. R. Alms, J. I. Brauman and R. Pecora, *J. Chem. Phys.* 61, 2255 (1974).
61. J. E. Anderson and P. A. Fryer, *J. Chem. Phys.* 50, 3784 (1969).
62. J. E. Anderson and C. P. Smythe, *J. Am. Chem. Soc.* 85, 2904 (1963).
63. J. P. Behr and J. M. Lehn, *J. Am. Chem. Soc.* 98, 1743 (1976).
64. Ch. Brevard and J. M. Lehn, *J. Am. Chem. Soc.* 92, 4987 (1970).
65. D. J. Pasto and C. R. Johnson, "Organic Structure Determination", Prentice-Hall, Englewood Cliffs, N. J. (1969).
66. K. Clusius and H. R. Weisser, *Helvetica Chimica Acta*, Vol XXXV, 400 (1952).
67. H. Posvic, R. Dombro, H. Ito and T. Telinski, *J. Org. Chem.* 39, 2575 (1974).
68. R. G. Parker and J. D. Roberts, *J. Org. Chem.* 35, 996 (1970).
69. J. L. Johnson, *Diss. Abstr. Int. B* 38, 3696 (1978).
70. K. K. Deb, T. C. Cole and J. E. Bloor, *Org. Mag. Res.* 2, 491 (1970).

71. J. A. Pople and D. L. Beveridge, "Approximate Molecular Orbital Theory", McGraw-Hill, New York (1970).
72. G. C. Levy and I. R. Peat, J. Mag. Res. 18, 500 (1975).
73. I. M. Armitage, H. Huber, D. H. Live, H. Pearson and J. D. Roberts, J. Mag. Res. 15, 142 (1974).
74. G. C. Levy, J. D. Cargioli and F. A. L. Anet, J. Am. Chem. Soc. 95, 1527 (1973).
75. J. M. Lehn, private communication, 1977.
76. "Physical Methods in Heterocyclic Chemistry", Vol. 5, edited by A. R. Katritzky, Academic Press, New York (1972).
77. International Critical Tables, Vol. 7, p213, McGraw-Hill, New York (1930).
78. International Critical Tables, Vol. 6, p84, McGraw-Hill, New York (1929).

VI. APPENDICESA. 'SHIFT'

The APL program 'SHIFT' was used in the determination of equilibrium constants from chemical shift data, providing the user with a choice of two concentration scales.

```

      ▼ SHIFT
[1]  RCALN OF EQUIL CONSTANT BY SUCCESSIVE APPROXIMATIONS,
[2]  RFROM CHEMICAL SHIFT DATA,
[3]  'ENTER WT OF MINOR COMPONENT IN EACH SOLN'
[4]  A←[]
[5]  'ENTER WT OF MAJOR COMPONENT IN EACH SOLN'
[6]  D←[]
[7]  'ENTER WT OF SOLVENT IN EACH SOLN'
[8]  S←[]
[9]  'ENTER MW OF MINOR COMPONENT'
[10] MWA←[]
[11] 'ENTER MW OF MAJOR COMPONENT'
[12] MWD←[]
[13] 'FOR KG SOLVENT/M TYPE X, KG SOLN/M TYPE Z'
[14] →(Z='Z')/LOOP
[15] CA←(1000÷S)XA÷MWA
[16] CD←(1000÷S)XD÷MWD
[17] →STEP
[18] LOOP:CA←(1000÷S+A+D)XA÷MWA
[19] CD←(1000÷S+A+D)XD÷MWD
[20] STEP:'ENTER OBSERVED SHIFT FOR EACH SOLN IN HZ'
[21] Δ←[]
[22] Y←Δ÷CD
[23] L←Δ LSFIT] Y
[24] ' '
[25] ' '
[26] '          CA          CD          Δ          Δ/CD'
[27] ARRAY←CA,((fCA),1)fCD
[28] ARRAY←ARRAY,Δ
[29] ARRAY,Y
[30] ' '
[31] ' '
[32] 'RESULTS OF LSFIT:'
[33] L
[34] K←-L[2]
[35] DX←CD
[36] I←0
[37] →CALC
[38] CON:K←KA
[39] →CALC
[40] IT:DX←DE

```

```

[41] CALC:I←I+1
[42] DE←CD-(KXDXXCA)÷1+KXDX
[43] →(1E-6∑|DX-DE)/IT
[44] ' '
[45] (↑'NO OF ITERATIONS: ') , ↑I
[46] X←Δ÷DE
[47] M←Δ LSFIT] X
[48] ' '
[49] ' '
[50] '          DE          Δ/DE '
[51] T←DE , ((↑DE) , 1) , X
[52] T
[53] ' '
[54] ' '
[55] 'RESULTS OF LSFIT:'
[56] M
[57] KA←-M[2]
[58] →(0.00001∑|KA-K)/CON
[59] ' '
[60] ' '
[61] 'PLOT OF Δ/DE VS Δ:'
[62] ' '
[63] ' '
[64] 40 40 PLOT Δ VS X
[65] ' '
[66] 'END SHIFT'

```

▽

## B. 'EDA'

The APL program 'EDA', offering the user a choice of two concentration scales, was used in the determination of equilibrium constants from  $T_1$  data. The program was also used in the determination of  $T_1$  in the pure complex.

▽ EDA

```

[1] RCALC OF EQUIL CONST FROM SPIN LATTICE RELAXN TIMES
[2] RWHERE CHEMICAL EXCHANGE IS SLOW REL TO MOLECULAR REORIENTN
[3] 'PART A. DETERMINATION OF THE EQUILIBRIUM CONSTANT'
[4] 'ENTER WT OF MINOR COMP IN REFERENCE SOLN'
[5] AO←[]
[6] 'ENTER WT OF SOLVENT IN REF SOLN'
[7] SO←[]

```



```

[8]  'ENTER OBSVD T1 OF REF SOLN (SEC)'
[9]  TF←[]
[10] 'ENTER VISCOSITY OF REF SOLN (CPOISE)'
[11] VO←[]
[12] 'ENTER WT OF MINOR COMP IN EACH SOLN'
[13] A←[]
[14] 'ENTER WT OF MAJOR COMP IN EACH SOLN'
[15] D←[]
[16] 'ENTER WT OF SOLVENT IN EACH SOLN'
[17] S←[]
[18] 'ENTER MW OF MINOR COMP'
[19] MWA←[]
[20] 'ENTER MW OF MAJOR COMP'
[21] MWD←[]
[22] 'ENTER OBSVD T1 FOR EACH SOLN (SEC)'
[23] T1←[]
[24] 'ENTER VISCOSITY OF EACH SOLN'
[25] V←[]
[26] 'FOR KG SOLVENT/M TYPE X, KG SOLN/M TYPE Z'
[27] →([]='Z')/LOOP
[28] CA←(1000÷S)xA÷MWA
[29] CD←(1000÷S)xD÷MWD
[30] CAO←(1000÷S0)xA0÷MWA
[31] →STEP
[32] LOOP:CA←(1000÷S+A+D)xA÷MWA
[33] CD←(1000÷S+A+D)xD÷MWD
[34] CAO←(1000÷S0+A0)xA0÷MWA
[35] STEP:''
[36] 'CONC OF MINOR COMP IN REF SOLN:',+CAO
[37] ''
[38] '          CA          CD          T1(SEC)          VISC(CP) '
[39] ''
[40] ARRAY←CA,((/CA),1)P CD
[41] ARRAY←ARRAY,T1
[42] ARRAY,V
[43] ''
[44] XX←VO÷VXT1
[45] YY←((VO÷VXT1)-1÷TF)X1÷CD
[46] MM←XX LSFIT1 YY
[47] ' '
[48] K←-MM[2]
[49] 'FIRST ESTIMATE OF K FROM INITIAL CONCENTRATIONS:',+K
[50] DX←CD
[51] I←0
[52] →CALC
[53] CON:K←KA
[54] →CALC
[55] IT:DX←DE
[56] CALC:I←I+1

```

```

[57] DE←CD-(KXDXxCA)÷1+KXDX
[58] →(0.0001≤|DX-DE)/IT
[59] ''
[60] 'NO OF ITERATIONS:',I
[61] Y←((VO÷VXT1)-1÷TF)X1÷DE
[62] X←VO÷VXT1
[63] M←X LSFIT1 Y
[64] ''
[65] 'RESULTS OF LSFIT1: '
[66] M
[67] ''
[68] '      Y      X'
[69] R←Y,((FY),1)FX
[70] R
[71] ''
[72] KA←-M[2]
[73] →(0.01≤|KA-K)/COM
[74] 'FOR PLOT OF RESULTS TYPE U, OTHERWISE TYPE N'
[75] →(U='N')/SKIP
[76] 'PLOT OF Y VS X: '
[77] ''
[78] 40 40 PLOT X VS Y
[79] SKIP: ' '
[80] ''
[81] ''
[82] ''
[83] 'PART B,      DETERMINATION OF THE T1 OF THE PURE COMPLEX'
[84] E←DE÷((VO÷V)X(1÷T1))-(1÷TF)
[85] J←DE
[86] B←E LSFIT1 J
[87] 'RESULTS OF LSFIT1: '
[88] B
[89] ''
[90] '      E      J      '
[91] R←E,((FE),1)FJ
[92] R
[93] ''
[94] 'T1 OF PURE COMPLEX AT REF VISC'
[95] G←B[2]+1÷TF
[96] H←1÷G
[97] H
[98] ''
[99] 'FIN'

```

▽

C. 'QUADEX'

The Fortran program 'QUADEX' was used in the determination of the molecular dynamics of complex formation.

```

1      DIMENSION K4(100),D(10),A(10),TDEXP(10),V(10),
          TDEXPV(10),
          ITTHEO(10,100),TDIF(10,100),DEVN(100),C(50),
          TCALC(50)
2      DOUBLE PRECISION K1,K2,K3,K4,LP,LM,QP,QM,KP,KM
3      REAL K
4      IE=5
5      IS=6
6      READ (IE,001)K1,BDIP,K,TDCOMP,N,ITER
7      001 FORMAT (2E11.4,2F8.4,2I3)
8      DO 0005 I=1,N
9      0005 READ (IE,0006)TDEXP(I),D(I),A(I),V(I)
10     0006 FORMAT (4F8.4)
11     VIS=V(1)
12     DO 0011 I=2,N
13     0011 TDEXPV(I)=TDEXP(I)*V(I)/VIS
14     DO 0007 J=1,ITER
15     K2=TDCOMP*BDIP
16     DO 0008 L=1,81
17     IF(L-9)0015,0015,0016
18     0015 K4(L)=0.00001*L*K2
19     GO TO 0033
20     0016 IF(L-18)0017,0017,0018
21     0017 K4(L)=0.0001*(L-9)*K2
22     GO TO 0033
23     0018 IF(L-27)0019,0019,0020
24     0019 K4(L)=0.001*(L-18)*K2
25     GO TO 0033
26     0020 IF(L-36)0021,0021,0022
27     0021 K4(L)=0.01*(L-27)*K2
28     GO TO 0033
29     0022 IF(L-45)0023,0023,0024
30     0023 K4(L)=0.1*(L-36)*K2
31     GO TO 0033
32     0024 IF(L-54)0025,0025,0026
33     0025 K4(L)=1*(L-45)*K2
34     GO TO 0033
35     0026 IF(L-63)0027,0027,0028
36     0027 K4(L)=10*(L-54)*K2
37     GO TO 0033
38     0028 IF(L-72)0029,0029,0030
39     0029 K4(L)=100*(L-63)*K2
40     GO TO 0033
41     0030 IF(L-81)0031,0031,0032
42     0031 K4(L)=1000*(L-72)*K2
43     GO TO 0033
44     0032 GO TO 500

```

```

45 0033 DO 0009 I=2,N
46     ALFA=K*D(I)
47     BETA=-K*D(I)-K*A(I)-1.0
48     GAMA=K*A(I)
49     C(I)=(-BETA-SQRT(BETA**2-4*ALFA*GAMA))/(2*ALFA)
50     F=A(I)-C(I)*D(I)
51     K3=K*K4(L)
52     LP=0.5*(K1+K2+K3*F+K4(L))+0.5*DSQRT((K1+K3*F-K2
                                     -K4(L))**2+4*K3*F*K
14(L))
53     LM=0.5*(K1+K2+K3*F+K4(L))-0.5*DSQRT((K1+K3*F-K2
                                     -K4(L))**2+4*K3*F*K
14(L))
54     KP=K4(L)/(LP-K1-K3*F)
55     KM=K4(L)/(LM-K1-K3*F)
56     QP=(KP-1)*(1-(1-KM)*C(I))/(KP-KM)
57     QM=(1-KM)*(1-(1-KP)*C(I))/(KP-KM)
58     TTHEO(I,L)=1.0/(BDIP*((QP/LP)+(QM/LM)))
59 0009 TDIF(I,L)=ABS(TTHEO(I,L)-TDEXPV(I))*100
60     DEVN(L)=TDIF(2,L)
61     DO 0010 I=3,N

62 0010 DEVN(L)=DEVN(L)+TDIF(I,L)
63     SUM=0.0
64     DO 0014 I=2,N
65 0014 SUM=SUM+TDEXPV(I)
66     DEVN(L)=DEVN(L)/SUM
67 0008 CONTINUE
68     SMIN=100000
69     DO 0012 L=1,81
70     IF(DEVN(L)-SMIN)0013,0013,0012
71 0013 MO=L
72     SMIN=DEVN(MO)
73 0012 CONTINUE
74     RATIO=K4(MO)/K2
75     WRITE(IS,800)SMIN,RATIO,K4(MO),K2,K1
76     WRITE(IS,801)TDCOMP
77     WRITE(IS,802)(C(I),TTHEO(I,MO),TDEXPV(I),I=2,N)
78 800 FORMAT (30H)DEVIATION FOR BEST FIT DATA ,E11.4
                                     ///60H RATE OF
1EXCHANGE RELATIVE TO RATE OF ROTATION OF COMPLEX,
                                     E11.4///35H RATE
1OF DISSOCIATION OF COMPLEX ,E11.4///35H RATE OF
                                     ROTATION OF
1COMPLEX ,E11.4///35H RATE OF ROTATION OF FREE
                                     MOLECULE ,E11.4)
79 801 FORMAT (///15H TD OF COMPLEX ,F8.4)
80 802 FORMAT (///60H FRACTION COMPLEXED TD THEOR
                                     (BEST-FIT) TD

```

```

      1EXPV      //(8X,F8.4,12X,F8.4,12X,F8.4)
81      ACC=0.10
82      DO 1000 I=1,27
83      ALFA=K*0.10
84      BETA=-K*0.10-K*ACC-1.0
85      GAMA=K*ACC
86      C(I)=(-BETA-SQRT(BETA**2-4*ALFA*GAMA))/(2*ALFA)
87      F=ACC-C(I)*0.10
88      L=M0
89      K3=K4(M0)*K
90      LP=0.5*(K1+K2+K3*F+K4(L))+0.5*DSQRT((K1+K3*F-K2
      -K4(L))**2+4*K3*F*K
91      14(L))
      LM=0.5*(K1+K2+K3*F+K4(L))-0.5*DSQRT((K1+K3*F-K2
      -K4(L))**2+4*K3*F*K
92      14(L))
92      KP=K4(L)/(LP-K1-K3*F)
93      KM=K4(L)/(LM-K1-K3*F)
94      QP=(KP-1)*(1-(1-KM)*C(I))/(KP-KM)
95      QM=(1-KM)*(1-(1-KP)*C(I))/(KP-KM)
96      TCALC(I)=1.0/(BDIP*((QP/LP)+(QM/LM)))
97      1000 ACC=ACC+0.10
98      WRITE(IS,900)(C(I),TCALC(I),I=1,27)
99      900 FORMAT(35H1FRACTION COMPLEXED      TD THEOR      //
      (8X,F8.4,8X,F8.4))
100     0007 TDCOMP=TDCOMP+0.10
101     500 STOP
102     END

```